A FITNESS-FOR-PURPOSE EVALUATION OF ELECTRO-SLAG FLANGE BUTT WELDS

FINAL REPORT

by

Steven C. Lovejoy, P.E.
Senior Mechanical Engineer
Bridge Engineering Section
Oregon Department of Transportation

for

Oregon Department of Transportation
Research Group
200 Hawthorne Avenue SE, Suite B-240
Salem, OR 97301-5192

April 2002

Technical Report Documentation Page

1. Report No.	2. Government Accession No.	3. Recipient's Catalog No.
OR-RD-02-15		

4. Title and Subtitle	5. Report Date
A Fitness-For-Purpose Evaluation of Electro-slag Flange Butt Welds Final Report	April 2002
	6. Performing Organization Code

7. Author(s)	8. Performing Organization Report No.
Steven C. Lovejoy, P.E., Senior Mechanical Engineer Bridge Engineering Section, Oregon Department of Transportation	

9. Performing Organization Name and Address	10. Work Unit No. (TRAIS)
Oregon Department of Transportation Research Group 200 Hawthorne Ave. SE, Suite B-240 Salem, OR 97301-5192	11. Contract or Grant No. 02BR7410

12. Sponsoring Agency Name and Address	13. Type of Report and Period Covered
Oregon Department of Transportation Research Group 200 Hawthorne Ave. SE, Suite B-240 Salem, OR 97301-5192 and Federal Highway Administration 400 Seventh Street SW Washington, DC 20590	Final Report
	14. Sponsoring Agency Code

15. Supplementary Notes

16. Abstract

A fitness-for-purpose evaluation was performed on the electroslag flange butt welds of the I-205, George Abernethy Bridge as per the request of FHWA notices N5040.23 and 5040.29 dated 2/16/77 and 2/23/77 respectively as well as Memorandum HNG-30 dated 6/21/78. This evaluation required gathering knowledge of the material properties, fabrication defects, and service loads pertaining to the weldments in question. With these data the serviceability of the weldments was assessed and retrofit or monitoring requirements were developed that would assure public safety at reasonable operational costs. After 23 years of ongoing testing and study the plan to monitor the welds in question was developed and justified saving the taxpayers over 6 million dollars in retrofitting construction expenses.

17. Key Words	18. Distribution Statement
electroslag, weld, fracture, steel, strain, stress, girder, NDE, NDT, residual, toughness, crack growth, nondestructive	Available from NTIS and Oregon Department of Transportation (http://www.odot.state.or.us/tddresearch)

19. Security Classification (of this report)	20. Security Classification (of this page)	21. No. of Pages	22. Price
Unclassified	Unclassified	86 + appendices	

Technical Report Form DOT F 1700.7 (8-72) Reproduction of completed page authorized ⊕ Printed on recycled paper

SI* (MODERN METRIC) CONVERSION FACTORS

APPROXIMATE CONVERSIONS TO SI UNITS

Symbol	When You Know	Multiply By	To Find	Symbol
		LENGTH		
in	inches	25.4	millimeters	mm
ft	feet	0.305	meters	m
yd	yards	0.914	meters	m
mi	miles	1.61	kilometers	km
		AREA		
in^2	square inches	645.2	millimeters squared	mm^2
ft^2	square feet	0.093	meters squared	m^2
yd^2	square yards	0.836	meters squared	m^2
ac	acres	0.405	hectares	ha
mi^2	square miles	2.59	kilometers squared	km^2
		VOLUME		
fl oz	fluid ounces	29.57	milliliters	mL
gal	gallons	3.785	liters	L
ft^3	cubic feet	0.028	meters cubed	m^3
yd^3	cubic yards	0.765	meters cubed	m^3
NOTE: Volumes greater than 1000 L shall be shown in m^3.				
		MASS		
oz	ounces	28.35	grams	g
lb	pounds	0.454	kilograms	kg
T	short tons (2000 lb)	0.907	megagrams	Mg
		TEMPERATURE (exact)		
°F	Fahrenheit temperature	5(F-32)/9	Celsius temperature	°C

APPROXIMATE CONVERSIONS FROM SI UNITS

Symbol	When You Know	Multiply By	To Find	Symbol
		LENGTH		
mm	millimeters	0.039	inches	in
m	meters	3.28	feet	ft
m	meters	1.09	yards	yd
km	kilometers	0.621	miles	mi
		AREA		
mm^2	millimeters squared	0.0016	square inches	in^2
m^2	meters squared	10.764	square feet	ft^2
ha	hectares	2.47	acres	ac
km^2	kilometers squared	0.386	square miles	mi^2
		VOLUME		
mL	milliliters	0.034	fluid ounces	fl oz
L	liters	0.264	gallons	gal
m^3	meters cubed	35.315	cubic feet	ft^3
m^3	meters cubed	1.308	cubic yards	yd^3
		MASS		
g	grams	0.035	ounces	oz
kg	kilograms	2.205	pounds	lb
Mg	megagrams	1.102	short tons (2000 lb)	T
		TEMPERATURE (exact)		
°C	Celsius temperature	1.8C + 32	Fahrenheit	°F

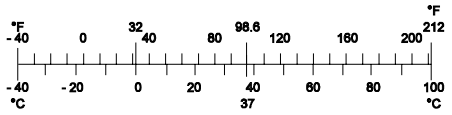

* SI is the symbol for the International System of Measurement

(4-7-94 jbp)

ACKNOWLEDGEMENTS

This project has spanned the course of over 23 years with thousands of hours of discussion, inspection, testing and analysis by people at ODOT, FHWA and the private sector. No one person can take credit for the entire project because so many people made major contributions. As the primary investigator and author of this report, I have the pleasure of acknowledging some of the people that have made great contributions to this project. From the Oregon Department of Transportation: John C. Jenkins, Jim Poore, Frank J. Nelson, Jim Sabel, Leslie Harkama, Steven Soltesz, and Alan Kirk. From the Oregon Graduate Institute of Science and Technology: Jack Devletian and Jinhong Yang. The Technical Review Committee: Warren Alexander, John Barsom, Dave McQuaid, Stan Rolfe, Bill Wood, Krishna Verma, and Bruce Johnson.

A FITNESS-FOR-PURPOSE EVALUATION OF ELECTRO-SLAG FLANGE BUTT WELDS

TABLE OF CONTENTS

LIST OF FIGURES

LIST OF TABLES

1.0 PURPOSE AND BACKGROUND OF FRACTURE ASSESSMENT

1.1 PURPOSE AND OBJECTIVES

This report summarizes the fracture assessment of the flange plate butt welds in the four 1030-foot box girders of the George Abernethy Bridge (West Linn Bridge) on the I-205 crossing of the Willamette River at West Linn, Oregon. This study was undertaken at the request of the Federal Highway Administration (FHWA), per FHWA Notice numbers N5040.23 dated 2/16/1977, N5040.29 dated 2/23/1977 and HNG-30 dated 6/21/1978. The purpose of this study was to satisfy the FHWA request and insure the safety and serviceability of this structure. The objectives were to quantify the fracture potential of the welds in question and assess their suitability for continued service. The end result of this work is to provide a recommendation on whether to leave the welds in service or to make repairs.

1.2 BACKGROUND

This study was focused around a particular type of welding process known as Electroslag Welding (ESW) that was commonly used in the joining of thick plates in bridges, buildings and marine vessels in the 1960's and early 1970's. The process was developed in Russia by B.E. Paton and was pursued in this country due to the economy realized on thick plate butt and T-welds (*Paton 1962*). Welding of thick plates, i.e., two inches and thicker, using conventional processes such as Submerged Arc and Shielded Metal Arc Welding, requires numerous weld passes and long welding times. The ESW process is more like a casting process and joins the plates in a single, high heat input pass.

Unfortunately, due to high production rates, poor quality control, poor quality assurance and poor welding practices in some fabrication facilities, a few bridges were put into service with fracture critical ESW that had poor toughness and weld defects. They were also difficult to inspect using Ultrasonic Testing (UT) due to the microstructure. This problem was brought to public attention with the failure of a box girder in Pennsylvania on an Interstate route near Pittsburgh in 1977. After this incident, a detailed investigation of other bridges with ESW was begun by Pense, Wood, and Fisher (*1981*). Information from this study was used by FHWA to restrict the use of ESW on fracture critical members as stated in Notice N5040.23 (see Appendix A, Exhibit 1). This notice also called for the evaluation of existing fracture critical ESW.

To emphasize the importance of these evaluations, FHWA put out a second notice, N5040.29 (see Appendix A, Exhibit 2). It authorizes the use of Federal-aid funds to perform the investigation. A fracture control plan for existing ESW fracture critical members was also

distributed as part of FHWA Memorandum HNG-30 (Appendix A, Exhibit 3; the fracture control plan details are not shown in this exhibit, however).

FHWA's position was that all fracture critical structures that have ESW must be either retrofitted or thoroughly analyzed and proven safe. A structure is fracture critical if it has no load path redundancy and any of its critical members experience a net tensile stress (combination of all design stresses). A fracture critical member of such a structure is a tension member or a member with tension components that would cause the structure to collapse if the member failed. Therefore, only the welds that experience tension under the combination of dead and live loads are affected by FHWA's position.

The fracture control plan utilized the concepts of fracture mechanics, which were only starting to make their way into the bridge engineering community at the time. Based on a review of the numerous discussions, memorandums and correspondence in the archived files for this bridge, it was evident that there was much discourse over the details and consequences of this plan. From the engineering side there was both concern and uncertainty as to how this plan would be executed. From the managerial side there was serious doubt that these concerns applied to ODOT structures. Nonetheless FHWA was persistent and ODOT proceeded with the study.

The essence of the fracture control plan was to quantify the stresses, defects, and toughness of the welds in question. With this information a safety factor with respect to failure by fracture was quantified and used in the decision of whether or not retrofitting was required.

In 1978 ODOT began the investigation with the Ultrasonic Testing (UT) and Radiographic Testing (RT) examination of six welds on the George Abernethy Bridge and some welds in the approach ramps of the Fremont Bridge over the Willamette River in Portland, Oregon. Three cores were trepanned from two compression welds and sent to a testing laboratory at the California Department of Transportation (Caltrans). The UT examinations performed on the bridge produced defect indications that were difficult to interpret. Some of the defect indications were extracted with the cores for material testing and upon sectioning were found to be a form of intergranular cracking. The material testing found a wide range of toughness as indicated by the Charpy V-Notch test. See Appendix B for the 1978 report. FHWA decided that more in-depth testing and analysis was required to determine whether the welds were acceptable. Otherwise, the welds would need to be retrofitted.

A second series of UT and RT inspections began in 1986 and continued until 1991. This effort inspected 11 welds and found no rejectable defects. Alternatives for full inspection, repair and partial inspection plans were presented.

In 1993 it was decided to perform the full investigation of these welds, as prescribed in the fracture control plan from FHWA. This would involve both full Non-Destructive Testing (NDT) of all 112 fracture critical welds, material testing and in-service strain measurements. In 1995 contracts were assembled to perform the material testing and NDT. In-service strain measurements were also made.

The second series of material testing was more extensive than the 1978 effort. The actual toughness of the base, weld metal, and heat affected zones (HAZ) were quantified with fracture

toughness testing as opposed to being qualified by impact testing. The material testing was divided into two phases. Phase I removed four cores to characterize the weld morphology and qualify the toughness. Based on results from Phase 1, Phase 2 of the testing quantified the toughness and crack growth characteristics of the base, weld, and HAZ material.

In 1996 weld, HAZ, and base metal cores were extracted from the compression flange welds in the B, C, and D girders of the George Abernethy Bridge for the second series of material testing. UT and Magnetic Particle Testing (MT) were performed on all 112 fracture critical welds as well as Phase 1 material testing. Between 1997 and 1998 Phase 2 material testing was performed. The final analysis of all testing (material, NDT, and structural) was performed and the report written and submitted to FHWA. In 2000 a committee of national experts in the fields of welding, NDT, and fracture mechanics reviewed the report and suggested retesting one of the crack growth test samples and performing a very close UT / RT examination on four of the welds with questionable UT defect indications. This work was performed and the results submitted to the committee in 2001. In January of 2002 the committee reconvened and approved the report.

After hundreds of hours of testing and research into the fitness-for-purpose of the electroslag welds on the George Abernethy Bridge, ODOT was able to convince FHWA that a rigorous inspection program could be implemented in lieu of retrofitting the welds in question. The analysis cost the tax payers less than $600,000 over the 23 years of the study and saved them more than $6,000,000 in retrofitting construction costs, not including the disruptions to vehicular traffic. Oregon is the only state to have completed this analysis option as opposed to retrofitting.

1.3 STRUCTURE DESCRIPTION

The George Abernethy Bridge was constructed in 1970. It carries six lanes of highway traffic, three in each direction, along a total length of 1687 ft. Each direction of traffic is supported by two, 1030 ft long, continuous box girders across three spans. The box girders are 5 feet wide and vary in depth from 12 to 21 feet. The continuous box girders were erected in 9 sections that were field spliced with bolted connections. Each section contains an average of eight ESW in the top and bottom flange plates; both flange plates and welds range in thickness from 2 to 3½ inches. The Bridge has an Average Daily Traffic (ADT) of 100,000 vehicles (both directions combined), with approximately 7% truck traffic. No recorded deficiencies had been recorded other than the welds in question.

Figure 1.1 shows the plan and elevation views of the overall structure. Figure 1.2 shows the ESW locations in each box girder. The fracture critical welds are circled. Figures 1.6 through 1.9 show details of the box girders. Figure 1.10 shows a typical cross section of a box girder.

Retrofitting of the ESW with splice plates was considered. The estimated cost of such an endeavor was 6.5 million dollars with considerable inconvenience to the flow of traffic on this bridge (see Appendix C).

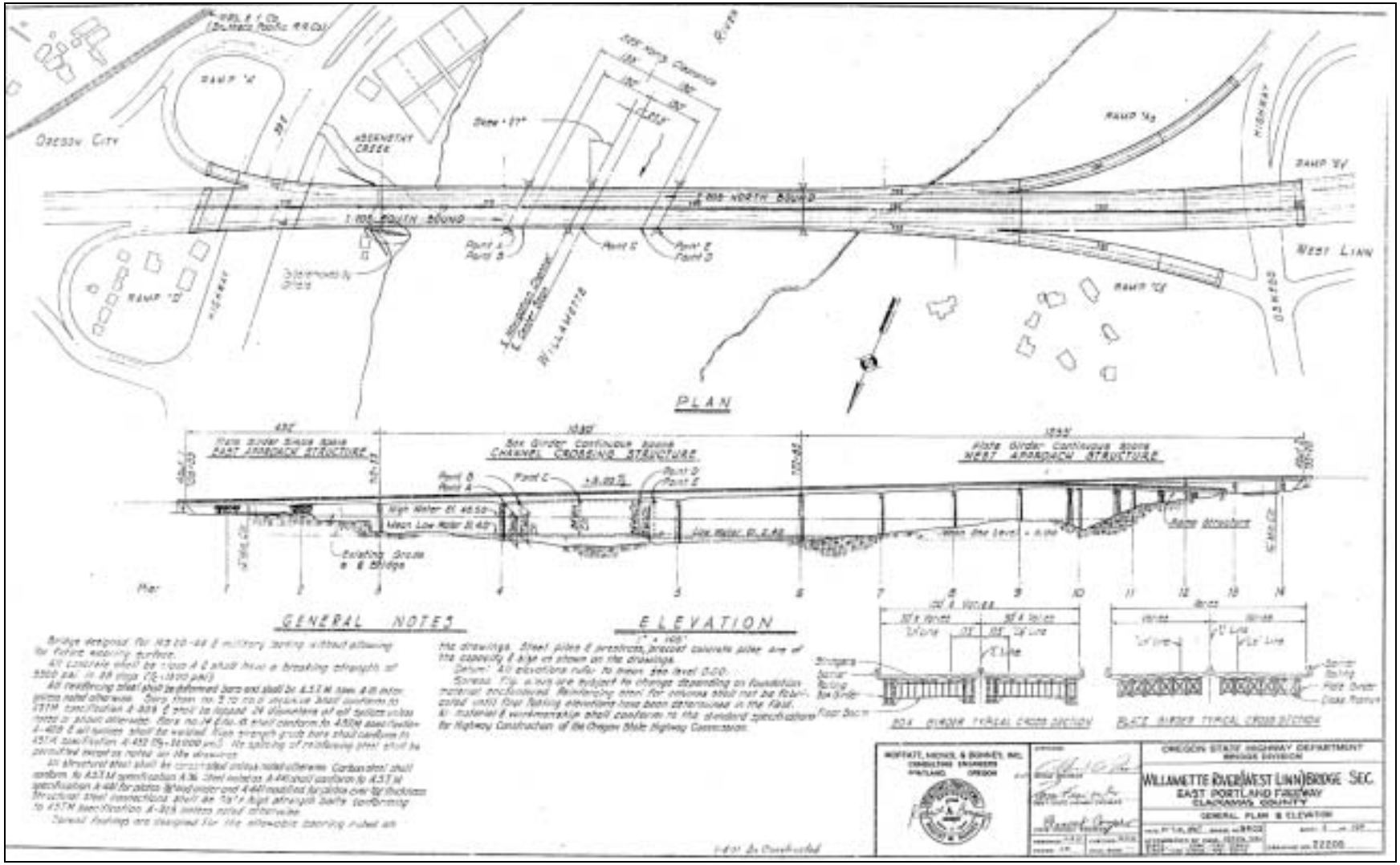

Figure 1.1: Plan and elevation of the George Abernethy bridge crossing the Willamette river at Oregon City – West Linn, Oregon

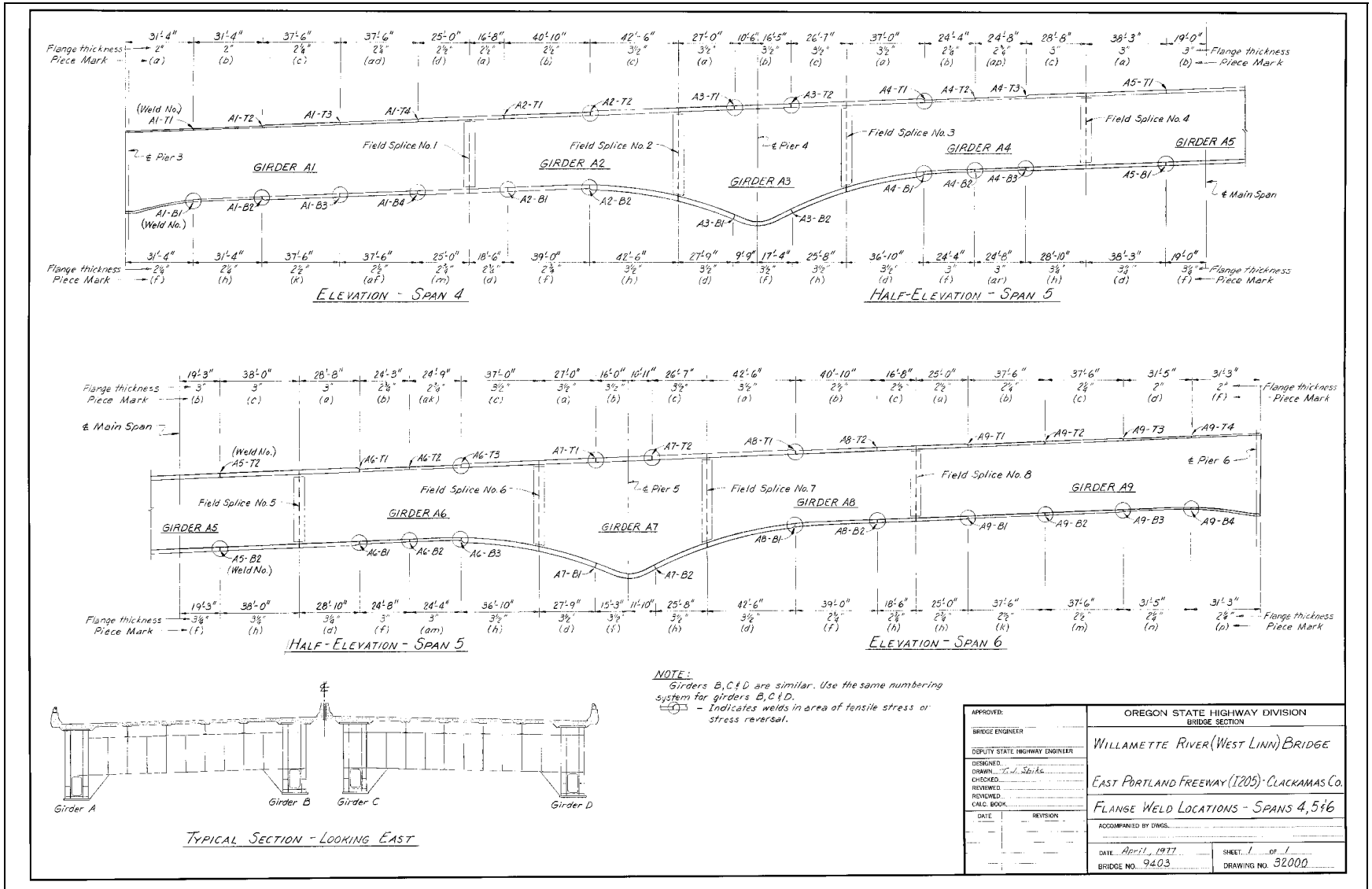

Figure 1.2: Electroslag weld locations in box girders

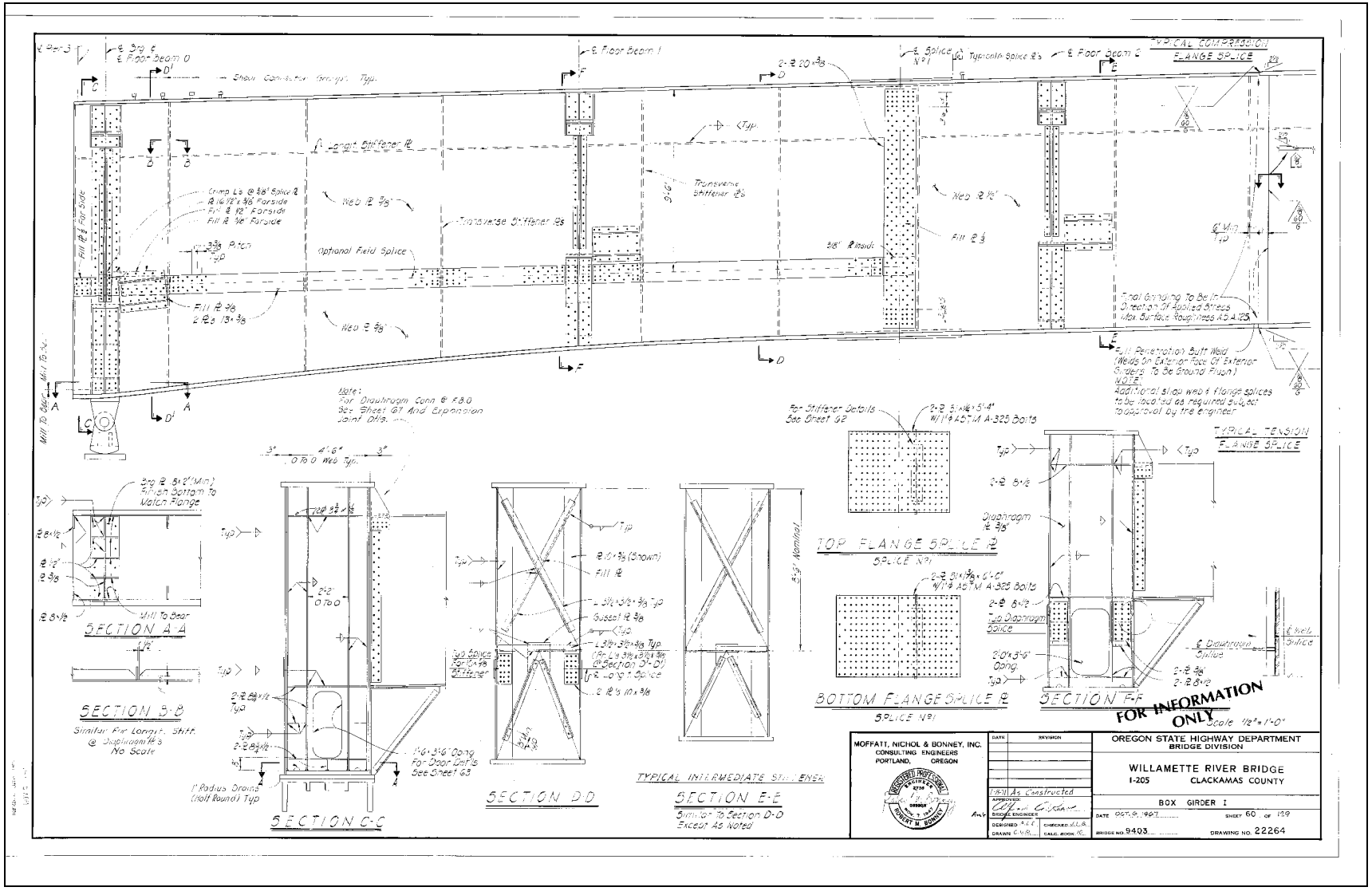

Figure 1.3: Details of box girders, Part I

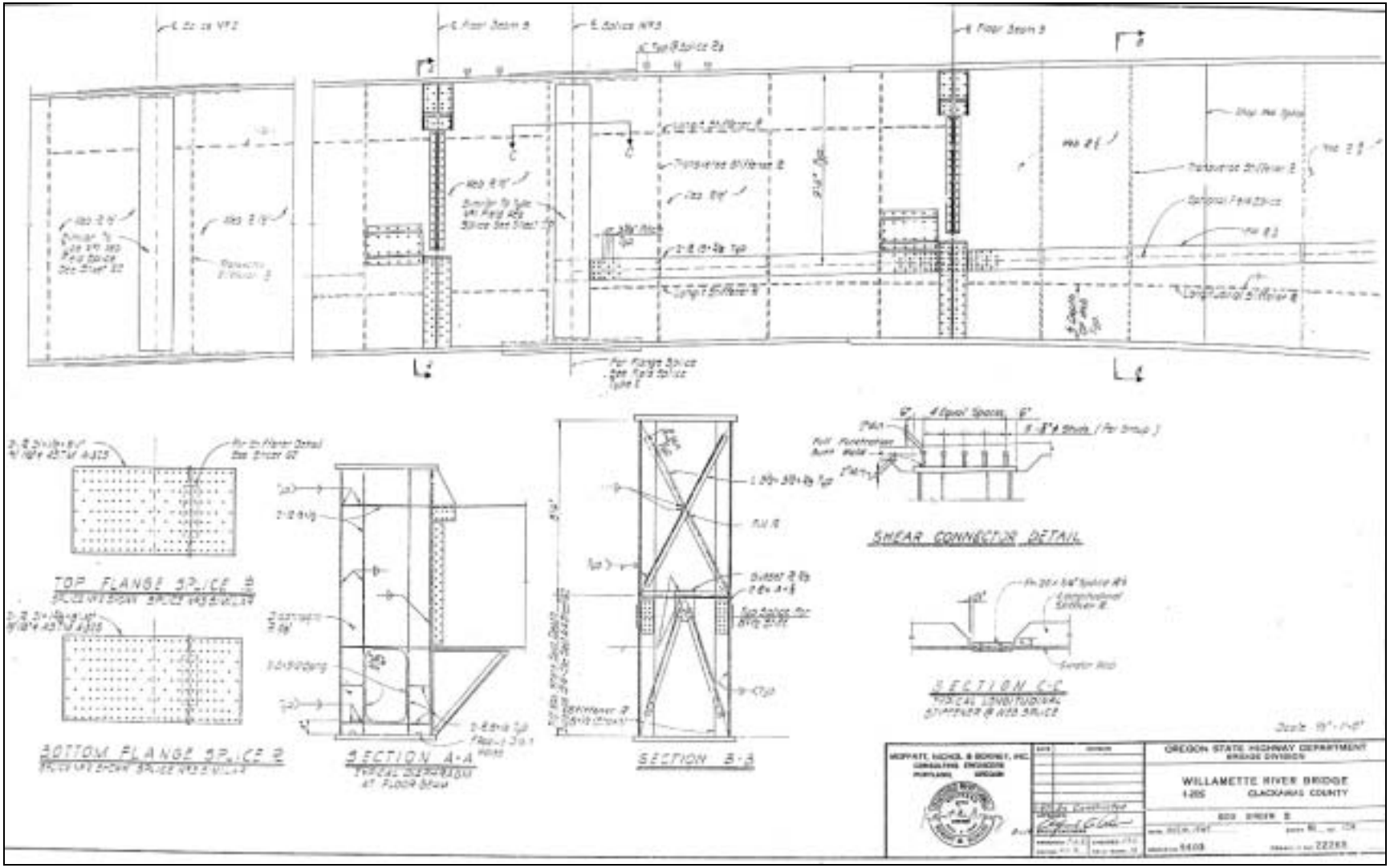

Figure 1.4: Details of box girder, Part II

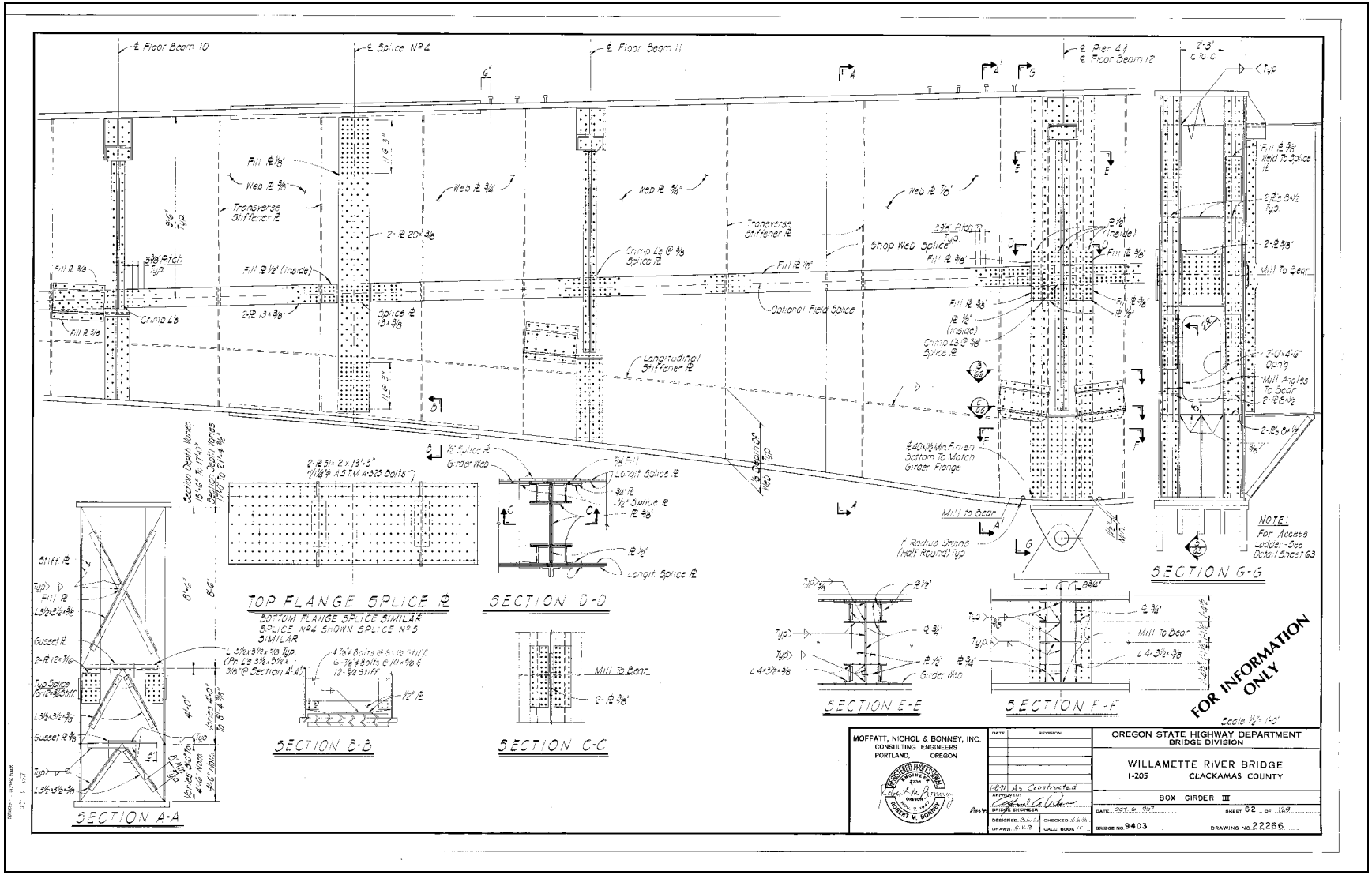

Figure 1.5: Details of box girder, Part III

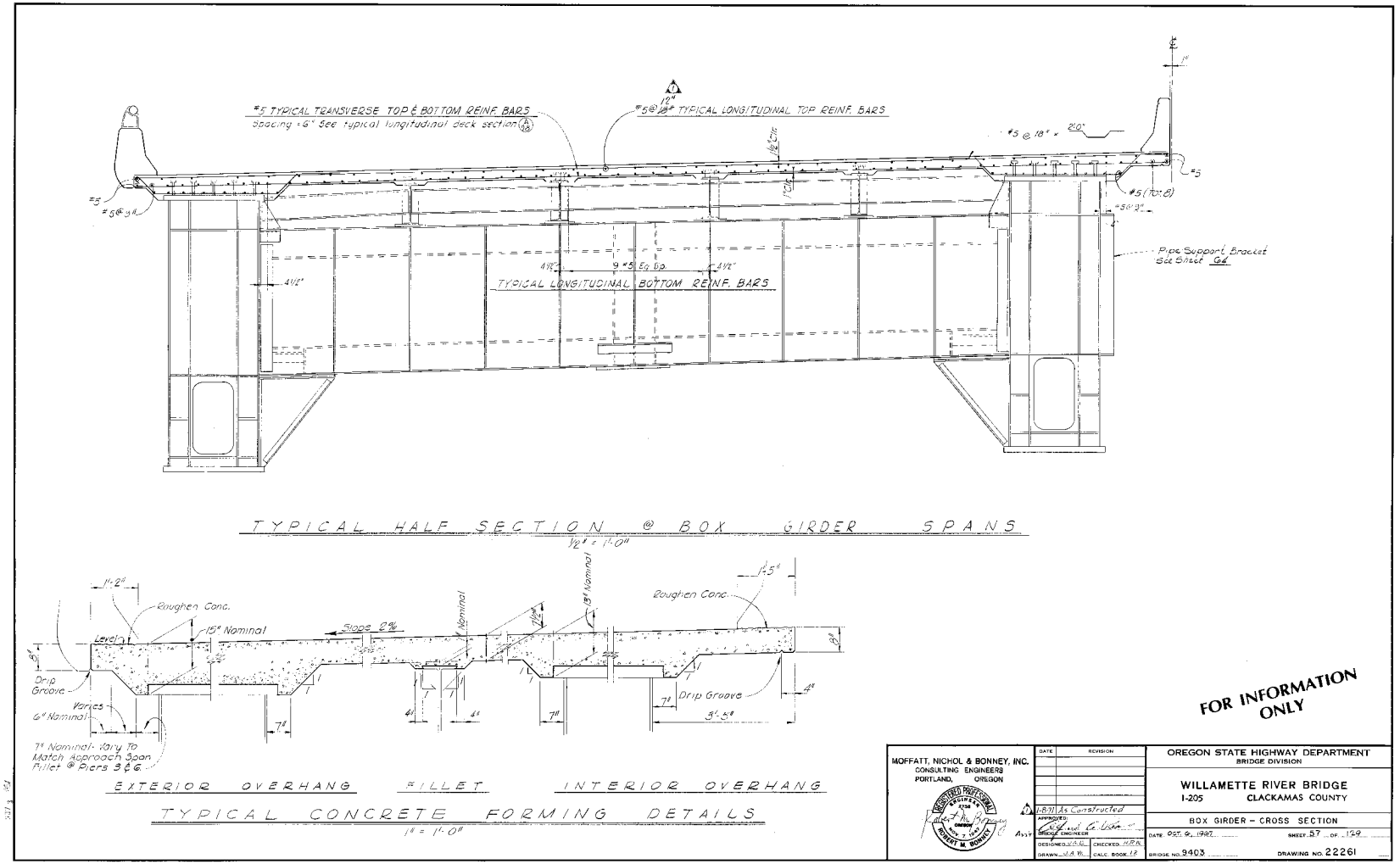

Figure 1.6: Cross section of box girder span

2.0 LOAD ANALYSIS

The function of the load analysis is to characterize the fracture potential and crack growth driving forces. For this analysis the maximum stress is required to calculate critical crack size, and the stress range from cyclic loading is needed to calculate fatigue crack growth. The maximum stress in the flange welds is a combination of dead load, live load, temperature induced load, possible seismic load and residual load from the fabrication process. The dead and live loads are reasonably easy to calculate and vary over the length of the girders in a smooth or gradual manner. Temperature induced load is similar. Fabrication induced loads, especially residual stresses from welding, pose a more difficult problem to quantify, and they typically have large magnitudes with steep spatial gradients.

This analysis looks at the loads and stresses in the box girder flange plates. The conclusion of this analysis shows that the dead load is the largest portion of structural loading and that the combination of live, thermal and seismic loads is nearly the same as the dead load. The total gross structural stress in any flange plate does not exceed 20.4 ksi. It is also shown that the flange butt welds have a compressive residual stress at the surface and a triaxial, tensile residual stress at the core of the welds. The magnitude of both of these regions is on the order of the yield stress of the weld metal.

2.1 DESIGN LOADS

The information described below is the author's interpretation of the design calculation books from Moffatt, Nichol and Bonney, Inc., the design engineers in the official record for this 1970 structure. These records are kept in the ODOT archives under Calculation Books 10 and 10A.

The steel box girders were designed for HS 20-44 and military loading. The design stress sheet for the box girders is shown in Figure 2.1. These loads apply to the superstructure as a whole and not to an individual box girder. Note that the dead load moments are many times larger than the live load moments, as is typical for long span structures. Design moments were based on a model that used the steel section properties for dead load and composite sections for live load. Inflection points for the dead load analysis were used for the composite section live load analysis. Negative moment regions were assumed to be cracked and did not include any contribution from the concrete deck.

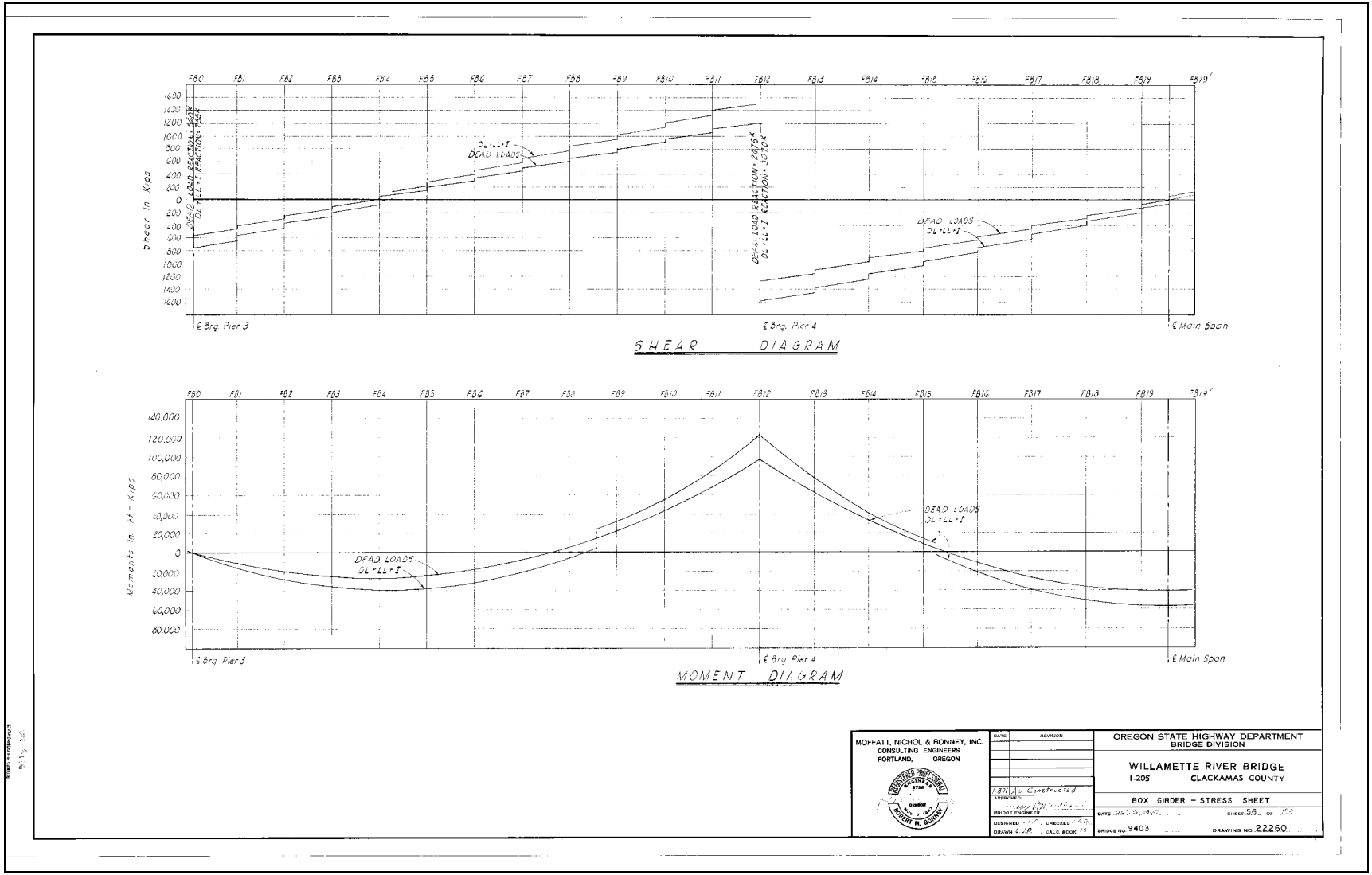

Figure 2.1: Design stress sheet for box girders

As part of the original design a finite element (FE) model was used to analyze the box girders. Taking advantage of symmetry, an edge and inner girder were each discretized into 20 elements over half their length (half of 1030 ft). In the model, floor beam elements connected the two girders. Both steel-only and composite sections were calculated. Eighty-seven inches of the 10-inch thick concrete deck were assumed to participate in the composite section of each girder. Torsional stiffness of the box girders was also quantified. Plate action from the concrete deck does not appear to be incorporated into the finite element model.

For the dead load, the stresses in the steel section were calculated assuming no composite action with the deck. Figure 2.2 shows the calculated bottom flange stresses due to dead load. Considering the top and bottom flange plates are nearly identical over the length of the girder, the neutral axis was assumed to be at mid-depth. Therefore the predicted top flange stresses are the same magnitude but opposite sign of the bottom flange stresses. The maximum dead load stresses are over the cantilever piers (4 and 5) with a magnitude of 9.3 ksi.

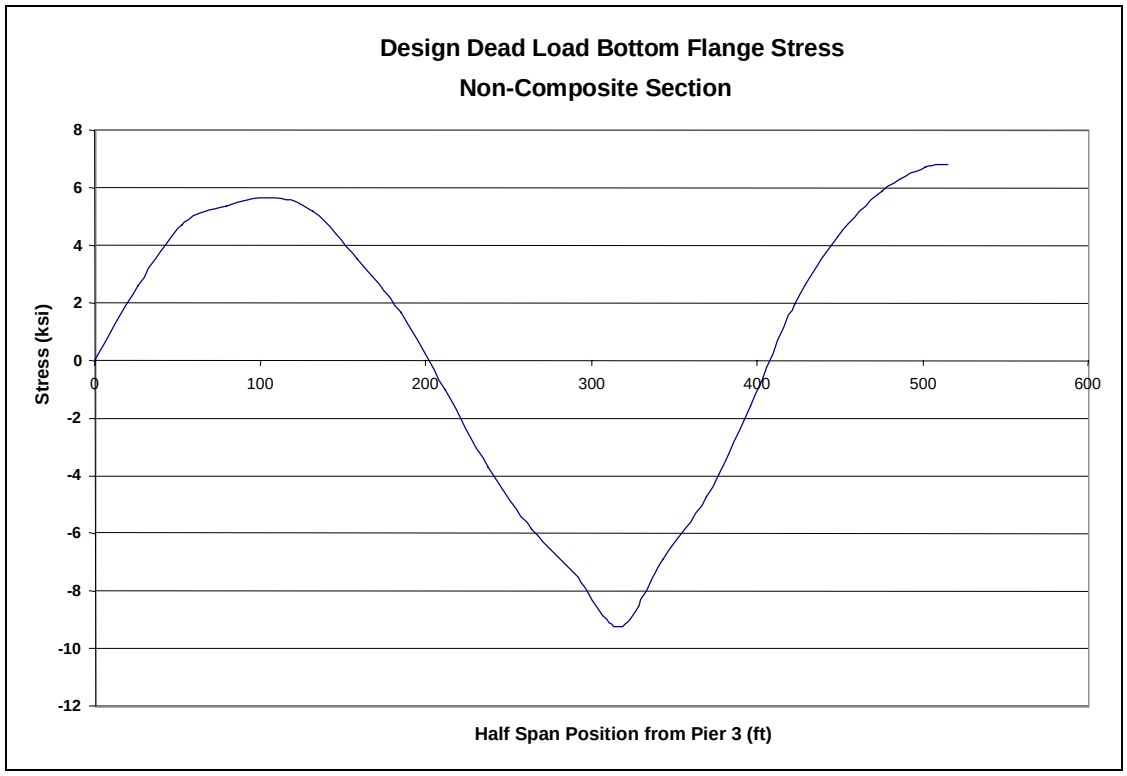

Figure 2.2: Calculated bottom flange stress from design dead loads

Using the inflection points from the non-composite section and dead loads, a live load model was developed using composite section properties in the positive moment regions. The negative moment regions were left non-composite. Uniform lane loading was applied over the entire model, and point loads were applied mid-span between piers 4 and 5. Figure 2.3 shows the resulting live load stress influence lines for the top and bottom flanges of the box girder. The maximum live load stress range is 2.8 ksi and occurs near $0.4L_1$ in the bottom flange of span 4

between piers 3 and 4. L_1 is the length of the end span in a three-span structure. Span 5 between piers 4 and 5 has a bottom flange stress range of 2.7 ksi and the stress in the top flange above the cantilever piers is 2.3 ksi.

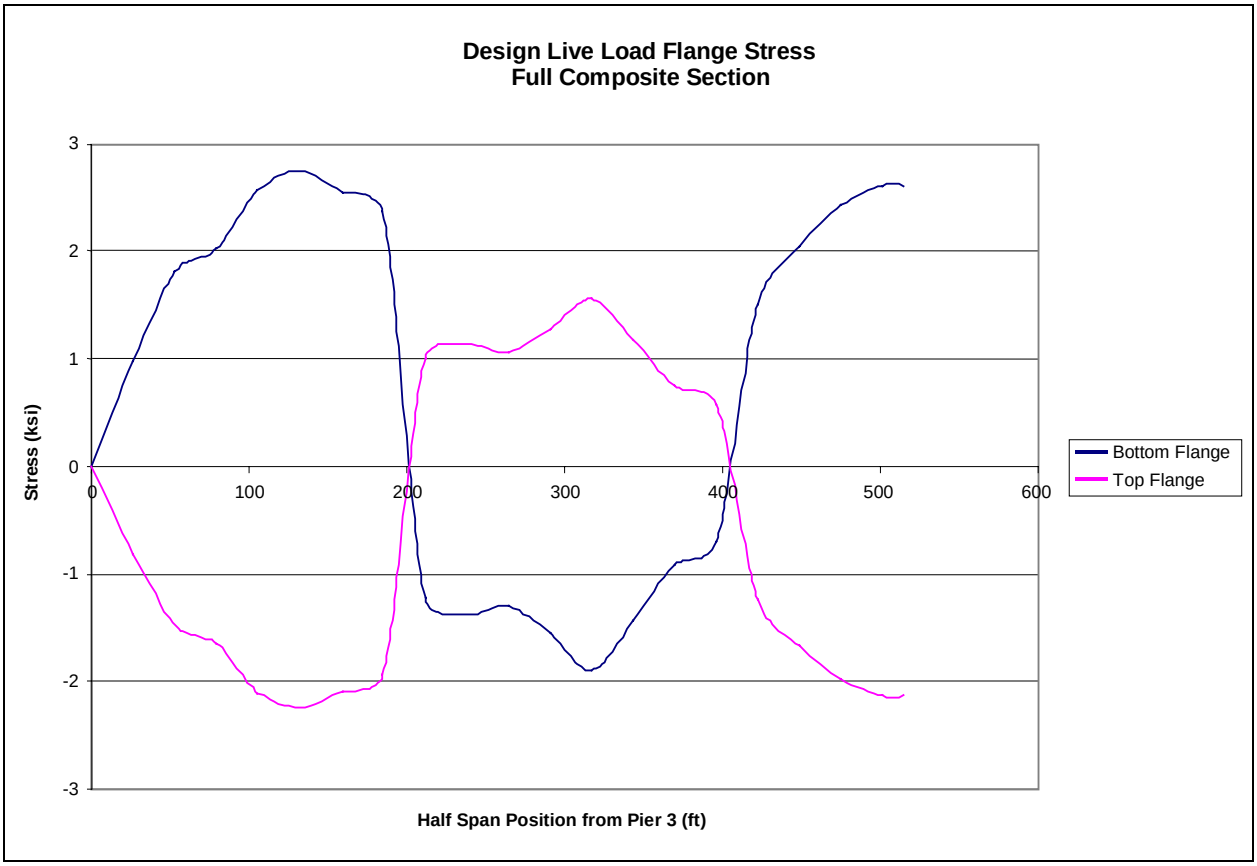

Figure 2.3: Calculated flange stresses from design live loads

Stresses due to concrete shrinkage in the deck were also calculated and shown to range from 0.5 ksi at mid-span between piers 4 and 5 to 4.2 ksi near the first floor beam of the span. These are compressive stresses.

To summarize the design dead and live load stresses in the box girders, dead load bending stress in the bottom flange ranged from –9.3 ksi (compression) to 6.8 ksi (tension). The top flange dead load bending stress ranged from –6.8 ksi to 9.3 ksi. The bottom flange live load stress ranged from –2.3ksi to 2.8 ksi. The top flange live load stress ranged from –2.1 to 2.3 ksi. The total maximum stress in any flange plate under design loads was 10 ksi.

2.2 STRAIN GAUGE TESTING OF LIVE LOAD STRESSES

2.2.1 Test description

In order to better characterize the live load spectrum, two of the four steel box girders were fitted with strain gauges. Uniaxial strain gauges were installed coincident with the longitudinal direction of the girder. The first location was inside the girder midway across span 4 on the upper surface of the bottom flange. This gauge is labeled GA1 and GB1 in girders A and B respectively in Figure 2.4. This location was subjected to positive bending and was near the theoretical position of maximum moment at $0.4L_1$.

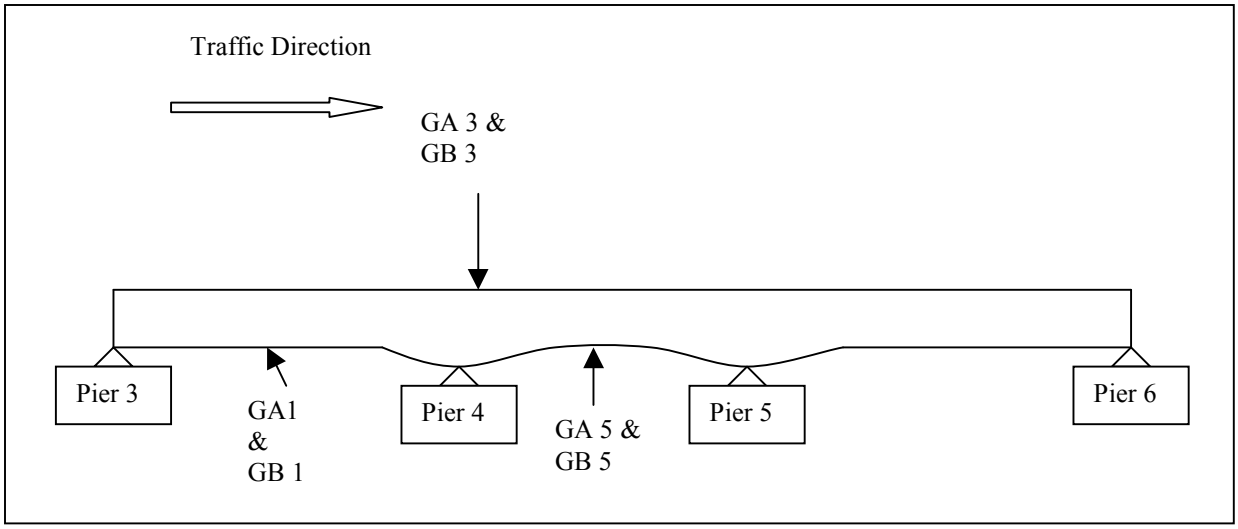

Figure 2.4: Location of strain gauges in A and B girders

The second location was on the underside of the top flange centered over Pier 4. This was the position of maximum negative bending moment. The gauges at this location are labeled GA3 and GB3 in Figure 2.4 for girders A and B respectively. The third gauge installation was midway across span 5, the navigation channel. This was a region of large positive bending moments. Gauges labeled GA5 and GB5 were mounted to the top surface of the bottom flange in girders A and B respectively. Figure 2.4 shows the gauge locations in elevation view.

Two forms of data collection were used. Stress cycle counting using the rainflow method was recorded at each gauge location (*Watson and Dabell 1975*). Burst time histories were also collected during peak stress cycles. Girder A was fitted with quarter Wheatstone bridge circuits and all gauges were read simultaneously. Burst time histories of strain at each location were recorded simultaneously once gauge GA1 had reached a critical level of strain. On the A/B girder structure traffic flows from span 4 to 5 to 6; thus gauge GA1 is the first to sense a live load. The precision of these strain measurements was on the order of ±10 microstrain. This

series of testing spanned continuously over a 30-day period in the early spring of 1999. Long-term thermal drift of the instrument zero was a challenging yet not insurmountable problem.

In Girder B a half Wheatstone bridge circuit was used with both gauges reading the same strain. This was done to improve the sensitivity of the data collection system. Due to this particular Wheatstone bridge configuration, long lead wires could not be tolerated; thus all gauges were read independently. The precision of these strain measurements was on the order of ±5 microstrain. This series of tests was conducted discontinuously over a four-month period in the winter of 1995-96. Since the length of each test was shorter in this series, thermal drift was not a significant problem.

Test data were collected at sample rates ranging from 10 to 100 Hz, using a fourth-order Butterworth low-pass filter with a 10 Hz cut off. Hysteresis of the Rainflow counting was set for 10 microstrain on the ¼ bridge transducers and 5 microstrain for the ½ bridge transducers. Quarter bridge installations used a three-wire configuration to account for lead wire resistance. Strain gauges were of ½-inch gauge length and 350-ohm resistance. Data collection was performed using a Somat 2100 field computer.

2.2.2 Results of Rainflow data collection

Girder A had the longest test duration at 30 days or approximately 720 hours. Figures 2.5- 2.7 show the histograms of the stress cycle counting gauges GA1, GA3 and GA5 respectively. The maximum stress cycles recorded were 2175 psi, 1305 psi and 1885 psi. The root-mean-cube (r.m.c.) effective stress ranges, $\Delta\sigma_{rmc}$, for these distributions were 465 psi, 435 psi and 452 psi.

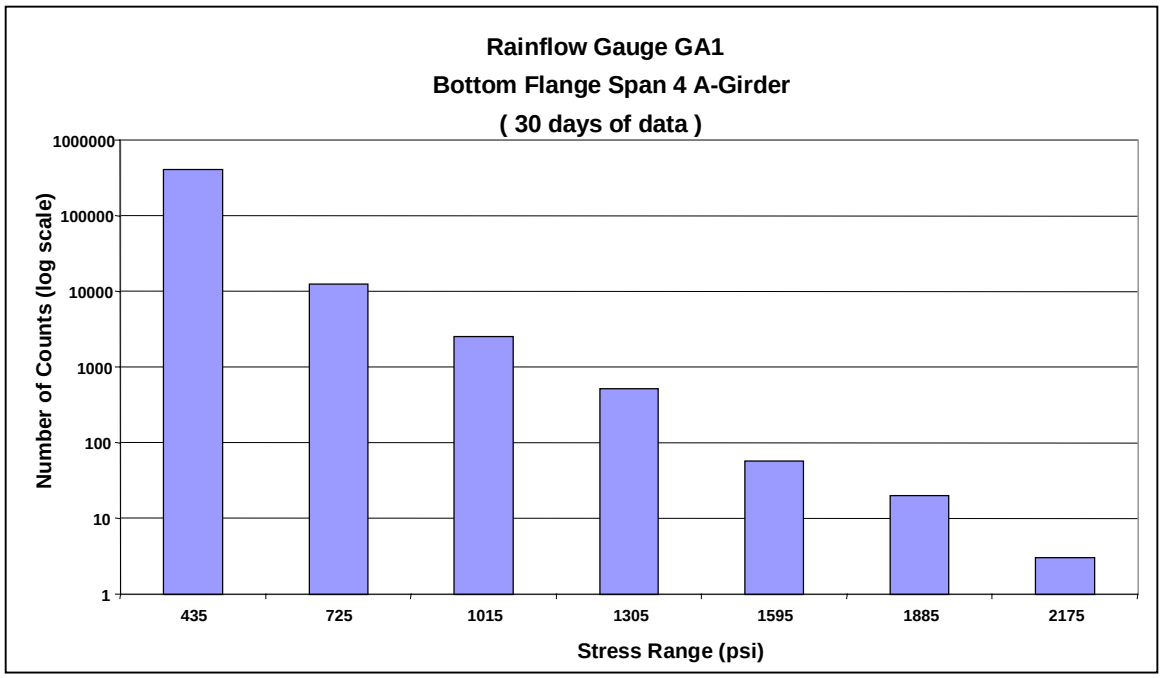

Figure 2.5: Rainflow histogram for gauge GA1

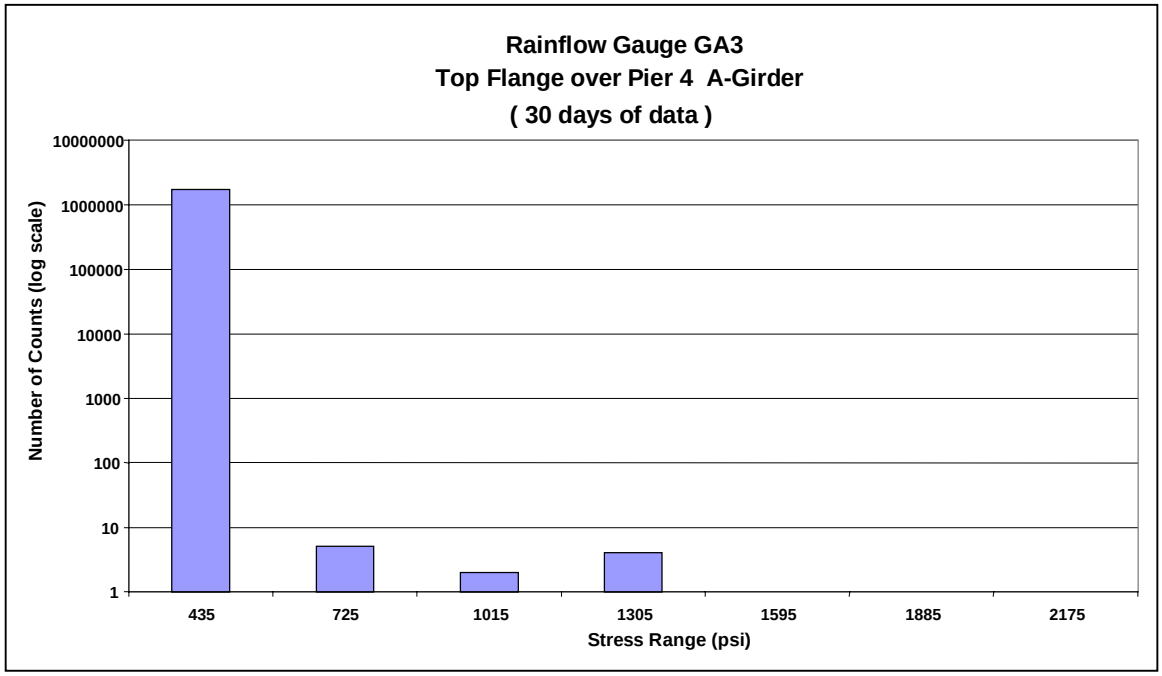

Figure 2.6: Rainflow histogram for gauge GA3

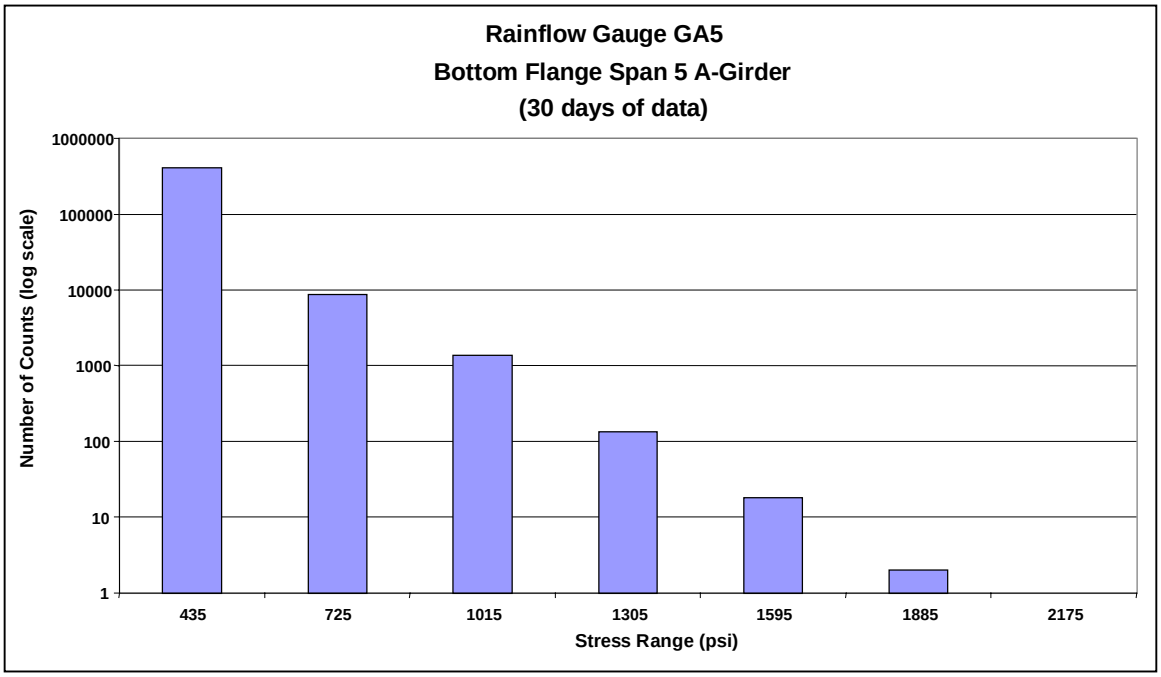

Figure 2.7: Rainflow histogram for gauge GA5

The effective stress range for these distributions was greatly influenced by the large number of low stress cycles from lighter vehicles. If only stress cycles with magnitudes above 500 psi are counted, then the effective stress range increases to 831 psi, 1054 psi and 795 psi respectively. These could be considered the r.m.c. stress ranges for truck traffic. Both of the mid-span positive moment locations showed higher stress ranges than did the negative moment location over pier 4. As expected, the pier 4 location showed a much higher number of measurable cycles, since trucks on spans 4, 5 and 6 could cause load changes in these flange plates.

Girder B had test lengths ranging form 94 to 169 hours. Figures 2.8 - 2.10 show the histograms of the stress cycle counting for gauges GB1, GB3 and GB5 respectively. The maximum stress cycles recorded were 1812 psi, 1233 psi and 1812 psi for GB1, GB3 and GB5 respectively. The $\Delta\sigma_{rmc}$ for these distributions were 694 psi, 577 psi and 689 psi. If only stress cycles with a magnitude greater than 500 psi are counted the effective stress ranges become 764 psi, 835 psi and 1060 psi. These data are summarized in Table 2.1.

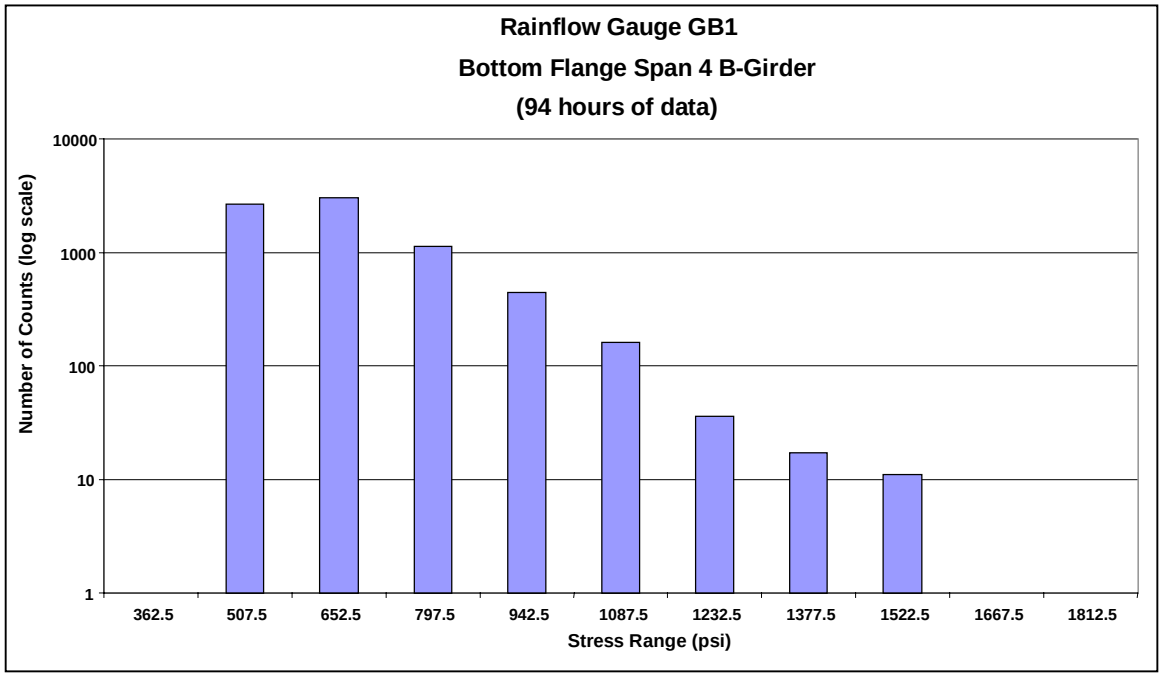

Figure 2.8: Rainflow histogram from gauge GB1

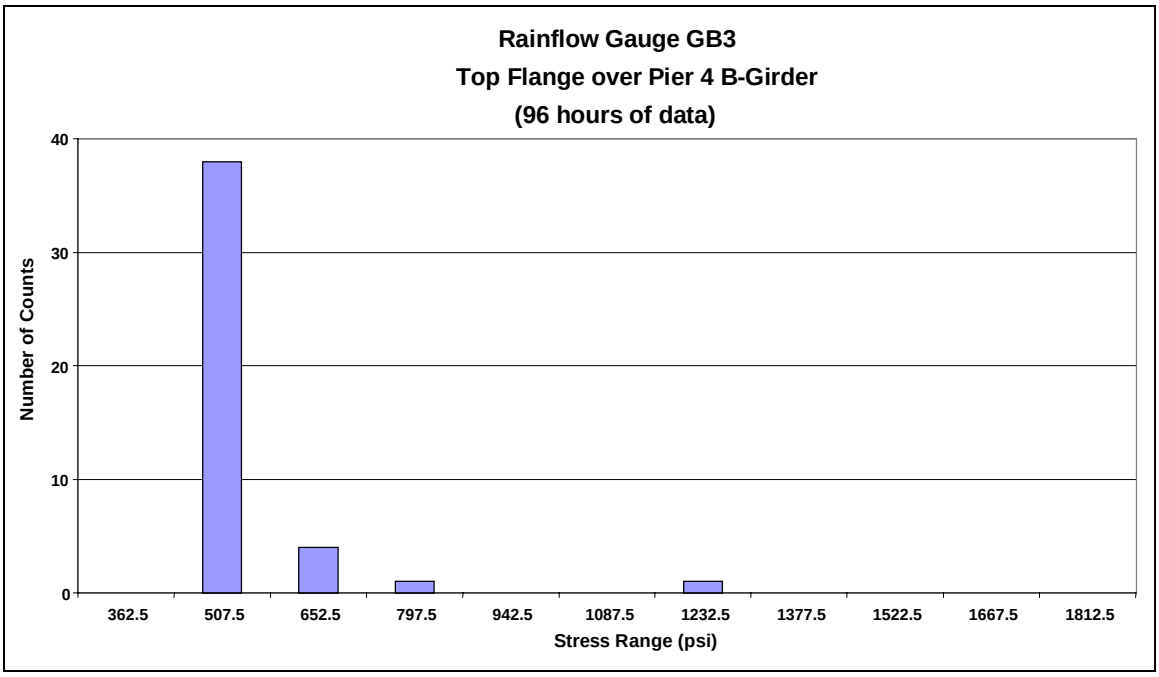

Figure 2.9: Rainflow histogram from gauge GB3

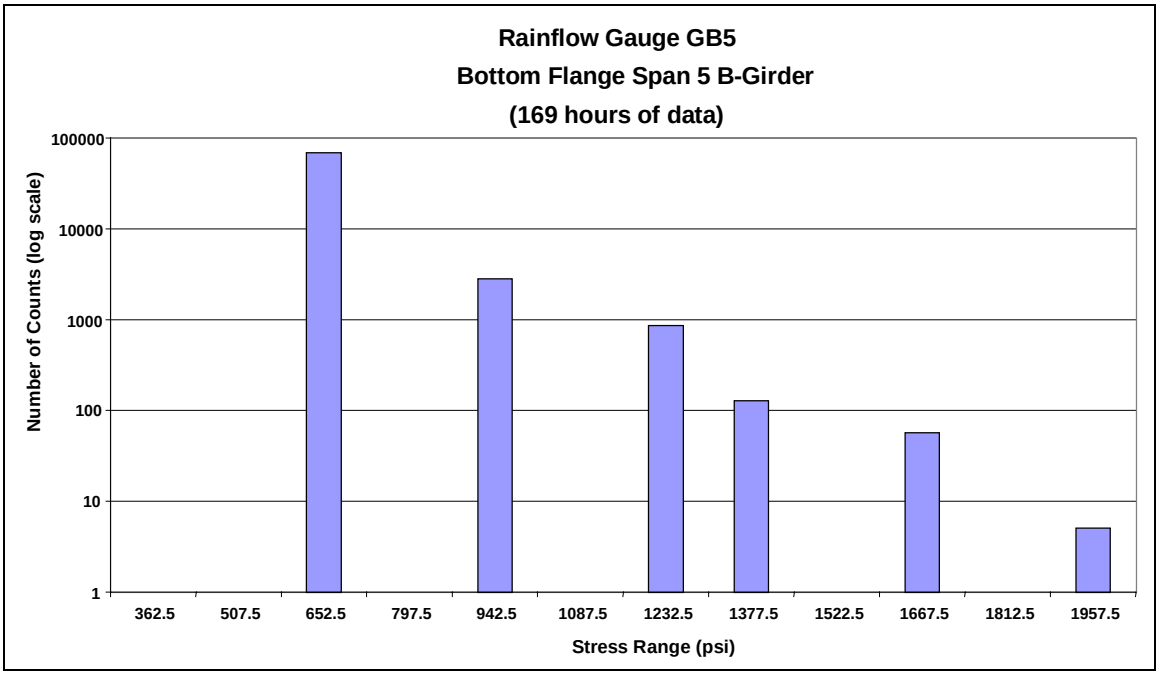

Figure 2.10: Rainflow histogram from gauge GB5

Table 2.1: Summary of load histories

Gauge I.D.	Gauge Location	Test duration (hours)	$\Delta\sigma_{max}$ (psi)	Total Distribution		Truck Distribution	
				$\Delta\sigma_{rmc}$ (psi)	# of counts, N	$\Delta\sigma_{rmc}$ (psi)	# of counts, N
GA1	Bottom Flange Span 4 @ 0.5L A-girder	720	2175	465	422,887	831	15,733
GA3	Top Flange Over Pier 4 A-girder	720	1305	435	1,714,115	1054	11
GA5	Bottom Flange Span 5 @ 0.5L A-girder	720	1885	425	422,699	795	10,200
GB1	Bottom Flange Span 4 @ 0.5L B-girder	94	1812	694	7,749	764	4,804
GB3	Top Flange Over Pier 4 B-girder	96	1233	577	44	835	6
GB5	Bottom Flange Span 4 @ 0.5L B-girder	169	1812	689	72,179	1060	3,876

2.2.3 Results of time history strain collection

Since the strain recording was performed inside the box girders over a long period of time it was not practical to correlate specific vehicles or loading conditions with specific strain time histories. By reviewing the many time histories recorded it was fairly easy to find what appeared to be single truck passing. Figure 2.11 shows the strain burst histories of the three gauges installed in girder A for typical legal weight trucks. Figure 2.12 shows a similar response with what appears to be two heavy trucks, one after the other. The actual time axis has been compressed and is thus of only qualitative significance. These strain response graphs both show that the positive bending moments regions in spans 4, 5 and hence 6, are significantly greater than the negative bending moment region over pier 4, and hence 5. The sensitivity of these measurements is more than adequate for the long-term rainflow cycle counting but is marginal for exacting analysis of the structural response to specific loads. Fortunately the strain ranges measured are of very low magnitude, and a precise analysis of live load behavior is not necessary.

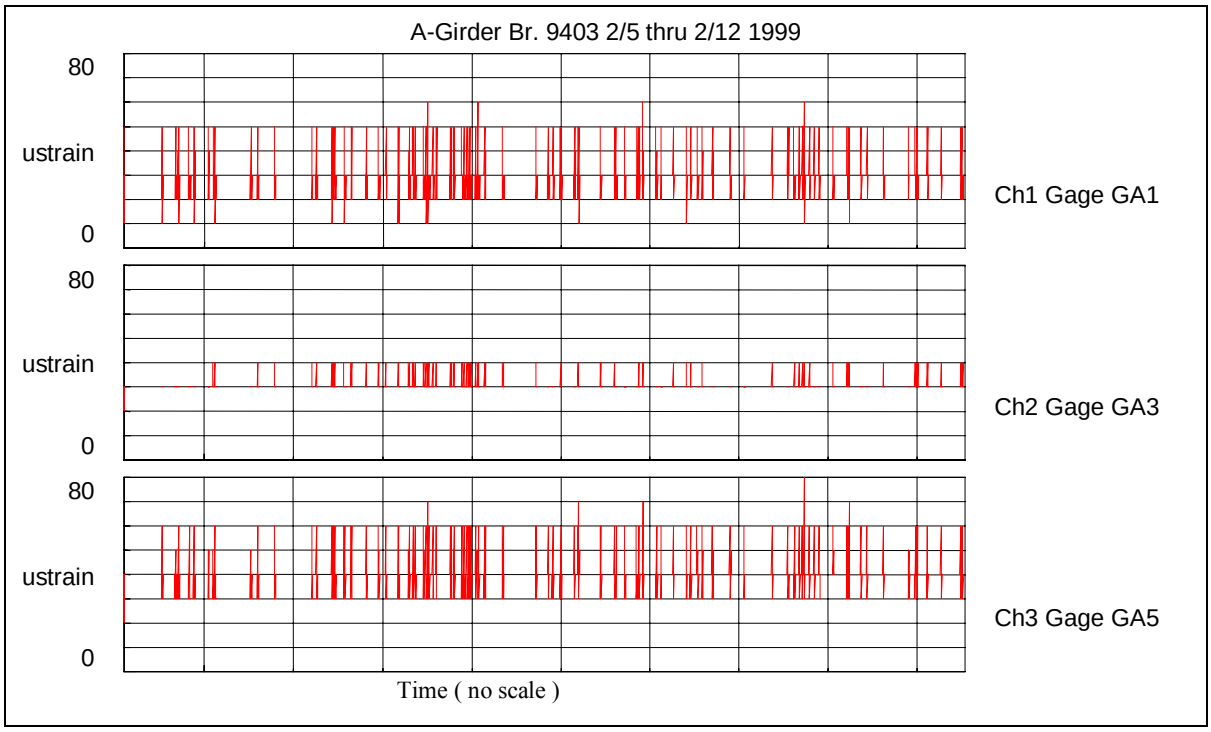

Figure 2.11: Collective Strain – Burst histories of live load on box girder A over a 7-day period

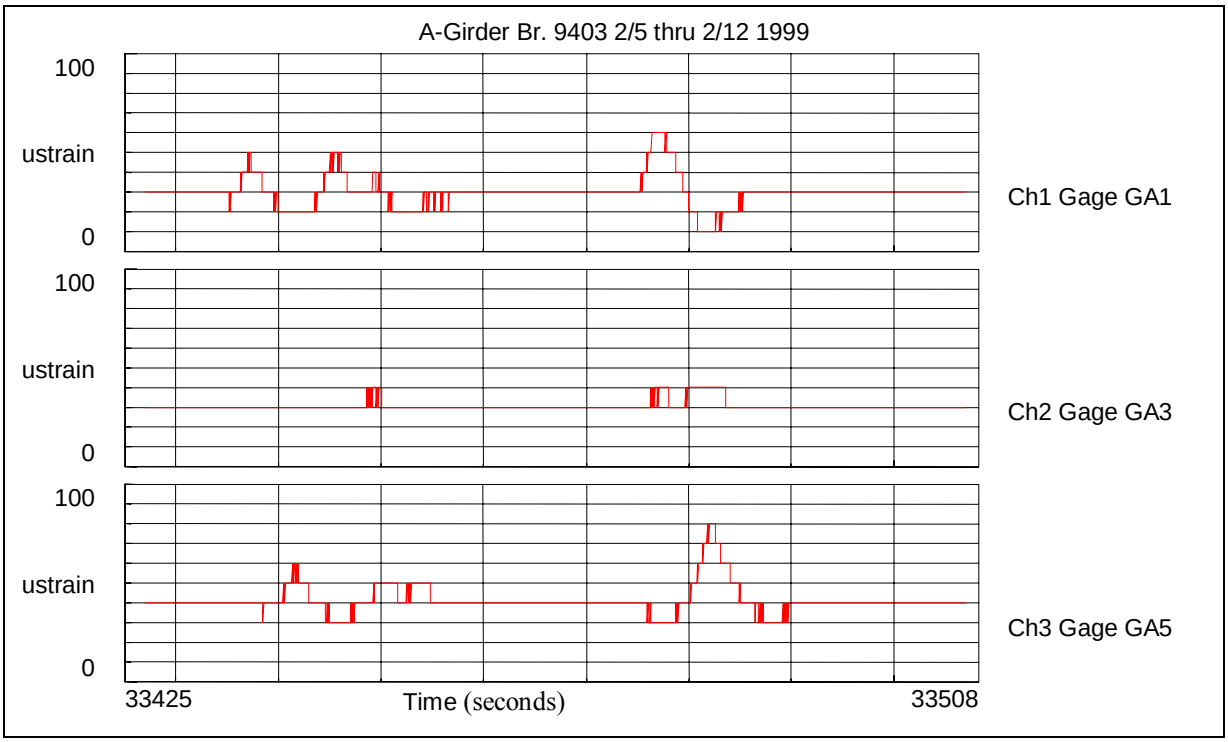

Figure 2.12: Individual Strain – Burst history from girder A

2.2.4 Summary of Strain Gauge Testing of Live Load on Box Girders

Both A and B girders were instrumented with strain gauges to quantify the live load strain spectrum at three critical locations in the three span continuos box girders. Rainflow strain cycle counting was used to quantify the spectrum, and strain time histories were recorded to verify the spectrum responses. Tension flange strain ranges measured were very low when compared to design strains/stresses. The maximum stress ranges measured over a one-month period are less then 2200 psi, with the r.m.c. stress ranges less than 1100 psi for truck traffic and near 500 psi for all traffic measured.

2.3 THERMAL STRESSES IN BOX GIRDERS

2.3.1 Temperatures measured inside box girder

It is likely the most significant temperature differential induced stresses in the box girder sections come from direct radiation heating from the sun. The D-girder is most strongly affected by this differential heating. The upstream web of this girder receives the most direct sunlight exposure, especially during the summer months. The downstream web is completely shaded and typically 30º to 40º F cooler than the upstream web. The air temperature in the D-girder also changes significantly during the summer, with daily temperature changes of 10º to 15º F being common. Table 2.2 shows the temperatures measured in the D-girder on a typical late summer or early fall day.

Table 2.2: Temperature (º F) in girder D on 10/9/96. Weather: sunny; highs in the low 80's.

	9:40 am	10:50 am	11:25 am	11:50 am	12:25 pm	4:30 pm
Upstream web (inside surface)	78	93	102	103	106	110
Downstream web (inside surface)	62	65	70	69	72	78
Bottom Flange 14 inches from downstream web	60	62	66	66	66	N/A
Inside air temperature	70	73	75	79	N/A	N/A

2.3.2 Flange stresses from thermal gradients

The original design calculations for the box girders (ODOT calculation books 10 and 10A) make no reference to thermal stress analysis. From experience and measurements inside the D-girder, the upstream web plate changes temperature rapidly relative to the flange and downstream web plate. As the upstream web plate increases in temperature, it is resisted by the top and bottom flange plates that are slower to heat. This action would put the upstream web plate in compression along the longitudinal direction of the girder. The flange plates will then experience a combination of tension along the longitudinal direction and in-plane bending about an axis normal to the surface of the flange plate. The bending stress gradient is such that the maximum tension from bending is on the hot side of the girder.

An attempt to quantity thermal stresses was made using finite element analysis (FEA). Figure 2.13 shows the mesh of a thermal stress model of a section of box girder. One web plate was given an increasing thermal load while the other was held at constant temperature. The flange plates were also held at the same temperature as the cooler web plate. As the heated web plate increased in temperature, internal forces shift and the flanges were put into in-plane bending due to the difference in thermal strain in the webs. Longitudinal stiffeners were added to prevent buckling of the web plates, which would manifest itself as a numerical instability in the FEA model. The stiffeners incorporated into the model supplied slightly more stiffness than those in the real girders. This error, though necessary for numerical stability, yielded conservative results due to the extra section that imparted larger thermal loads into the flanges. Based on the measured temperature data, a temperature gradient between opposite web plates of less then 50º F was typical for a sunny summer day.

Figure 2.13: End view of finite element model used to estimate thermal stresses in flange of box girders

The resulting stress gradient in the top and bottom flange plate is shown in Figure 2.14. At a temperature differential of 50º F the maximum in-plane bending stress was 4,800 psi. Thermal stress cycles such as those discussed above would have a frequency of occurrence on the order of 100 cycles per year, since the majority of days in this location have mild temperatures in the range of 50º to 60º F, with partial to full overcast skies.

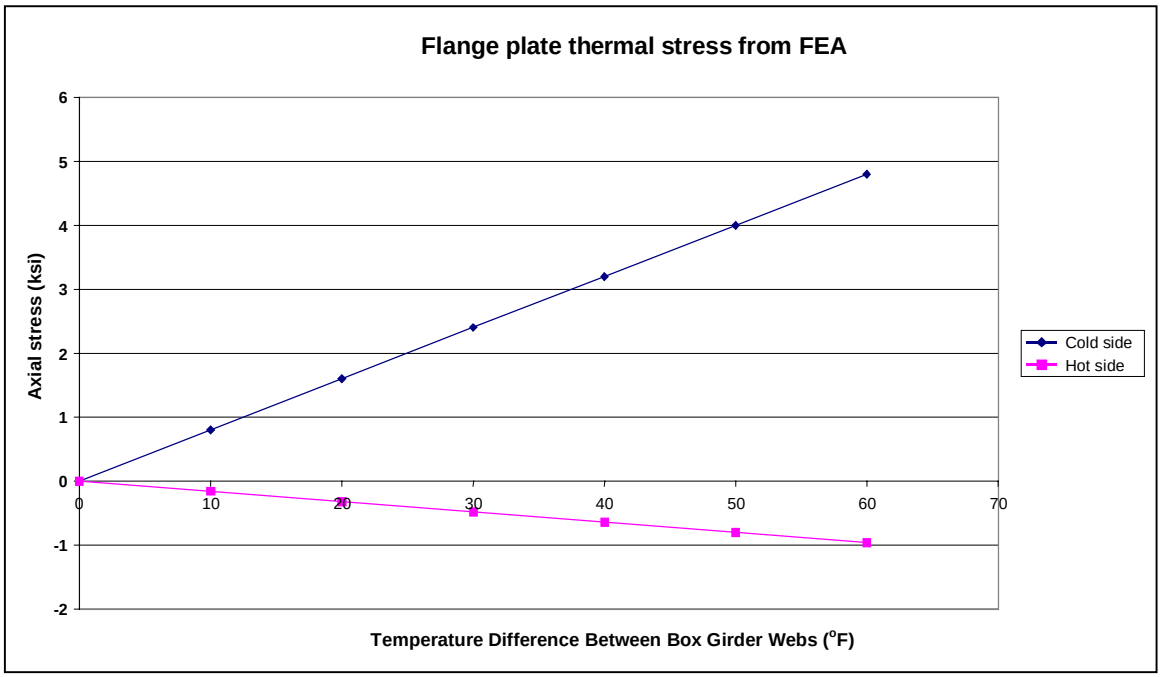

Figure 2.14: Calculated thermal stress in flange plates (in-plane bending)

2.4 SEISMIC LOADING

A seismic analysis was performed on the box girders as part of the 1999 Seismic Retrofit project on the structure (*ODOT 1999*). All flange stresses from the assumed seismic loading were less than 4.5 ksi.

2.5 RESIDUAL STRESS ANALYSIS OF FLANGE PLATES

The flange plates in these large box girders are very much three-dimensional when viewed from a macro perspective. Thicknesses range from 2 to 3½ inches in both top and bottom flanges with 192 butt welds. Refer to Chapter 1 for a structural description. In addition to the dead, live and thermal loads, stresses in the flange plates and welds include internal and external residual stresses from fabrication operations. The external source is from welded attachments, specifically the webs. The internal sources of residual stresses come from the rolling of the steel plate from a cast ingot and the thermal and shrinkage stresses from the butt welds.

Of these sources of residual stress in the flange plates, the butt welds have the largest magnitude over the greatest depth into the plates. Rolling stresses are also significant but of limited depth, especially in the thicker plates. The stresses imparted by the welding of the web to the flange are large in magnitude but limited in depth when compared to the butt welds, and they are generally orthogonal to the direction of main focus – the longitudinal direction of the girder.

The internal residual stresses from the butt welds are of large magnitude and have very steep spatial gradients, especially in the plane of the thickness and longitudinal direction of the girder. The ESW is made in what can be thought of as a continuous casting process, where the casting is joining the two plates being welded. Figure 2.15 depicts an ESW weld in plan and section elevation views. This welding process basically pours a casting into the gap between the ends of the plates to be welded. The outer surface of the gap is faced off with a pair of water cooled copper shoes.

The weld region cools from the outside in as heat is conducted through the plates and copper shoes. As the weld metal and melted base metal cool, a solidified shell forms around the core of the weld. The solidification front moves progressively towards the core until all metal returns to a solid phase. The liquid to solid phase transformation is accompanied by a change in density and a change in shear strength. The solid becomes more dense and develops the ability to resist shear deformation, i.e., flow of material. As this cooling progresses the cooled outer shell develops compressive stresses as the core increases in density and pulls on the outer shell. The inner core ends up in triaxial tension.

This description of the development of these stresses is quite well known both from a qualitative and quantitative perspective. Analytical and experimental research have shown these stresses to exist as such and with magnitudes on the order of the yield stress of the steel (*Ferrill, et al. 1966; Ruud, et al. 1981; Ruud, et al. 1993*).

Rolling stresses can also reach these magnitudes but generally form a compressive stress in the surface or x-y plane that diminish rapidly in the thickness or z direction. These intense yet thin compressive layers – top and bottom – are balanced by a low magnitude tensile field over the majority of the thickness.

Because the ESW process is of such high heat input and slow cooling rate, much of the rolling stresses in the vicinity of the welds are both annealed from the temperature time history and dominated by the introduction of welding stresses. Thus a strong case can be made to not have to consider the interaction of these residual stresses and focus on the dominant welding-induced residual stresses.

2.5.1 Experimental verification of residual stresses

Accurately quantifying the internal stress distribution for the welds on this structure, though not impossible, is a difficult and time-consuming problem. As shown in the cited references, the stresses are intense in magnitude and spatial gradients. An effort was made to verify the general conclusions drawn about the stress field in the flange plates. Two types of measurements were made for this purpose.

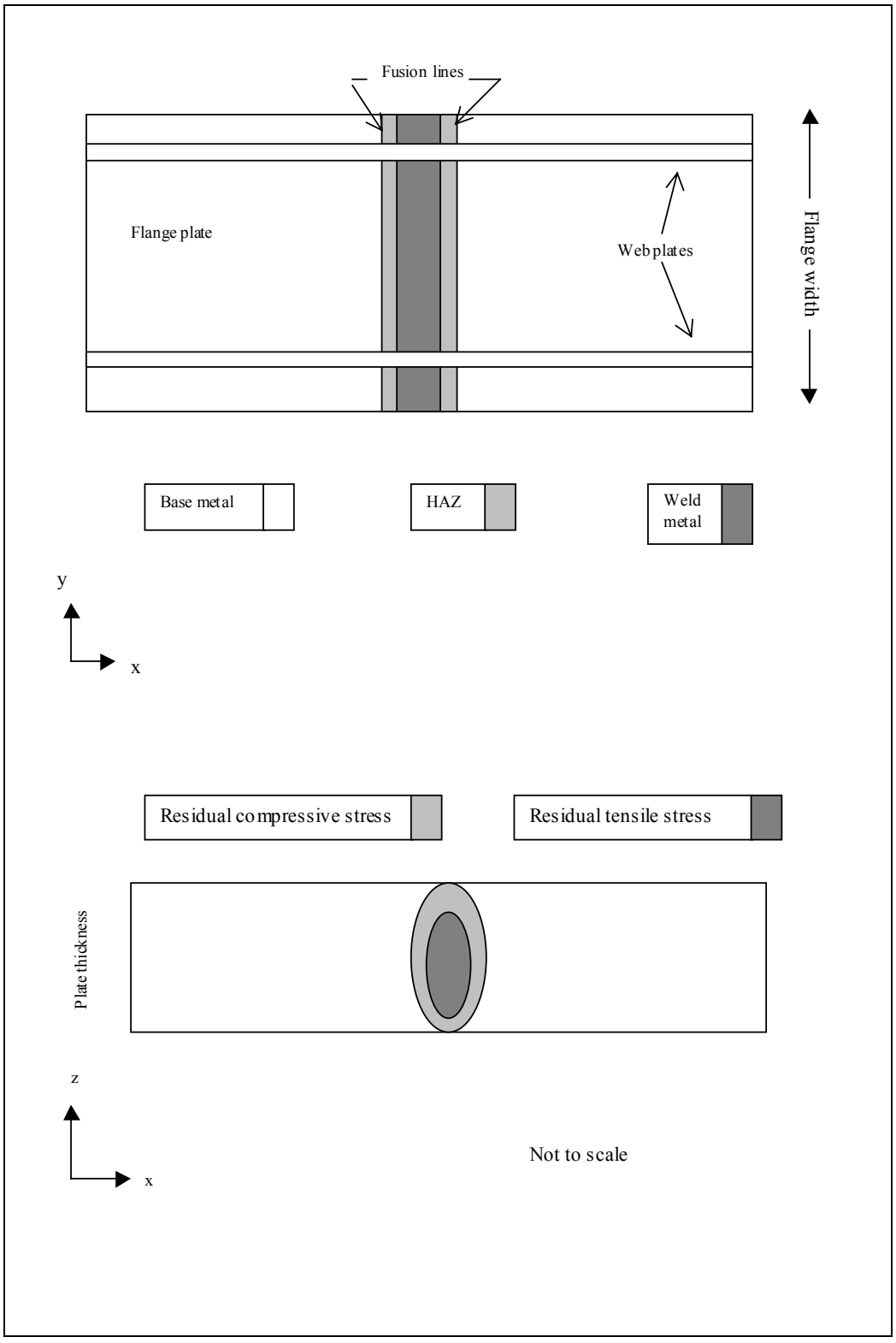

Figure 2.15: Plan and elevation view of the Electroslag butt welded flanges. Metallurgical and stress field regions are shown qualitatively

The first measurement was coupled to the weld and base metal core extractions for the material testing program. Through-thickness cores of 3 ¾ inch diameter were extracted from compression flanges in the B, C and D girders. These cores were centered over base, HAZ and all weld metal regions. Biaxial strain gages were attached to the top face (top surface of bottom flange) of the core. The gauges were lined up with the longitudinal and lateral directions of the flange. The gauges were read before and after the trepanning operation.

As the core is removed from the flange plate the stresses acting on the circumference of the core are relieved, and the core will undergo a change in shape. The gauges measure this change and provide a rough estimate of the stresses acting in the plate prior to removal. Table 2.3 summarizes the results. The data indicate that in the longitudinal direction (x) of the plate there is a compressive strain on the order of 1000 με and a tensile strain in the lateral direction (y) of the same magnitude, equivalent to a stress of 29,000 psi. Only two base metal cores were removed, so little can be inferred from these data other than there appears to be compressive surface stresses present.

Table 2.3: Residual stress estimates from core removal strain measurements. All cores 3½ inch in diameter and 3½ inch thick.

Core Location	Metal Type	Design Dead Load Stress in x-Direction (ksi)*	Estimated Stress Prior to Removal (ksi)	
			x-Direction	y-Direction
D3B2	Weld center	-14.0	-26.7	+20.6
B3B1	Weld center	-14.0	-23.2	> +29.5
C7B2	Weld center	-14.0	-33.1	+18.0
D7B1	HAZ	-14.0	-26.7	+20.6
D3B2	HAZ	-14.0	-26.7	+26.7
D3B1	HAZ	-14.0	-14.8	+31.0
B3B2	HAZ	-14.0	-27.8	> +29.5
B7B1	HAZ	-14.0	-25.5	+19.4
B7B2	HAZ	-14.0	-20.6	+25.5
C7B1	HAZ	-14.0	-33.0	+18.0
D3B1+8	Base metal	-13.5	-22.0	+0.3
B1+4**	Base metal	+0.2	-4.6	-12.5

*+ = tension; – = compression ** 2 inch thick core

The above measure is in a way the inverse of the hole-drilling method as defined by ASTM E837, which was also performed on a flange butt weld. A total of seven locations were instrumented and tested. The purpose was to quantify the residual stress field on the surface of the flange plate across a butt weld. Figure 2.16 shows the measured variation of σ_x, σ_y and τ_{xy} in the longitudinal direction of the flange plate across weld C1B1, which is 2 inches thick. The abscissa, y/t, is the position, y, relative to the weld centerline normalized with the plate thickness, t. The results indicate again a large magnitude compressive stress on the surface in the longitudinal direction over the weld. The lateral stress also shows compression of similar magnitude. The stresses ranged from 14 ksi tension to 56 ksi compression.

None of the test locations showed a uniform stress field in the through-thickness or z direction. Consequently the residual stress calculation coefficients do not hold exactly true, and the

calculated stresses using the blind hole calculations (as per ASTM E837) will be lower than actual stresses. Nonetheless this difficult test procedure was executed with great care, and the results are very plausible.

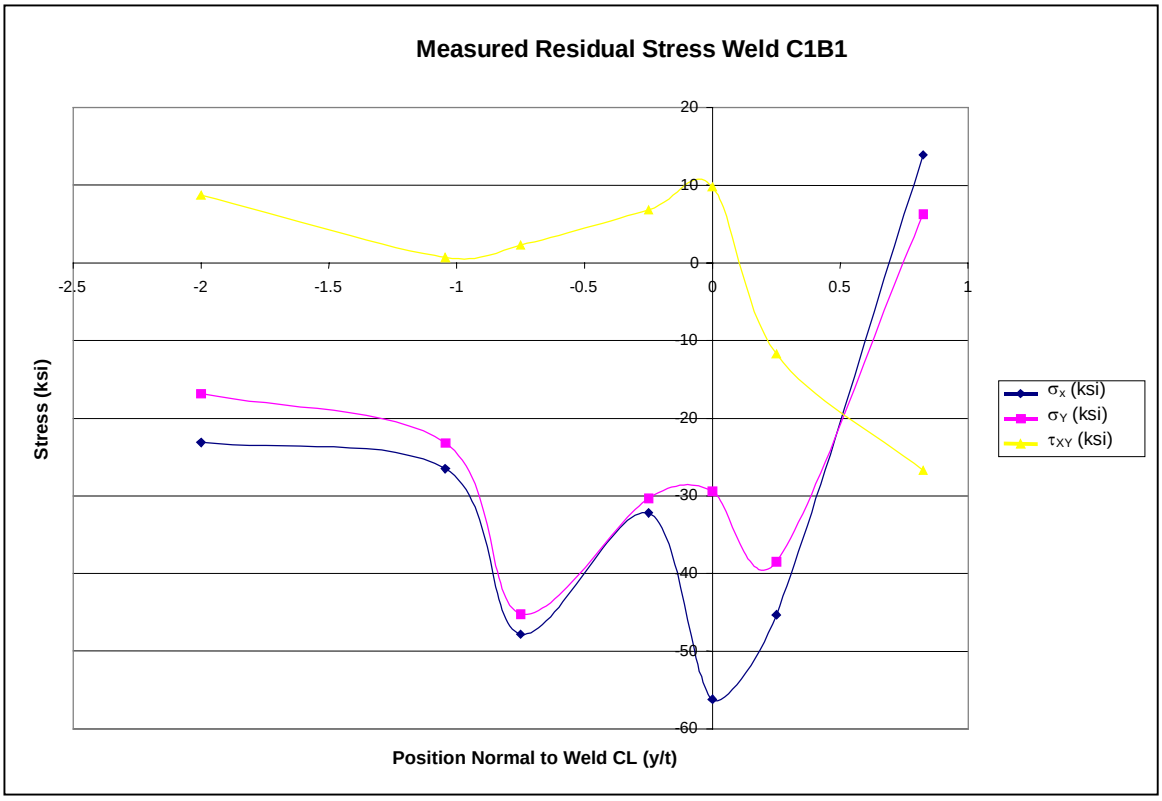

Figure 2.16: Results of ASTM E-837 residual stress measurements in ESW

Figure 2.17 shows core strain measurements before and after removal from the compression flanges. Figure 2.18 shows one of the strain rosettes being read during the hole-drilling method (E837) of residual stress measurement.

2.5.2 Summary of residual stress analysis

Various sources of residual stresses were discussed including welded attachments, rolling stresses and butt welding. A case was developed showing that the stress field developed by the butt welding of the flange plates dominated. The stress field in this region of the flange plate, including the weld metal, HAZ and local base metal, is subjected to a intense compressive shell filled with a triaxial tension zone in the core of the weld. The compressive zone was experimentally verified, and the corresponding tensile core was implied, both from prior analysis and experiments and from reason. Given the magnitude of the compressive stresses measured and the insight gained from prior work, it is prudent to assume the tensile stresses in the weld metal core are of a weld metal yield stress magnitude.

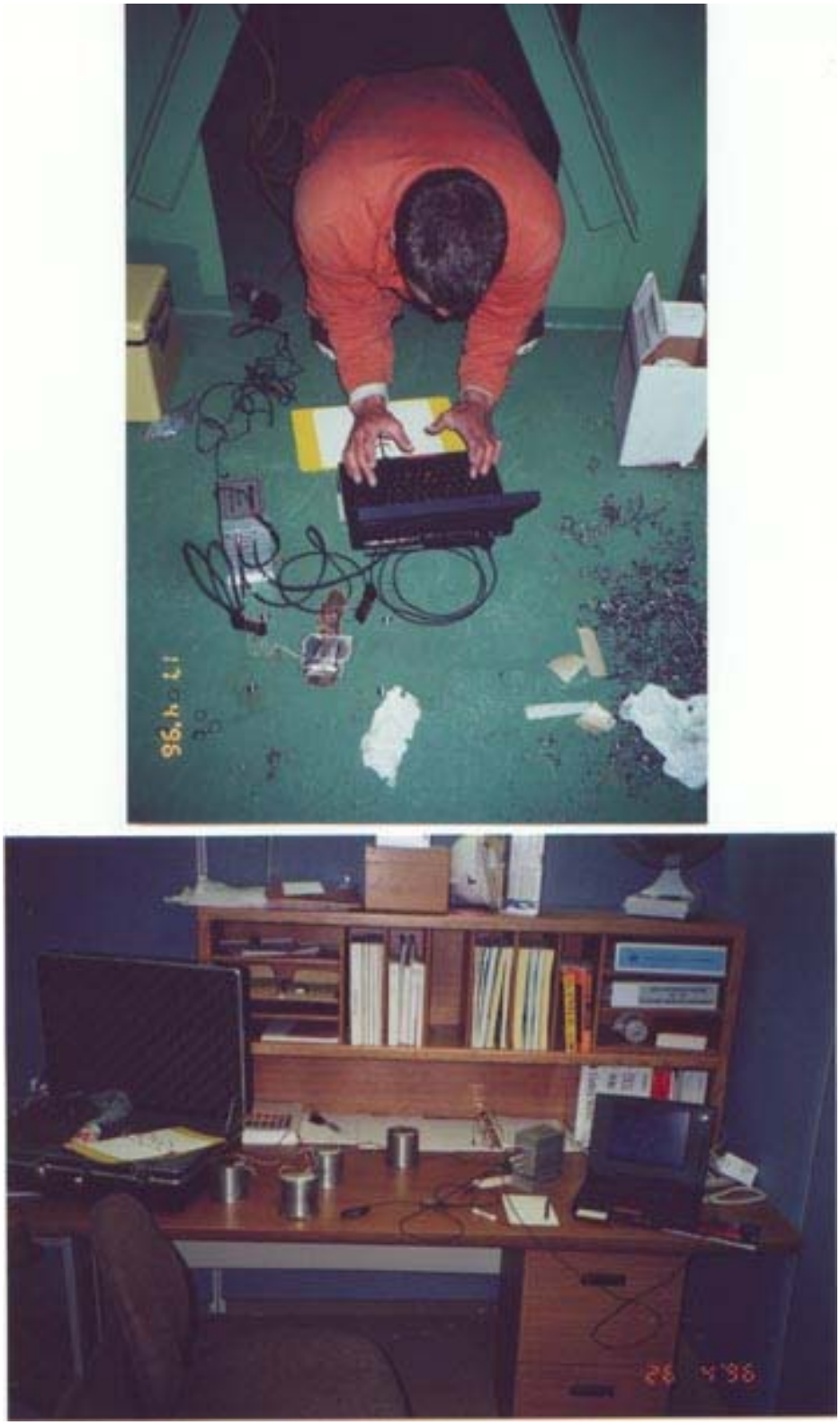

Figure 2.17: Weld metal core strain measurements. Top photo shows gauge reading prior to core removal and bottom photo shows strain measurements after cores were removed from flange ESW.

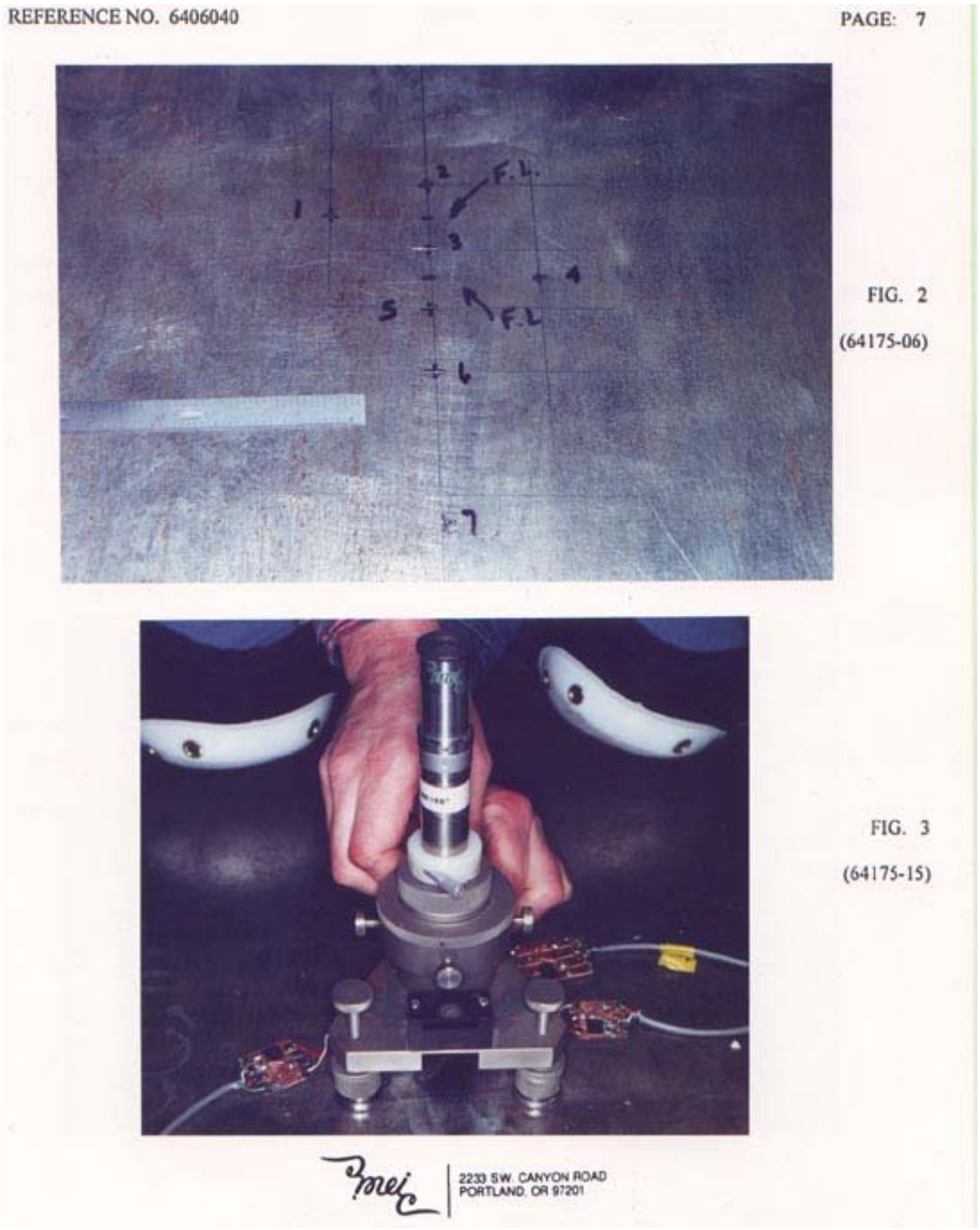

Figure 2.18: Residual stress measurements conducted according to ASTM E-837.
Photographs courtesy of MEI – Charlton, Inc. Portland, OR

3.0 MATERIAL TESTING

3.1 PURPOSE OF MATERIAL TESTING

In order to accurately assess the fitness-for-purpose of the ESW incorporated into the flanges of the box girders, the weld, base and heat affected zone (HAZ) metals needed to have pertinent material properties quantified. The primary characteristics to be investigated were the fracture toughness and fatigue crack growth. Other properties such as hardness, tensile, Charpy - V notch (CVN), chemistry and microstructure were investigated as supportive data. The fracture toughness of a material is very much effected by the thickness, temperature and load rate and thus is not an intrinsic material property. This testing program was tailored to the specific environment, thickness and loading requirements of this bridge.

3.1.1 Previous work

In 1978 three 2 ¾-in diameter by 3 3/8-in long cores were removed from a compression flange in the A-girder for UT and CVN testing. One of the cores contained UT defects found during an in-service inspection, and the other two were used for CVN testing of the weld metal and HAZ. The cores were sent to the Caltrans Materials laboratory and tested under the direction of Eric Nordlin (*Caltrans 1978*). The ultrasonic testing was reported as successful, in that UT defects were confirmed by sectioning. All defects examined were found to be grain boundary cracking. The CVN study showed that the fine grained weld metal at the center of the weld core had an average CVN value of 13 ft-lbs; the course grained weld metal had an average CVN value of 24 ft-lbs; and the HAZ had an average CVN value of 58 ft-lbs. All testing was conducted at 0º F. The 1996 AISI/AASHTO/AWS requirement for welding processes other than ESW and EGW is 15 ft-lbs at 0º F.

These earlier core extractions revealed that the course grained weld metal had grain dimensions on the order of 7 mm. This is a very course grain structure to be tested with the 10 mm by 10 mm CVN specimen and thus provides a plausible explanation to the large extreme spread of the reported values.

3.2 INVESTIGATION REOPENED

In 1992 a second look into the suitability of these welds was begun. With the knowledge gained in the first investigation, it was clear that a more detailed testing plane would be required. The second approach was essentially a continuation of the original Fracture Control Plan (FCP) for Existing Electroslag-Welded Fracture Critical Members, published by FHWA in 1976, which was started with the Caltrans report sited above. Using the principals of the FCP a detailed material coring plan was developed.

3.3 WELD, HAZ AND BASE METAL CORES REMOVED FOR BOX GIRDERS

The material testing plan required compact tension specimens with a thickness on the order of 1 inch, which means that the size of the core extracted from the flange needed to be at least 3 inches in diameter. The largest trepanning type core drill located would remove a 3½-inch diameter core. Finding a portable machine to operate this cutter at its recommended speed was very difficult. The cutter is designed for fast and efficient stock removal used in production work. Cutting a 4-inch diameter hole 3½ inches deep in less than 60 seconds requires large values of torque and horsepower for a portable machine. A custom drill was designed and fabricated, as shown in Figure 3.1. This unit developed over 800 ft-lbs of torque at the cutter and required nearly 27 hp to run the hydraulic pump, which was remotely located on the roadway.

At the recommendation of FHWA, the Oregon Graduate Institute (OGI) was contracted to perform the testing of the cores, once removed from the bridge (see Appendix D). OGI has been an expert in the field of ESW since the 1980's and provided guidance into the selection of coring operation locations in order to maximize the usefulness of the weld and HAZ metal.

Fourteen cores were removed from various compression flanges in the B-, C- and D-girders for material characterization. The holes were fitted with expanding plugs that acted structurally to fill the holes. Of the fourteen cores that were removed from the bridge, two were base metal specimens, five were weld centerline specimens, and the remaining seven were heat affected zone (HAZ) specimens.

The weld centerline specimens were centered between the weld fusion zone edges, visible after grinding and etching the surface of the weld. The center point of the HAZ specimens was placed ½ to $^{5}/_{8}$ inch out from the fusion line edge. This offset was found to optimize material usage for HAZ test specimens. Figure 3.2 depicts the coring relative to the weld geometry.

Figure 3.1: Coring ESW for material testing: 1) top left: close-up view of 4-inch diameter cutter; 2) top right: custom built drill; 3) bottom left: drilling and tapping mounting holes; 4) drill in place ready to core

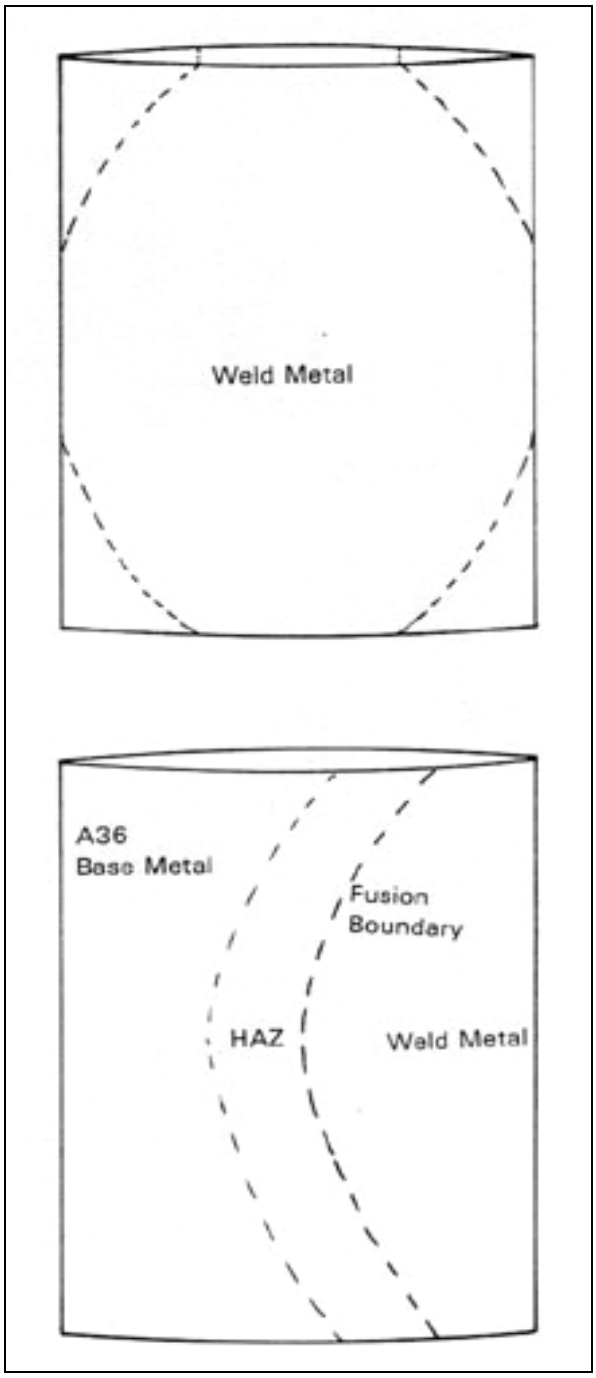

Figure 3.2: Depiction of how cores were centered to maximize weld and HAZ material of the ESW

3.4 PHASE 1 TESTING

When performing fracture toughness tests it is very helpful to know ahead of time the values of the parameters you are testing for. This knowledge can greatly improve the validity of the test, especially when testing specimens with a thickness dimension significantly smaller than the plates used in service. For this reason a few of the cores removed from the structure were subjected to CVN, hardness, composition and microstructural characterization prior to designing the more in-depth fracture toughness testing plan. Information from Phase 1 would help quantify the testing requirements needed for more accurate fracture toughness tests such as ASTM E399, E813, E1024 and E647 that were being considered for Phase 2 testing. The CVN testing performed in 1978 tested several metallurgically different regions, but all at the same temperature. In order to estimate real fracture properties, a CVN versus temperature relationship was required.

3.4.1 CVN testing

CVN toughness specimens were machined from the weld center at mid-thickness, quarter thickness and near the surface. In addition, CVN specimens were machined at the mid-thickness HAZ location within 1 mm (0.040 in) from the fusion line. These specimens were tested over a range of temperatures as reported in Figure 3.3.

It can be seen that the transition from a brittle to a ductile failure mode occurred around 50º F at dynamic strain rates. Tensile tests were also performed on the weld metal (*Koon-Hall-Adrian 1997*). The results of transverse and longitudinal (relative to welding direction) tensile tests are shown in Table 3.1.

Table 3.1: All weld metal tensile properties at mid thickness

Orientation Relative to weld direction	σ_{ult} (psi)	0.2% offset σ_{ys} (psi)	Elongation in 4D (%)	Reduction of area (%)	Temp	I.D.
Parallel y-dir.	87,300	65,000	22.0	63.5	Room	C7B2 (mid.)
Transverse x-dir.	84,400	59,400	22.0	59.5	Room	C7B2 (mid.)

The Barsom-Rolfe two stage correlation was used to estimate plane strain fracture toughness from CVN and tensile data (*Barsom and Rolfe 1987*). Then an estimate of the expected toughness at the lowest anticipated service temperature (LAST) and in-service strain rate of the structure of 0º F and 10^{-3} sec^{-1} respectively, was developed. A temperature shift of 94º F was calculated as the difference between the dynamic strain rate of the CVN test and in-service strain rate. Refer to Equation 1 for the temperature shift and Equation 2 for CVN-K_{Id} relationship.

Using this correlation, a critical stress intensity estimate of 105 ksi-in$^{1/2}$ at 0º F was calculated for the all weld metal region at mid-thickness. See Figure 3.3.

$$T_{shift} = 0.75(215 - 1.5\sigma_{ys})^{o} F \quad (1)$$

$$\text{for } 36 \text{ ksi} < \sigma_{ys} < 140 \text{ ksi}$$

$$K^2_{Id} / E = 5 \text{ (CVN) impact (psi-in., ft-lb)} \quad (2)$$

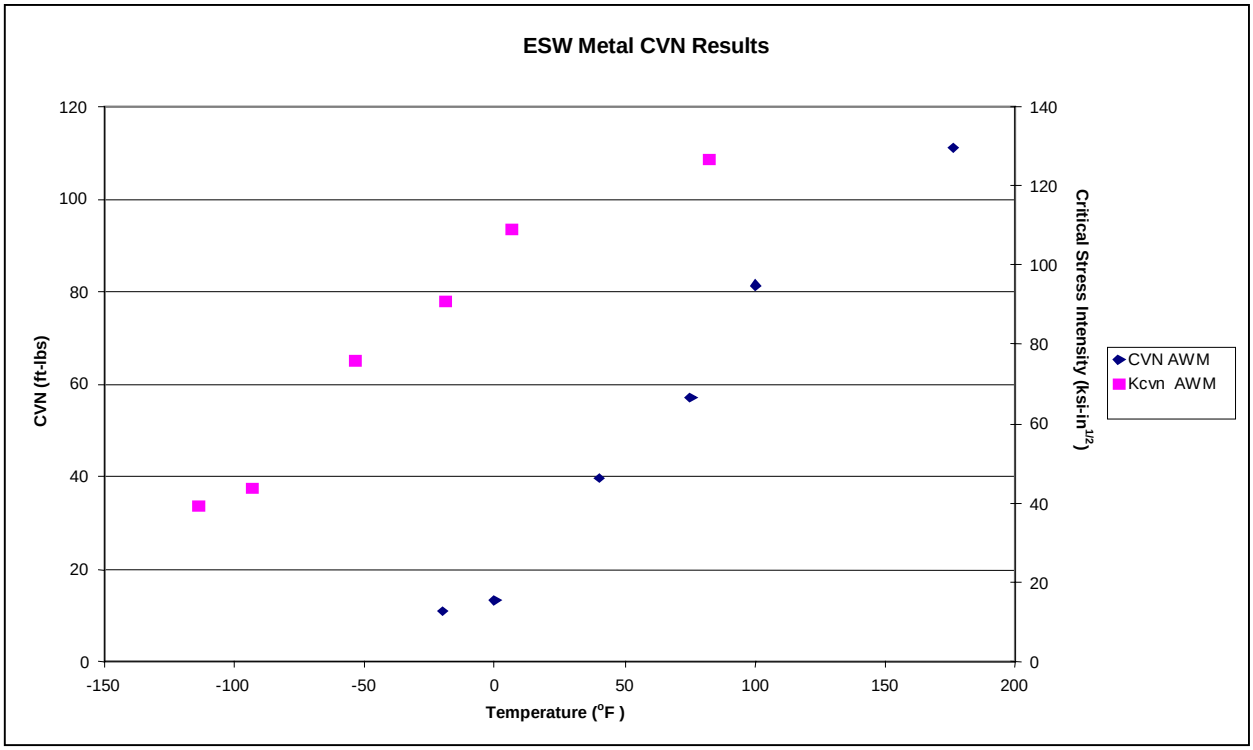

Figure 3.3: Toughness data of ESW metal from Charpy V-notch testing. Diamonds read on the CVN scale on left, squares correlate to the predicted fracture toughness read on right scale.

3.4.2 Chemical Composition and Weldability

Representative samples of weld metal and A36 base metal were chemically analyzed as shown in Table 3.2. The only differences between the weld metal and base metal compositions were lower carbon and greater alloy content of the weld metal resulting in a similar P_{cm} but higher

CE_{IIW} [1]of the weld metal. The differences between weld metal and base metal were on the same order relative to the variations from weld to weld.

Table 3.2: Chemical composition of weld and base metals

Element	Weld Metal Core D7B2 (%)	Weld Metal Core C7B2 (%)	Base Metal (A36) (%)
C	.156	.21	.19
Mn	1.22	.75	1.01
Si	.26	N/A	.30
Cr	.07	N/A	.04
Ni	.55	N/A	.01
Mo	.10	<.005	-
Cu	.09	.10	.02
S	.014	N/A	.009
P	.013	N/A	.013
Al	.002	N/A	.013
Cb	.001	N/A	.001
P_{cm}	**.25**		**.25**
C_{IIW}	**.44**		**.37**

3.4.3 Microstructure

A detailed description of metallurgical regions found with the ESW is included in Appendices C and D. In summary, the welds examined on this structure were typical of the older technology standard-gap method. Water-cooled shoes were used but large grained weld and HAZ structures were common in all cores. SMAW repair welds were located on nearly all of the cores extracted.

3.5 PHASE II TESTING

Phase II testing was comprised of 1) using an appropriate fracture toughness test on compact tension specimens at the LAST and in-service strain rates; and 2) quantifying the crack growth threshold stress intensity range for the weld, HAZ and base metals.

3.5.1 Fracture toughness

The Phase I CVN data indicated that at the LAST of 0º F and in-service strain rate of 10^{-3} sec^{-1}, the failure mode would occur somewhere in the transition region from brittle to ductile behavior. This fact complicated selection of an appropriate method of quantifying toughness. Given the highly restrictive specimen size requirements of ASTM E399 it was foreseen that measuring a valid K_{Ic} value with a CT specimen thickness on the order of 1 inch was unlikely. If stable crack growth could be achieved then J_{Ic} may be attainable as defined in ASTM E813. Using a CTOD approach, as defined in ASTM E1290, was not practical, because it is generally recommended for full thickness test specimens. Anderson and Dodds found that when a fracture test specimen

[1] P_{cm} and CE_{IIW} are defined in Annex VIII of the AWS D1.5 Bridge Welding Code.

provided inadequate triaxial restraint for valid K_{Ic} measurements, yet did not achieve stable crack growth in order to satisfy J_{IC}, a correction could be made, based on small scale yield criteria that can predict the full thickness toughness of a material using a partial thickness specimen (*Anderson and Dodds 1991*).

This approach appeared well suited to this particular material, and the CT specimens were machined into the largest square specimen attainable from the 3.5-in diameter cores. ASTM E813 was chosen as the testing procedure. If the data revealed that the material was extremely brittle then it could be converted to K_{Ic} as defined in E399. Under linear elastic fracture mechanics (LEFM) assumptions it is not unreasonable to convert the load line displacements to the crack opening displacements (COD) required in E399.

Figure 3.4 show the CT specimen geometry. The specimens machined had a W dimension of 2.0 inches and a thickness B of 1.0 inches. Side notches were used to help maintain crack tip front uniformity under the intense residual stress state of weld metal resulting in an effective B dimension of 0.90 inches. Specimens were tested at room temperature and at 0º F under a load rate of 2 to 5 seconds to full load.

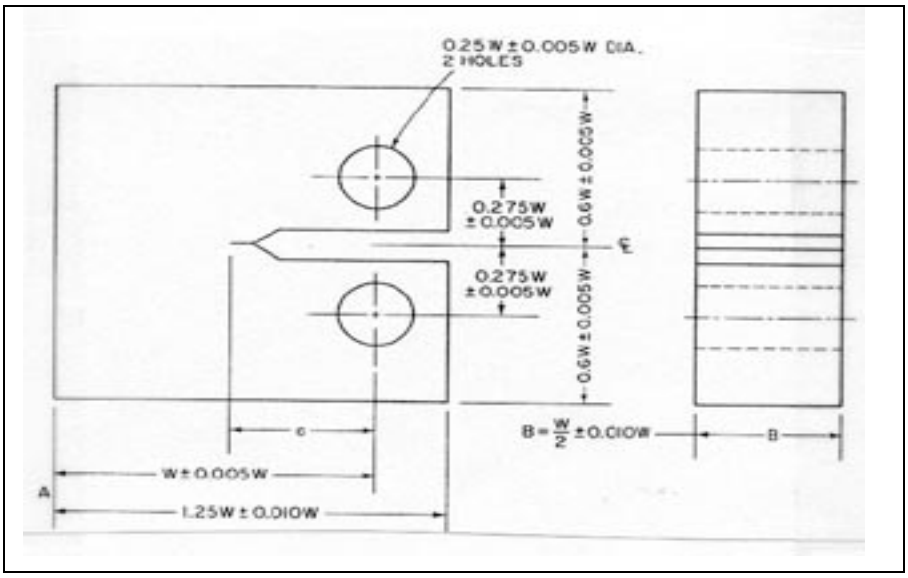

Figure 3.4: Compact tension specimen used for J-integral and crack growth testing of ESW metal

Table 3.3 and Figure 3.5 summarize the fracture toughness results using the CT specimens. The first four symbols of the ID code locate the portion of the bridge where the material originated. The remaining symbols identify whether the specimen was machined from the top (T), center (C), bottom (B) or heat affected zone (HAZ) of the core. All HAZ specimens were machined from the central section of the core thickness in order to sample as much representative material as possible. The fatigue crack length reported ranged from 1.19 to 1.26 inches. The side notches proved to be effective in maintaining crack front straightness. The maximum load path

displacement (LPD_{max}) was found to be as low as 0.042 inch for the brittle weld and HAZ metal and as large as 0.307 inch for the highly ductile base metal. It is clear from these lower values that stable crack growth was extremely difficult to achieve with most of the specimens.

Table 3.3: Results of fracture toughness testing

Sample (ID)	Temp (° F)	$B\sigma_y / J_{max}$	K_Q (ksi-in^{½})	K_{max} (ksi-in^{½})	K_c from J_{ssy} (ksi-in^{½})	J_{max} (in/lb)
B3B1-T	RT	77	59.7	95.6	145	991
B3B1-C	0° F	176	58.8	75.7	108	432
B3B1-B	0° F	52	57.5	109.4	159	1462
D3B1-T	RT	47	59.5	103.2	165	1627
D3B1-C	RT	53	59.5	99.2	164	1432
D3B1-B	RT	40	61.2	93.2	178	1898
B3B2-HAZ	0° F	213	54.6	63.6	101	358
B7B1-HAZ	0° F	231	56.8	69.5	97	329
D3B1+8	0° F	6	44.6	98.9	220	6008
C3B2-C	0° C	37	Not reported	Not reported	176	1416

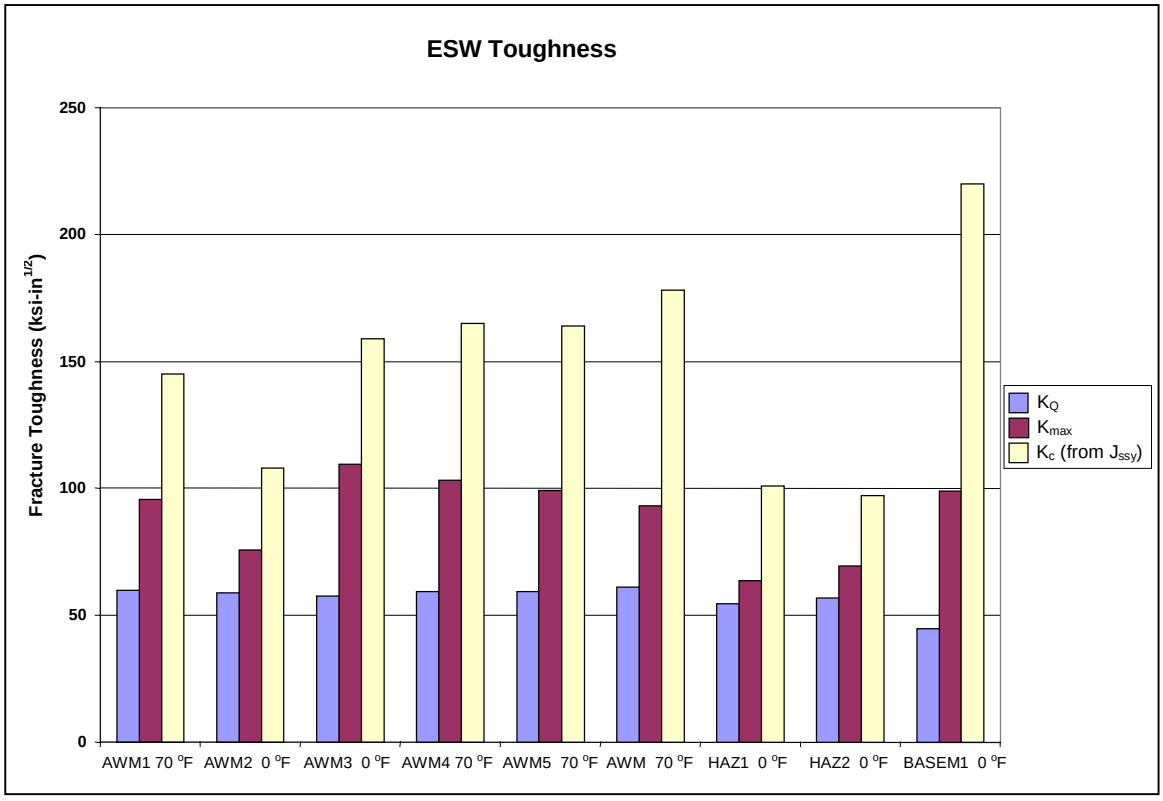

Figure 3.5: Fracture toughness of weld,HAZ and base metal. All data are calculated from J-integral (ASTM E813) test data

In all load - displacement records the ratio P_{max} / P_Q was substantially greater than 1.10, indicating that plane strain conditions were not achieved near the crack tip and that K_Q was not likely representative of K_{Ic}. This can also be interpreted that in order to achieve a valid K_{Ic} value from these materials, a specimen thickness of much greater than 1 inch would be required. Nonetheless, this material can still be considered to behave in a brittle manner under these test conditions and K_Q as well as K_{max} must be considered as reasonable parameters to assess the fitness-for-purpose of these welds in the 3½ inch thickness found in this bridge.

J_{max} had a much larger range than any other parameters investigated, with recorded values as low as 329 lbs/in and up to 6008 lbs/in, for a weld and base metal specimen, respectively. None of the weld or HAZ specimens met the criteria of stable crack extension as defined in E813. Nonetheless, a meaningful approximation of the actual toughness of the in-service weld and HAZ metal can still be made.

Figure 3.5 shows the parameter K_c (from J_{ssy}) as well as K_Q and K_{max}. K_c (from J_{ssy}) is the estimated value of K_c based on J_{max} data from the reduced thickness test specimens. The test specimens were thick enough to allow only small scale yielding near the crack tip. As the dimensionless parameter ($B\sigma_y/J_{max}$) becomes equal to and greater than 200, the measured value of J_{max} should approach the small scale yielding value of J. For values less than 200, corrections are made based on the hardening exponent of the material, which was found to be near 8.0. As stated above, this procedure was developed by Anderson and Dodd and is appropriate for J data that failed to meet the criteria of E813 due to insufficient stable crack extension. This approach accounts for the limited plasticity near the crack tip in the bridge welds, yet still allows the easy-to-calculate and understand LEFM assessment of critical crack size.

Figure 3.6(a) shows load-displacement curves from a typical ductile (upper plot) and brittle (lower plot) response in the E813 testing performed by OGI. Figure 3.6(b) shows the J-R curve for specimen C3B2-C tested at 0º C (as opposed to the 0º F test temperature used on the other specimens). Appendices E and F contain the photographs of the fractured compact tension test specimens. Appendix E contains the fatigue and fracture testing performed on the mid-thickness AWM specimen, C3B2-C.

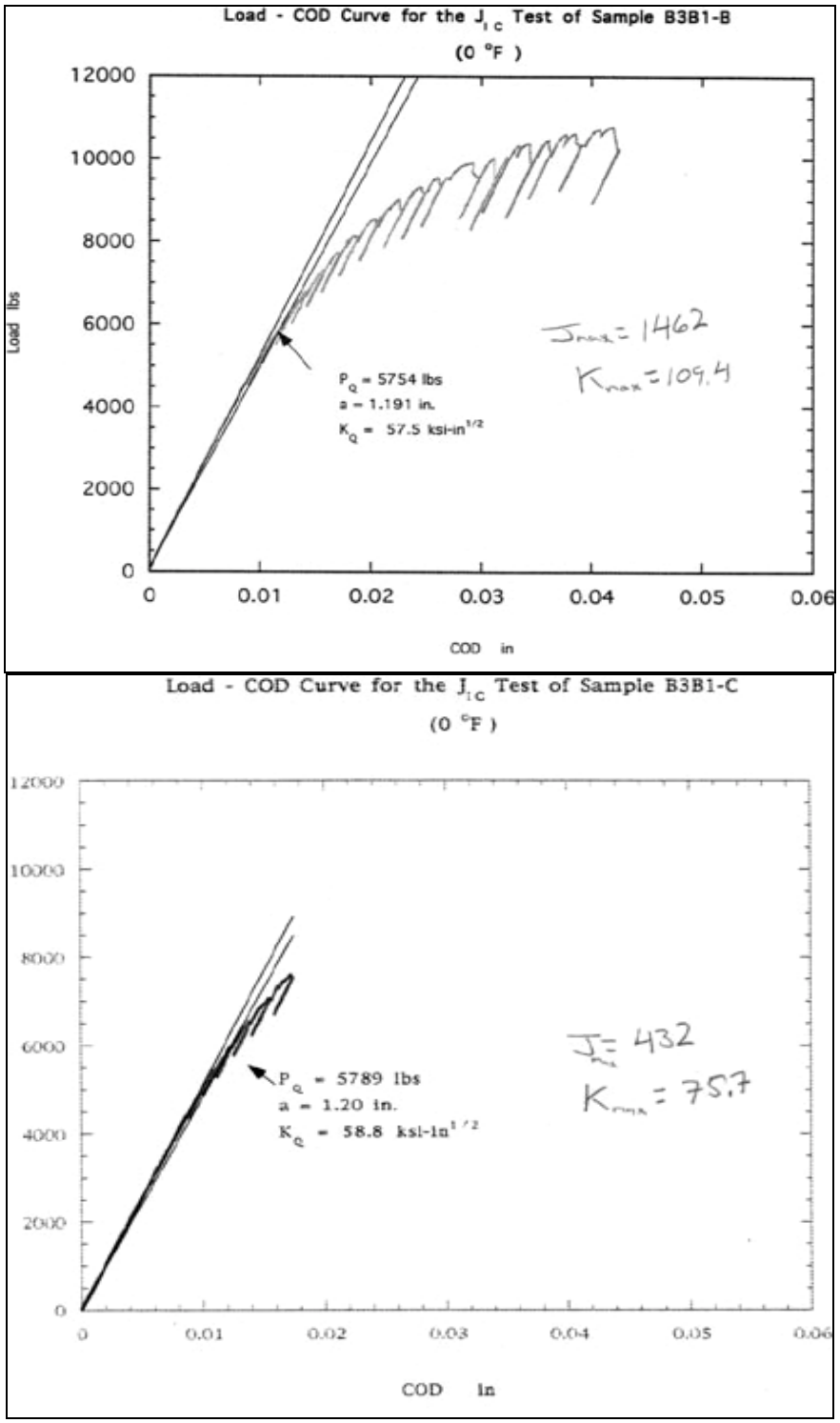

Figure 3.6 (a): Example ductile (upper) and brittle (lower) behavior in the load-displacement plots of ASTM E813 test data (OGI test results)

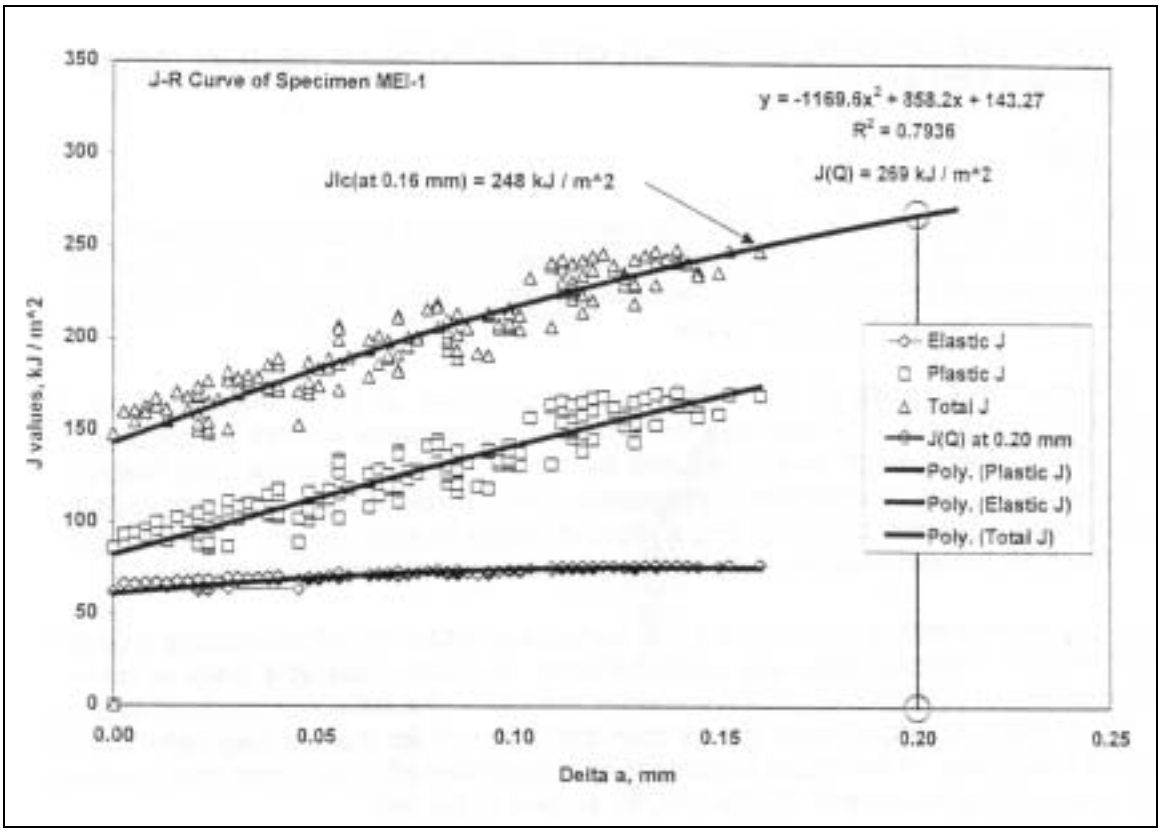

Figure 3.6 (b): J-R curve from AWM specimen C3-B2-C tested at 0º C by CC Technologies Inc.

3.5.2 Crack growth threshold

Fatigue crack growth threshold testing per ASTM E647 was conducted on the extracted weld, HAZ and base metal at room temperature. All fatigue crack growth testing was performed by OGI with the exception of specimen C3B2-C, which was tested by CC-Technologies Inc.

Threshold crack growth data is important because it represents the lowest possible stress intensity range that will induce an existing crack to grow under cyclic loading. Thus it can be used to assess the largest crack that would be expected to remain dormant in the structure when the live load or alternating stress field is known. Table 3.4 summarizes the results of the fatigue threshold measurements on the weld, HAZ and base metals. Values range from 10.9 to over 15 ksi-in^{½}. Figure 3.7 shows the threshold responses for both the HAZ (upper tested by OGI) and AWM (lower tested by CC Technologies). Figure 3.8 shows the crack tip progression down a coarse, prior austenitic, grain boundary.

Table 3.4: Fatigue crack growth threshold results

Specimen ID	Location	ΔK_{th} (ksi-in$^{1/2}$)
C3B2-B	Weld Metal surface	10.9
C3B2-C (*MEI-Charlton 2001*)	Weld Metal mid-thickness	12.0
C3B1-C	HAZ mid-thickness	15
C7B3-C	HAZ mid-thickness	12.7
D3B1+8	Base Metal mid-thickness	13.4

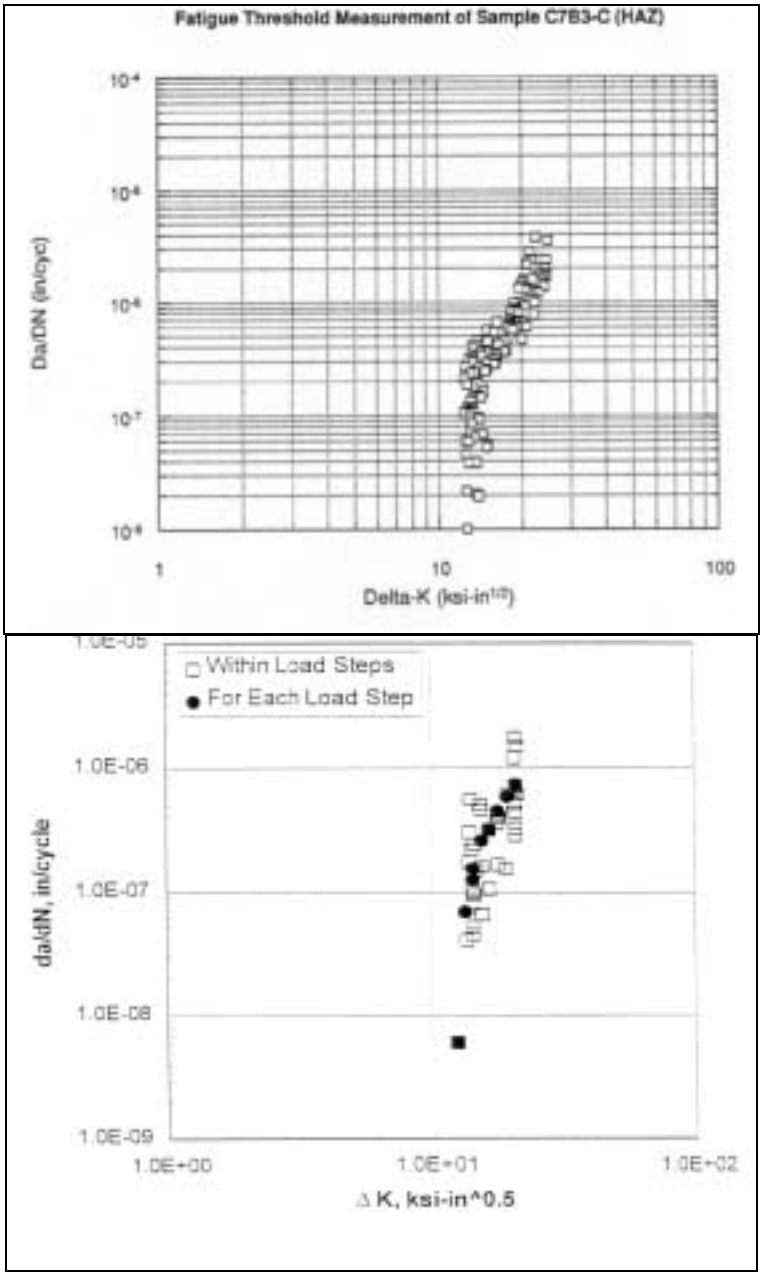

Figure 3.7: Fatigue crack growth threshold (ASTM E647) data. Upper plot HAZ threshold. Lower plot AWM threshold.

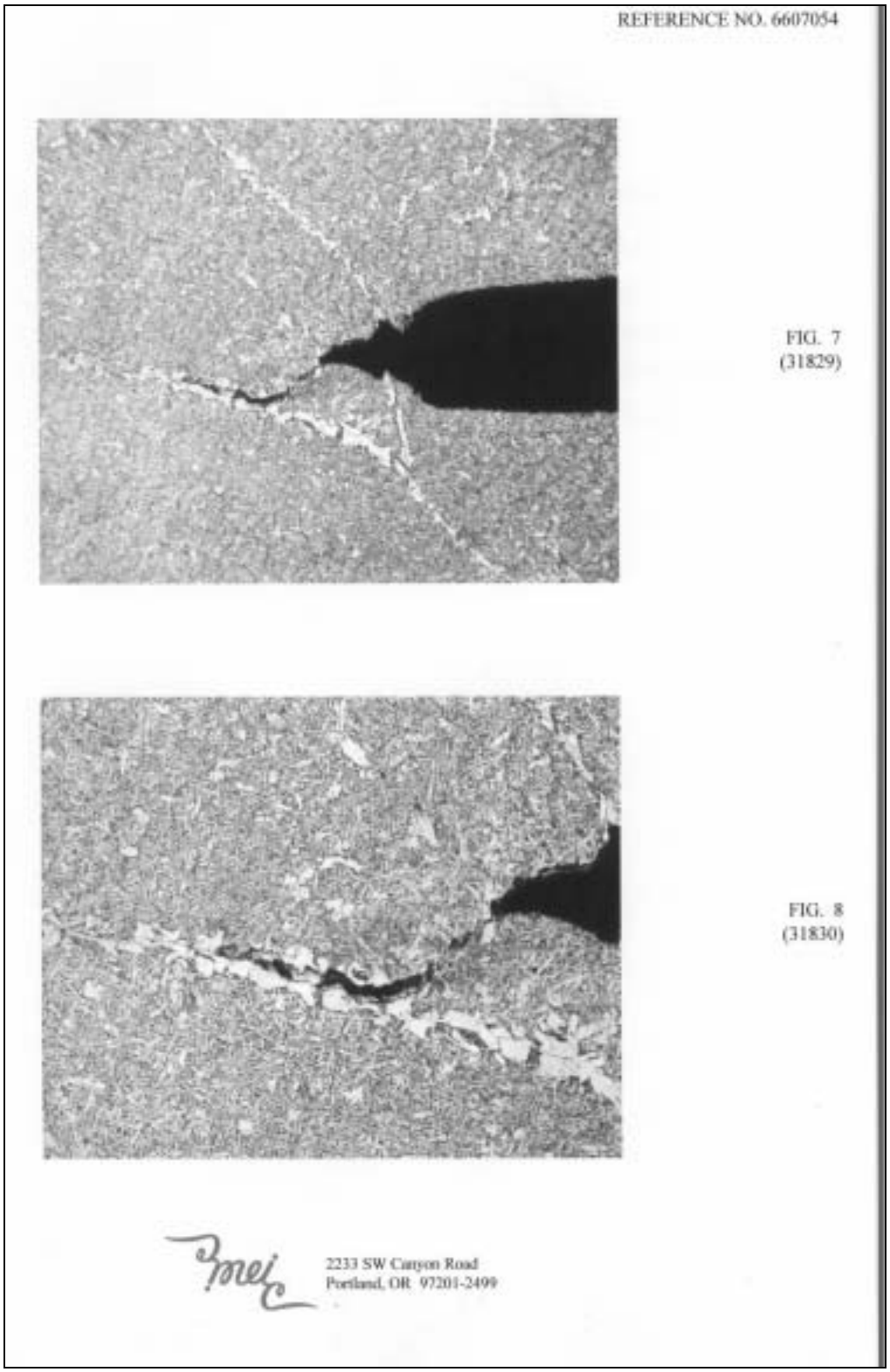

Figure 3.8: Fifty times (upper) and 100x (lower) photomicrographs of crack tip on specimen C3B3-C. Note that crack tip has connected to and is following a ferrite vein at a prior austenite grain boundary.

Residual stresses on the surface of the AWM compact tension specimen were quantified using ASTM E837 prior to crack growth threshold testing. The principal stresses on both sides of specimen C3B2-C between the back surface and crack tip were found to be very low (+600 and –400 psi). Figure 3.9 shows the specimen being tested for residual stress.

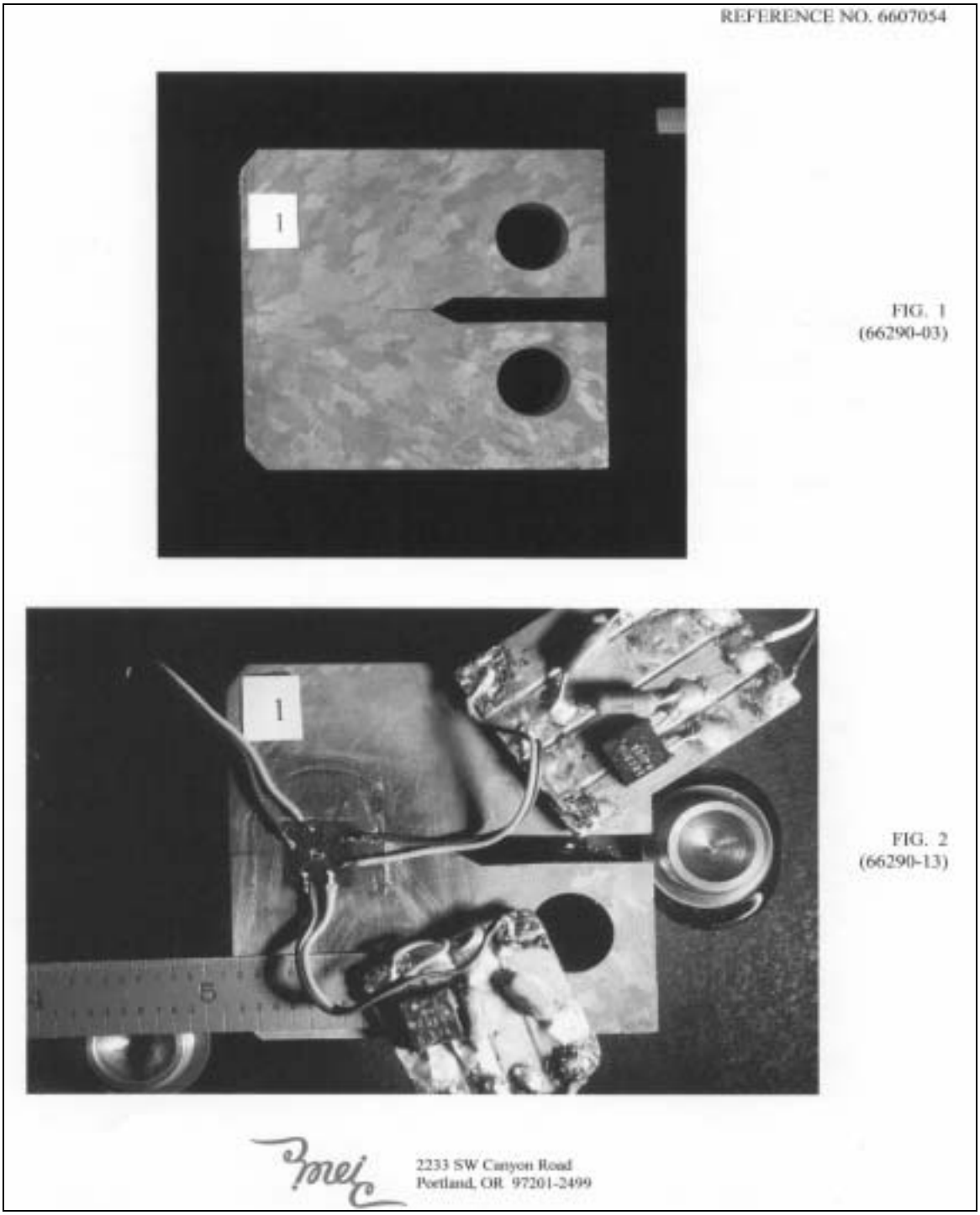

Figure 3.9: Etched compact tension specimen C3B2-C (upper) and residual stress measurement on specimen (lower)

3.6 FATIGUE CRACK GROWTH RATE

The crack growth rate parameters A and m as defined under ASTM E647 were to be quantified for the weld, HAZ and base metals as part of the material testing contract. This information, however, was not measured. Fortunately, as will be shown in Chapter 5, fatigue crack growth in these welds under service loads is very unlikely and not a critical piece of data to the overall evaluation.

3.7 SUMMARY OF MATERIAL TESTING PROGRAM

CVN impact, J integral and threshold fatigue tests were conducted on 3½-in diameter x 3½-in long cores of electroslag welds extracted from box girder flanges on the I-205 George Abernethy Bridge near Oregon City, Oregon. The results of those tests may be summarized as follows:

1) The welds incorporated into this bridge are typical standard gap ESW that are comprised of a coarse columnar grained weld metal, fine and coarse grained HAZ and SMAW repair welds near the ESW – base metal fusion zone.

2) The indicated critical fracture toughness based on CVN data for AWM material and the two-stage Barsom-Rolfe correlation predicted a K_c value of 105 ksi-in^{½} at the in-service temperature and strain rate of 0º F and 10^{-3} sec $^{-1}$ respectively.

3) As expected, neither the ASTM E399 "Plane Strain Fracture Toughness" nor the E813 "Elastic/Plastic Fracture Toughness" specification were perfectly suited to this material under the service strain rate and temperature. The material tested was too tough for passing K_{Ic} criteria yet too brittle to pass J_{IC} testing criteria using the 1 inch thick CT specimens. Toughness based on the E399 approach had a K_c range of 55 to 60 ksi-in^{½} for the weld metal and HAZ. K_{max} ranged from 75 to 110 ksi-in^{½} for the weld metal and 65 to 70 ksi-in^{½} for the HAZ.

4) Previous work from Anderson and Dodds allows an estimate of the toughness in the full thickness plates in the bridge to be made from the E813 data. Critical stress intensity values based on the small scale yielding values of the J integral ranged from 108 to 178 ksi-in^{½} for the weld metal and near 100 ksi-in^{½} for the HAZ.

5) The threshold fatigue value was found to have a low of 10.9 ksi-in^{½} in the weld metal at mid-thickness and a high of over 15 ksi-in^{½} in the HAZ. The base metal had a similar resistance to crack growth of 13.4 ksi-in^{½}.

4.0 NONDESTRUCTIVE EVALUATION OF BOX GIRDER ESW

4.1 PURPOSE OF NDT PROGRAM

The purpose for performing NDT (nondestructive testing) on the ESW is to identify sub-critical cracks or other flaws that degrade the integrity of the welds and/or present a risk of fatigue crack growth under service conditions. This chapter summarizes the testing performed on the flange butt welds.

4.2 APPLICABLE METHODS OF NDT

There are several NDT methods that are useful for examining the flange butt welds in question. They are Radiography (RT), Ultrasonic (UT), Magnetic Particle (MT) and Acoustic Emissions (AE) testing. Strain measurements can also be considered a form of NDT but is discussed in the Chapter 2 - Load Analysis. A brief description and discussion of each form of NDT is presented below.

4.2.1 Radiography

Also called X-ray testing, this form of testing uses a point source of electromagnetic radiation typically from a radioactive metal. A sheet of film is used to permanently record the results. The weld is placed between the radioactive source and the film. Changes in density of the weld are recorded on the film. This method is most sensitive to flaws that are oriented in the direction of the radiation. Because of this anisotropic sensitivity, the subject is usually X-rayed from two or more directions. This method can identify three-dimensional flaws or defects with excellent sensitivity, on the order of 1/50 of an inch. Planar (2D) flaws can often cause sensitivity to go down to 1/10 of an inch or more. Competent technicians can usually detect planar flaws larger that 1/5 of an inch in geometry, such as the welds in question.

4.2.2 Ultrasonic Testing

This method uses sound waves to detect flaws. A transducer is acoustically coupled to the weld and base metals and sound waves are interjected into the material in a specific direction, at various energy levels and frequencies. This transducer also receives any returned waves that are reflected off of surfaces (impedance mismatches) encountered during propagation. Time differences between sent and returned signal are measured. Knowing the speed at which various types of sound or stress waves propagate in the material the time differences can be converted to distances. Also the energy level of the returned wave can be used to indicate size and severity of the reflector inside the material.

UT is more sensitive to flaws or defects that are oriented perpendicular to the direction of wave propagation. As with RT, more than one direction of inspection is used. UT can reliably detect 3D and planar flaws down to very small dimensions in good geometry and a clean material. The ESW have highly variable grain structure with some grains being very large or coarse. The intergranular boundaries present reflectors and attenuation to the UT wave and thus can greatly reduce the signal-to-noise ratio of the instrument. Proper techniques executed by an experienced technician can identify flaws on the order of $^1/_5$ of an inch or larger. In general, the UT results from a thick, coarse-grained ESW requires more experience to interpret than the radiograph.

4.2.3 Magnetic Particle Testing

This is a surface inspection tool. MT uses magnetic flux lines that are made visible with iron power. Flaws and defects on or within approximately $^1/_{10}$ of an inch below the surface will appear as a discontinuity in the flux line. This method can reliably detect flaws on the order of $^1/_5$ of an inch on or near the surface.

4.2.4 Acoustic Emission Testing

This method is used for detecting fatigue crack growth. When cracks grow they do so in bursts and emit a stress wave in the parent material. Using several sensors that listen for such events, the location of the noise source can be identified. Unfortunately there are many other noise sources within in-service bridges, and the difficulty lays in signal-to-noise discrimination. Unlike the other methods discussed, this method is typically not used to size a flaw but to identify any flaw activity such as crack face rubbing and crack tip extension. Experience and technical competence are paramount to the success of this NDT method.

4.3 PREVIOUS NDT

4.3.1 Construction

The girders were fabricated between April and October 1969 at American Pipe Construction in Portland, Oregon. The contract called for RT and MT examination of every ESW. Leslie Harkama (a retired ODOT employee) worked for American Pipe at the time of construction and performed much of the NDT on the welds as a Quality Control (QC) function. Harkama is an American Society for Nondestructive Testing (ASNT) Level III technician in MT, RT, PT and UT. This is the highest level attainable from ASNT. He is well known in the local NDT community as an expert with over 35 years of direct experience.

He firmly believes that the contractor did a very good job of QC and that the State inspectors did a good job of Quality Assurance (QA). As a consequence of this thorough NDT, many of the butt welds were repaired with shielded metal arc welding (SMAW) due to flaws and defects found to be rejectable by the D1.1 welding code. Though not required by contract, Harkama performed UT on many of the welds. All of the radiographs from this contract were destroyed sometime in the 1980's.

Notes from the State inspection files show that A and B girders were fabricated between April and June 1969. Table 4.1 summarizes the fracture critical ESW in the A- and B- girders that were repaired due to rejectable defects. Some repairs were made by excavating and rewelding with SMAW, and others were completely cut apart and started over. Eight of the 56 fracture critical welds have noted repairs; some such as A1B1 and B6T3 have over four repairs noted. All repairs were noted to have passed RT before acceptance.

Table 4.1: Repaired fracture critical butt welds

Weld Identification	Number of Recorded Repairs
A1B1	6
A6B2	1
A2B1	1
A7T1	1
B6T3	4
B8B1	4
A1B4	2
A6B1	2

Girders C and D were fabricated between August and October 1969. No defect repairs were directly noted but little other information was recorded other than section worked on and date. Coring from this evaluation in the C and D girders showed nearly every weld contained SMAW weld repairs, mostly to repair undercut.

4.3.2 First In-service inspection

In 1977, after FHWA requested all States to investigate fracture critical ESW, ODOT hired a UT consultant, Andrew Struzyk, to perform UT and Pittsburgh Testing Laboratory to perform RT on selected welds in both the Fremont bridge approach ramps and the box girders of the West Linn Bridge. The RT revealed no rejectable defects and the UT was inconclusive. UT flaw indications were located in the bottom compression flange over Pier 4 in girder A. Cores were extracted and sent down to Caltrans for evaluation of the UT flaw indications and material testing (*Caltrans 1978*). The UT indications were found to be grain boundaries with some intergranular cracking.

4.3.3 Second In-service inspection

In 1990 through 1992 Poore and Harkama performed the second in-service inspection of the ESW. A total of 30 ESW were randomly selected and then inspected with UT and MT. Five ESW were inspected with RT as well. Harkama developed the UT procedures with Poore using straight, 45-, 60- and 70-degree angle beam explorations. The RT was contracted to Professional Services Industries Inc. using an Iridium 192 source. Two welds were found to have a UT rejectable indication. No rejectable RT flaw indications were noted including one of the UT rejected defects.

4.3.4 Third In-service inspection

In 1994 Longview Inspection was contracted to inspect the outer edges of the 112 fracture critical ESW (*Longview Inspection, Inc. 1994*). One weld revealed code rejectable defects. In 1996, after a lengthy contract to clean up the interior of the box girders from lead paint dust and install lighting and electrical power, a third NDT program was finished under the direction of the author. A UT contract was awarded to Professional Services Industries, Inc. to inspect all of the 112 fracture critical ESW. Jim Sable, CWI and ASNT Level I UT, Level II MT, oversaw all testing inside the four girders. The UT operators were level II. Straight 45-, 60- and 70-degree angle beam transducers were used to inspect the welds. MT was also used. All testing was performed inside the box girders with the exception of the portion of the flange welds outside of the webs, which were inspected from both the top and bottom. Inside the box girders all paint was removed within 18 inches of each weld (*Professional Services Industries, Inc. 1996*).

Four of the 112 welds inspected showed rejectable UT indications. Rejection criteria were based on the 1988 AWS D1.5 "Bridge Welding Code" criteria for dynamically loaded members. The inspection of these four welds is discussed below.

4.3.4.1 Weld C1B2

Rejected due to 70-degree scan with a 60 dB indication level and a 50 dB reference level. Indication rating +4, length 2 inches. Field notes indicate the inspector could see the beginning of this flaw indication with both the 60- and 45-degree scans. Indication lies ⅝ inch from weld centerline at a depth into the plate of 0.6 inches. See Figure 4.1 for inspection form and 4.5(a) for a plot of the indication. For the 70-degree scan on 1½ to 2½ inch thick plates, like C1B2, a Class A flaw has an indication rating +4 and lower. Thus the UT indication in this weld is right on the border of being a Class A flaw severity.

4.3.4.2 Weld A1B2

Rejected due to 45-degree scan with a 50 dB indication level and a 40 dB reference level. Indication rating +6, length ½ inch. Field notes indicate the inspector could detect this indication over all of the length of the weld and felt it might be related to the transition in plate thickness. The indication appeared to follow grinding marks left from fabrication. See Figure 4.2 for inspection form and 4.5 (b) for a plot of the indication. For the 45-degree scan on 1½ to 2½ inch thick plates, like A1B2, a Class A flaw has an indication rating +9 and lower.

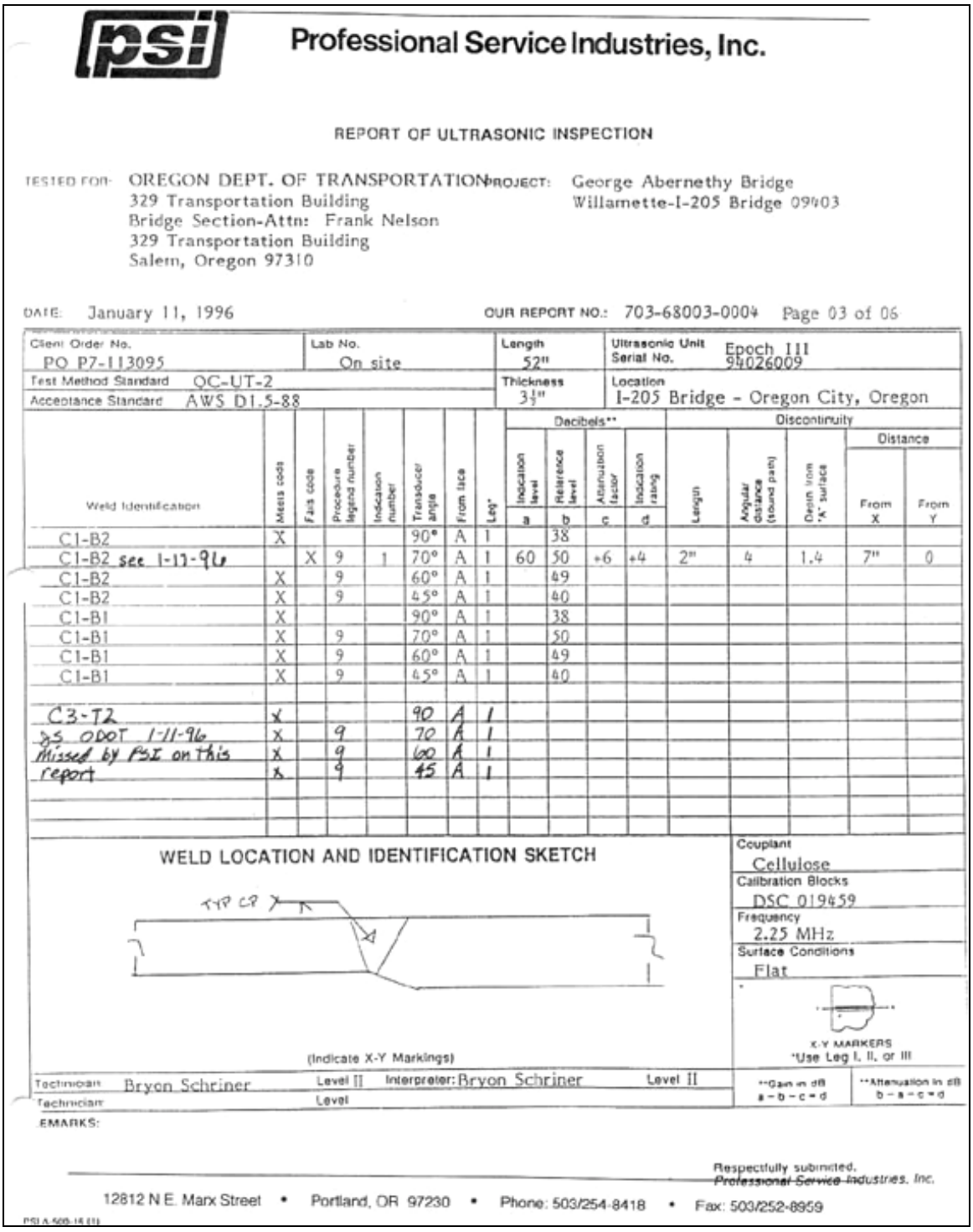

Professional Service Industries, Inc.

REPORT OF ULTRASONIC INSPECTION

TESTED FOR: OREGON DEPT. OF TRANSPORTATION
329 Transportation Building
Bridge Section-Attn: Frank Nelson
329 Transportation Building
Salem, Oregon 97310

PROJECT: George Abernethy Bridge
Willamette-I-205 Bridge 09903

DATE: January 11, 1996 OUR REPORT NO.: 703-68003-0004 Page 03 of 06

Client Order No.	Lab No.	Length	Ultrasonic Unit Serial No.
PO P7-113095	On site	52"	Epoch III 94026009
Test Method Standard: QC-UT-2		Thickness: 3½"	Location: I-205 Bridge - Oregon City, Oregon
Acceptance Standard: AWS D1.5-88			

Weld Identification	Meets code	Fails code	Procedure legend number	Indication number	Transducer angle	From face	Leg*	Decibels** a	b	c	d	Discontinuity Length	Angular distance (sound path)	Depth from "A" surface	Distance From X	From Y
C1-B2	X				90°	A	1		38							
C1-B2 see 1-17-96		X	9	1	70°	A	1	60	50	+6	+4	2"	4	1.4	7"	0
C1-B2	X		9		60°	A	1		49							
C1-B2	X		9		45°	A	1		40							
C1-B1	X				90°	A	1		38							
C1-B1	X		9		70°	A	1		50							
C1-B1	X		9		60°	A	1		49							
C1-B1	X		9		45°	A	1		40							
C3-T2	X				90	A	1									
25 ODOT 1-11-96	X		9		70	A	1									
Missed by PSI on this	X		9		60	A	1									
report	X		9		45	A	1									

WELD LOCATION AND IDENTIFICATION SKETCH

(Indicate X-Y Markings)

Couplant: Cellulose
Calibration Blocks: DSC 019459
Frequency: 2.25 MHz
Surface Conditions: Flat

X-Y MARKERS
*Use Leg I, II, or III

**Gain in dB a - b - c = d
**Attenuation in dB b - a - c = d

Technician: Bryon Schriner Level II Interpreter: Bryon Schriner Level II
Technician: Level

REMARKS:

Respectfully submitted,
Professional Service Industries, Inc.

12812 N.E. Marx Street • Portland, OR 97230 • Phone: 503/254-8418 • Fax: 503/252-8959

PSI A-509 (4-91)

Figure 4.1: UT report for 1996 inspection of ESW C1B2. The 70 degree scan does not meet the AWS D1.5-88 acceptance requirements.

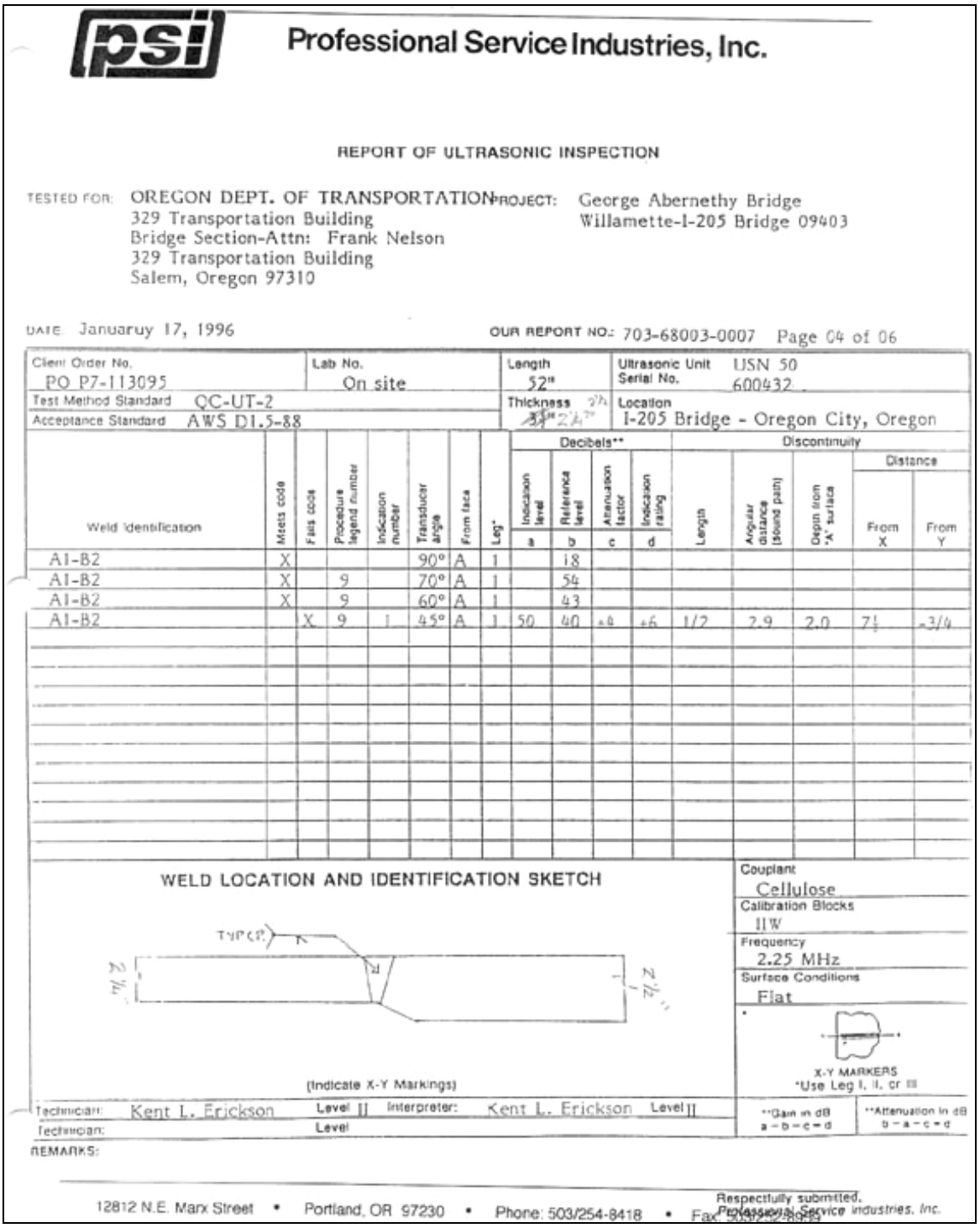

Professional Service Industries, Inc.

REPORT OF ULTRASONIC INSPECTION

TESTED FOR: OREGON DEPT. OF TRANSPORTATION
329 Transportation Building
Bridge Section-Attn: Frank Nelson
329 Transportation Building
Salem, Oregon 97310

PROJECT: George Abernethy Bridge
Willamette-I-205 Bridge 09403

DATE: Januaruy 17, 1996 OUR REPORT NO.: 703-68003-0007 Page 04 of 06

Client Order No.: PO P7-113095 | Lab No.: On site | Length: 52" | Ultrasonic Unit: USN 50 | Serial No.: 600432
Test Method Standard: QC-UT-2 | Thickness: 2¼" | Location: I-205 Bridge - Oregon City, Oregon
Acceptance Standard: AWS D1.5-88

Weld Identification	Meets code	Fails code	Procedure legend number	Indication number	Transducer angle	From face	Leg*	Decibels** Indication level a	Reference level b	Attenuation factor c	Indication rating d	Discontinuity Length	Angular distance (sound path)	Depth from "A" surface	Distance From X	Distance From Y
A1-B2	X				90°	A	1		18							
A1-B2	X		9		70°	A	1		54							
A1-B2	X		9		60°	A	1		43							
A1-B2		X	9	1	45°	A	1	50	40	+4	+6	1/2	2.9	2.0	7½	~3/4

WELD LOCATION AND IDENTIFICATION SKETCH

(Indicate X-Y Markings)

Couplant: Cellulose
Calibration Blocks: IIW
Frequency: 2.25 MHz
Surface Conditions: Flat

X-Y MARKERS
*Use Leg I, II, or III

Technician: Kent L. Erickson Level II Interpreter: Kent L. Erickson Level II
Technician: Level

**Gain in dB a – b – c = d
**Attenuation in dB b – a – c = d

REMARKS:

12812 N.E. Marx Street • Portland, OR 97230 • Phone: 503/254-8418 • Fax: 503/252-8089

Respectfully submitted,
Professional Service Industries, Inc.

Figure 4.2: UT report for 1996 inspection of ESW A1B2. The 45 degree scan does not meet the AWS D1.5-88 acceptance requirements.

4.3.4.3 Weld A4B2

Rejected due to 70-degree scan with a 64 dB indication level and a 54 dB reference level. Indication rating +5, length 3.5 inches. Field notes indicate that this indication appears to extend under the downstream web wall. Flange inspection outside the web showed no indication. See Figure 4.3 for inspection form and Figure 4.5 (c) for a plot of the indication. For the 70-degree scan on 2½ to 4 inch thick plates, like A4B2, a Class C flaw has an indication rating +4 to +5. Thus the UT indication in this weld is right on the border of being a Class D flaw severity.

4.3.4.4 Weld A8T1

Rejected due to 45-degree scan with a 49 dB indication level and a 39 dB reference level. Indication rating +5, length approximately 0.5 inches. Field notes indicate that this indication appears to extend under the downstream web wall. See Figure 4.4 for inspection form. This was located on the outer lip of weld.

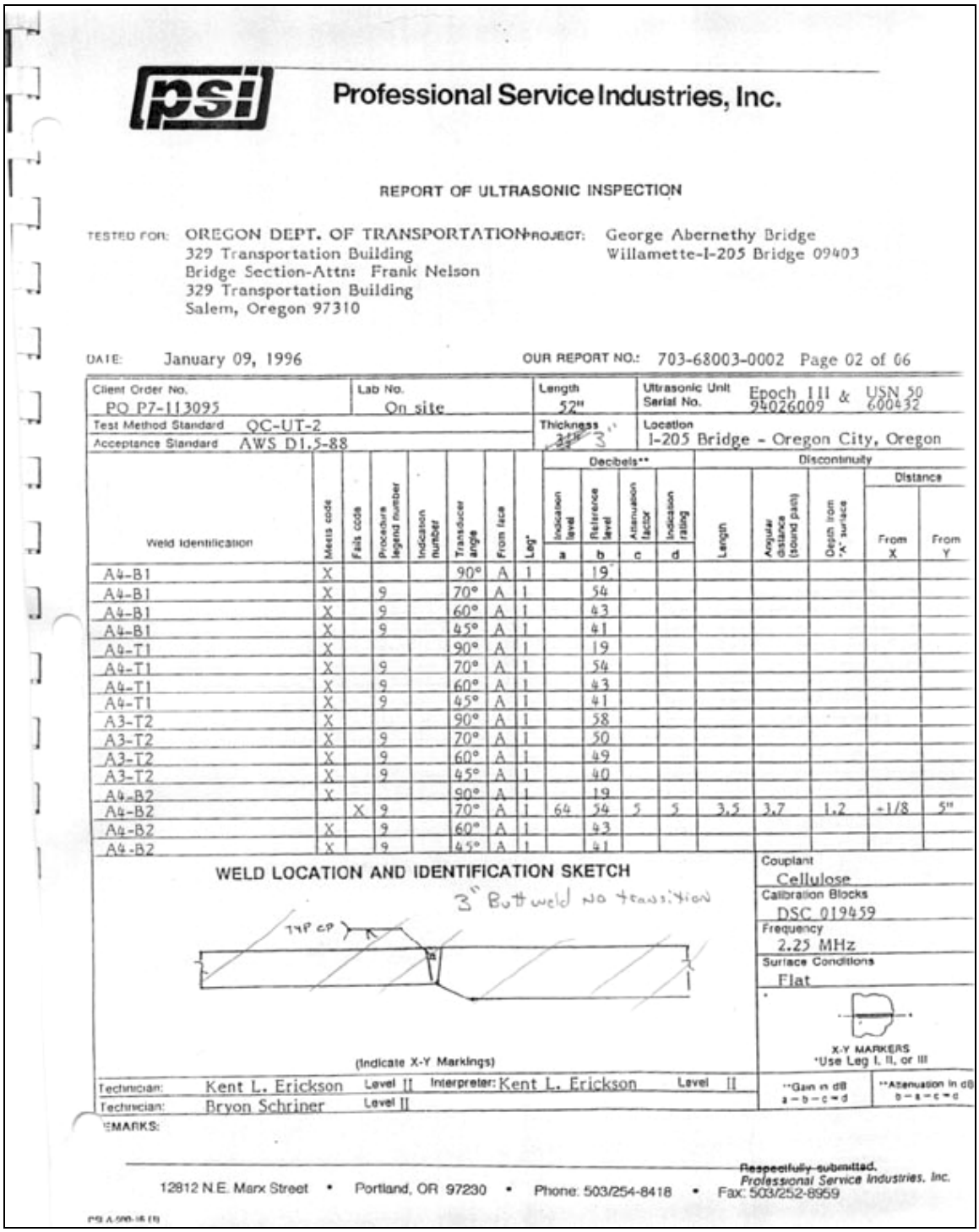

Professional Service Industries, Inc.

REPORT OF ULTRASONIC INSPECTION

TESTED FOR: OREGON DEPT. OF TRANSPORTATION
329 Transportation Building
Bridge Section-Attn: Frank Nelson
329 Transportation Building
Salem, Oregon 97310

PROJECT: George Abernethy Bridge
Willamette-I-205 Bridge 09403

DATE: January 09, 1996 OUR REPORT NO.: 703-68003-0002 Page 02 of 06

Client Order No.	Lab No.	Length	Ultrasonic Unit Serial No.
PO P7-113095	On site	52"	Epoch III & USN 50 94026009 & 600432
Test Method Standard QC-UT-2		Thickness 3"	Location I-205 Bridge - Oregon City, Oregon
Acceptance Standard AWS D1.5-88			

Weld Identification	Mess code	Fails code	Procedure legend number	Indication number	Transducer angle	From face	Leg*	Decibels** Indication level a	Reference level b	Attenuation factor c	Indication rating d	Discontinuity Length	Angular distance (sound path)	Depth from "X" surface	Distance From X	Distance From Y
A4-B1	X				90°	A	1		19							
A4-B1	X		9		70°	A	1		54							
A4-B1	X		9		60°	A	1		43							
A4-B1	X		9		45°	A	1		41							
A4-T1	X				90°	A	1		19							
A4-T1	X		9		70°	A	1		54							
A4-T1	X		9		60°	A	1		43							
A4-T1	X		9		45°	A	1		41							
A3-T2	X				90°	A	1		58							
A3-T2	X		9		70°	A	1		50							
A3-T2	X		9		60°	A	1		49							
A3-T2	X		9		45°	A	1		40							
A4-B2	X				90°	A	1		19							
A4-B2		X	9		70°	A	1	64	54	5	5	3.5	3.7	1.2	-1/8	5"
A4-B2	X		9		60°	A	1		43							
A4-B2	X		9		45°	A	1		41							

WELD LOCATION AND IDENTIFICATION SKETCH

3" Butt weld no transition

TYP CP

(Indicate X-Y Markings)

Couplant: Cellulose
Calibration Blocks: DSC 019459
Frequency: 2.25 MHz
Surface Conditions: Flat

X-Y MARKERS
*Use Leg I, II, or III

Technician: Kent L. Erickson Level II Interpreter: Kent L. Erickson Level II
Technician: Bryon Schriner Level II

**Gain in dB a - b - c = d
**Attenuation in dB b - a - c = d

REMARKS:

Respectfully submitted,
Professional Service Industries, Inc.

12812 N.E. Marx Street • Portland, OR 97230 • Phone: 503/254-8418 • Fax: 503/252-8959

Figure 4.3: UT report for 1996 inspection of ESW A4B2. The 70 degree scan does not meet the AWS D1.5-88 acceptance requirements.

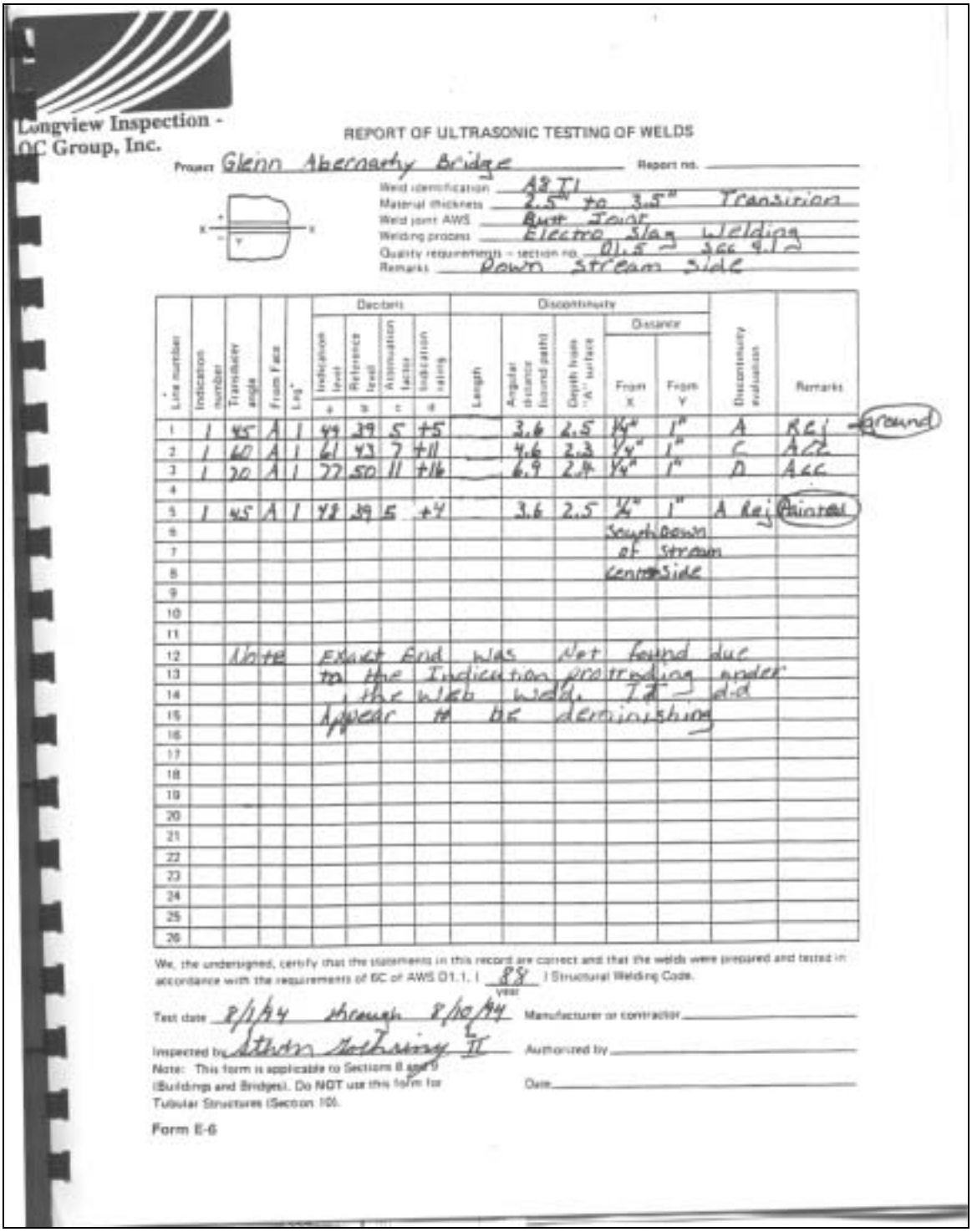

Longview Inspection - QC Group, Inc.

REPORT OF ULTRASONIC TESTING OF WELDS

Project: Glenn Abernathy Bridge — Report no.

Weld identification: A8 T1
Material thickness: 2.5" to 3.5" Transition
Weld joint AWS: Butt Joint
Welding process: Electro Slag Welding
Quality requirements – section no.: D1.5 → 3cc 9.1.2
Remarks: Down Stream Side

Line number	Indication number	Transducer angle	From Face	Leg	Decibels: Indication level (+)	Decibels: Reference level (=)	Decibels: Attenuation factor (=)	Decibels: Indication rating (dB)	Discontinuity: Length	Discontinuity: Angular distance (sound path)	Discontinuity: Depth from "A" surface	Distance: From X	Distance: From Y	Discontinuity evaluation	Remarks
1	1	45	A	1	44	39	5	+5		3.6	2.5	1/4"	1"	A	Rej - ground
2	1	60	A	1	61	43	7	+11		4.6	2.3	1/4"	1"	C	Acc
3	1	70	A	1	77	50	11	+16		6.9	2.4	1/4"	1"	D	Acc
4															
5	1	45	A	1	48	39	5	+4		3.6	2.5	1/4"	1"	A Rej	Painted
6												South Down			
7												at Stream			
8												Center Side			
9															
10															
11															
12		Note	Exact End						was	Not	found	due			
13			to the						Indication	protruding	under				
14			the web						weld.	It	did				
15			appear						to be	diminishing					
16															
17															
18															
19															
20															
21															
22															
23															
24															
25															
26															

We, the undersigned, certify that the statements in this record are correct and that the welds were prepared and tested in accordance with the requirements of 6C of AWS D1.1, [88] (year) Structural Welding Code.

Test date: 8/1/94 through 8/10/94 — Manufacturer or contractor:

Inspected by: Arthur Gothaway II — Authorized by:

Note: This form is applicable to Sections 8 and 9 (Buildings and Bridges). Do NOT use this form for Tubular Structures (Section 10). — Date:

Form E-6

Figure 4.4: UT report for 1994 inspection of ESW A8T1 downstream outer edge. The 45-degree scan does not meet the AWS D1.5-88 acceptance requirements.

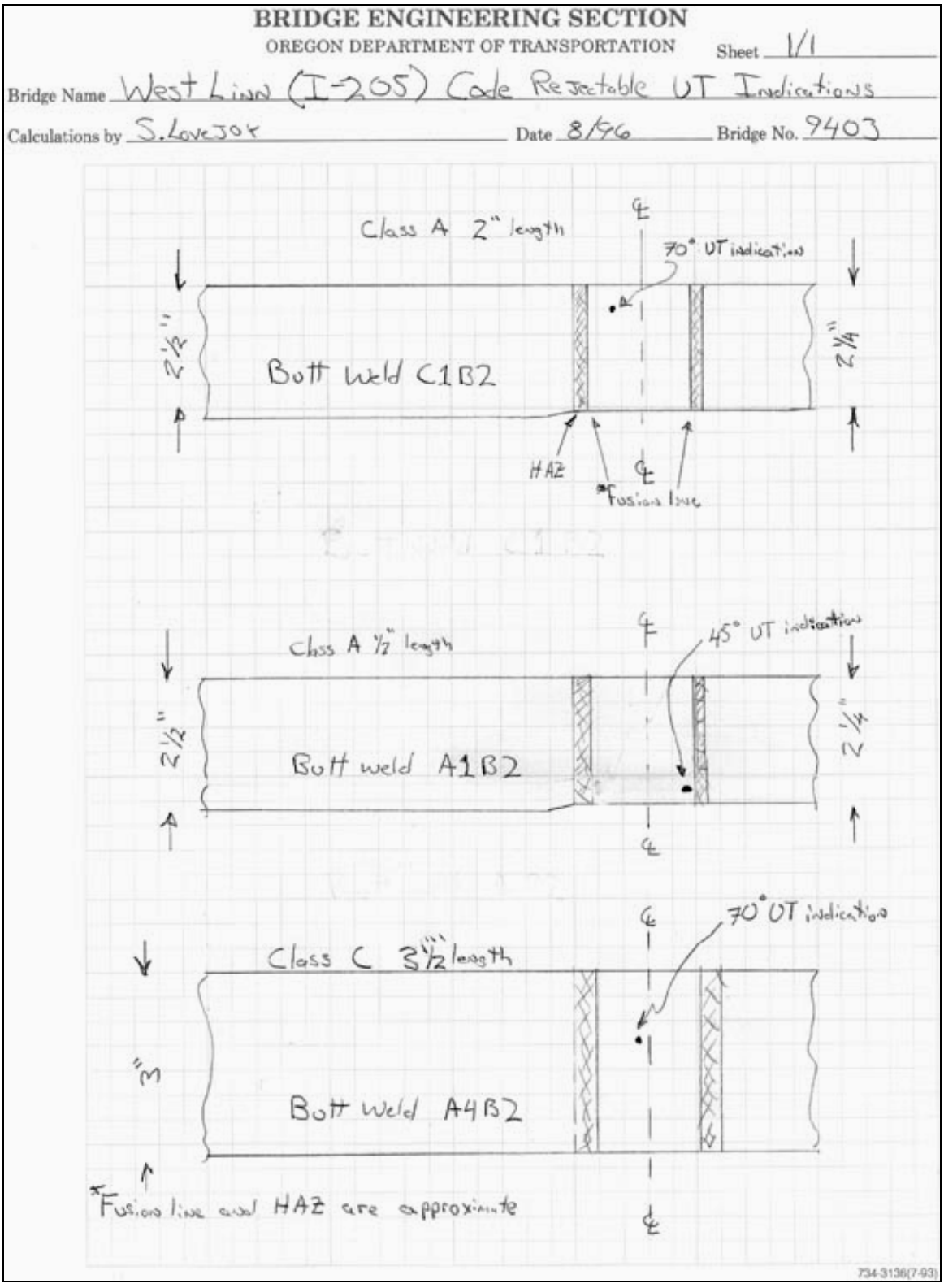

Figure 4.5: UT indication plots from 1996 inspection

Ultrasonic inspection of the coarse-grained, standard-gap ESW is far more difficult than welds with finer grain structure. Sound wave reflection and attenuation from the grain boundaries with in the metallurgical structure of these welds can adversely effect the signal to noise ratio of the test. Large amounts of energy must be input to compensate for the attenuation and often the large prior austenite grain boundaries form measurable reflectors to the sound waves giving false indications. Nonetheless, these four welds showed significant indications, whereas the other 108 welds inspected did not.

4.3.5 Acoustic Emission testing

In the Winter of 1993 limited AE inspection was performed on weld C1B2. This weld was chosen because it was easily accessible and contained some interesting UT flaw indications. This inspection was more of an FHWA-sponsored demonstration than an actual test. Nonetheless, a reputable AE expert listened to the weld in question under approximately 4 hours of heavy traffic. No evidence of crack growth was indicated (*Physical Acoustics Corporation, 1993*).

4.3.6 Fourth In-service Inspection (Y2KS)

During the winter of 2000 a fourth inspection effort was made to more closely examine the welds with code rejectable flaw indications. Wiss, Janney, Elstner Associates, Inc. was contracted to review all previous NDT on the subject welds and examine in detail welds A1B2, B1B2, C1B2, A4B2 and A8T1. Each of these five welds was thoroughly inspected with UT; the C1B2 weld was also inspected with RT. Four of the five welds inspected showed reject level indications with UT, as previous inspections had recorded. After a thorough review of previous work and detailed testing of these welds, both the author and the Y2KS inspector did not believe these defect indications to be crack-like in nature. This is best represented by quoting a portion of the report, (*Wiss, Janney, Elstner Associates, Inc. 2001*):

> "*A comprehensive review including data of Y2KS and prior nondestructive tests performed during the 1990's to study electroslag welded joints for characterization of detected indications was not conclusive; however, an increased confidence may be established in the stability of the joints. Although reject level indications were produced in ultrasonic examinations, their nature was characteristically random, and of relatively short length. Radiographs, where available, did not provide corroborating data. No indications from nondestructive tests were interpreted to represent crack-like discontinuities*." (*page 11*)

4.4 SUMMARY OF NDT ON FLANGE BUTT WELDS

The original fabrication of the box girders used both RT and MT as a NDT method. Although the original radiographs have been lost, there is strong evidence through personal testimony and field inspection notes of well-qualified people involved with the fabrication that all welds passed the requirements of AWS D1.1-69.

Post-construction UT revealed four out of the 112 fracture critical ESW had UT rejectable flaw indications based on the AWS D1.5-88 welding code. These rejection criteria were based on welding processes other than the standard gap ESW used for the fabrication on this bridge. In all four cases the indication was found to be rejectable on one of the four scan angles used. Three of the four welds with UT rejectable defect indications were subject to radiographic inspection that showed no defect indications.

There is substantial evidence that such coarse grained weld and HAZ metals may require more specific UT procedures and rejection criteria than those used for the other weld processes found in bridge construction. At this time it is the author's opinion that the four welds that contain UT rejectable defect indications should not be considered as having crack-like defects without concurrence with RT; thus the four welds in question are not considered to be crack-like.

Tables 4.2, 4.3, 4.4 and 4.5 summarize the NDT performed on the butt welds after construction.

Table 4.2: Summary of 1990 – 92 NDT of 30 Electroslag Welds

Weld I.D.	Flaw Severity Class	Scan angle (deg.)	D1.5-88 Reject	Comments
A1B2	A	45	N	100% RT no indications, transition reflection
B1B2	A	45	Y	100%RT no indications, incomplete fusion in web fillet
B8B2	D	45, 60	N	
C1B2	B	60	Y	
C4B2	D	45, 60	N	Partial RT no indications
C4B3	D	45	N	Poor signal to noise ratio, Partial RT no indications
D1B1	D	70	N	Porosity in web fillet, Partial RT confirmed UT
D1B2	D	70	N	Partial RT no indications
D1B4	D	45	N	

Table 4.3: Summary of 1994 UT of all fracture critical Electroslag Welds (outside of webs)

Weld I.D.	Flaw Severity Class	Scan angle (deg.)	D1.5-88 Reject	Comments
A8T1	A, C, D	45	Y	Down stream edge
B9B3	B, C	45	Y	Down stream edge
A4B2	D	60	N	Up stream edge, continues inside (see 1996 UT)
B2T2	D, D	45, 60	N	Down stream edge
B6B1	B, D	45	N	Down stream edge
B6B2	C	45	N	Down stream edge

Table 4.4: Summary of 1996 NDT of all fracture critical welds (inside of webs)

Weld I.D.	Flaw Severity Class	Scan angle (deg.)	D1.5-88 Reject	Comments
C1B2	A	70	Y	1992 UT noted same indications, AE tested in 1993
A1B2	A	45	Y	Passed 1992 100% RT
A4B2	C	70	Y	UT picked up from top and bottom surfaces, goes under upstream web.
D1B2	D	70	N	Passed partial RT in 1992
D6B3	B, B	60, 70	N	
D8B2	C	70	N	
A1B1	A	45	N	¼ inch length, not recorded in 1992 UT.
A2B2	C	45	N	
A8B1	B	70	N	
A9B1	C	60	N	
B1B2	D	45	N	Passed 100% RT in 1992, class A UT defect reported in 1992

Table 4.5: Summary of Y2KS NDT of selected welds

Weld I.D.	Flaw Severity Class	Scan angle (deg)	D1.5-88 Reject	Comments
A1B2	A	45	Y	Joint thickness transition is suspected of causing indication
B1B2	A	70	Y	Skewing transducer 15 to 25 degrees was required
C1B2	A	60, 70	Y	Y2KS radiograph did not corroborate UT findings
A4B2	D	70	N	Previously reported UT indication (1996) was not found
A8T1	A	45, 60	Y	Most difficult UT indications to evaluate

5.0 FITNESS FOR PURPOSE EVALUATION

5.1 OVERVIEW OF EVALUATION

In 1977, as a result of an earlier bridge girder failure, FHWA issued Notice N5040.23, directing state highway departments to examine in detail ESW in fracture critical bridge members. A detailed fracture control plan, developed by Dr. Stanley Rolfe for assessing the safety of these structures, was distributed by FHWA. A portion of this plan was executed in 1978 and 1979. The conclusion of this plan is contained in this report.

The George Abernethy Bridge contains fracture critical weldments that typically show substandard toughness, or crack tolerance, when compared to newer bridges designed and fabricated after execution of the FHWA fracture control plan. The FHWA fracture control requirements address the toughness of bridge steels and welds. If followed, the requirements almost guarantee ductile failure modes in all critical steel bridge members. Clouding this issue, however, is the fact that standard gap ESWs have a very coarse grain structure that can often lead to UT indications that RT does not pick up.

The purpose of the George Abernethy Bridge evaluation was to develop a fracture control plan that considered the possible crack-like defects in the welds, the weld metal's ability to tolerate cracks, and the service loading that may cause cracks to grow. The fracture control plan needed to insure public safety, structure serviceability, and maintain reasonable maintenance costs.

5.2 FAILURE OF THE BOX GIRDERS

According to NBIS standards, the Bridge does not have redundant load paths and is therefore considered fracture critical. However, the box girders are three-span continuous and thus offer the potential of structural redundancy via the moment carrying capacity of the haunched section over the interior piers. Calculations performed in 1980 indicated that if shear capacity could be maintained in the event of a fractured flange plate, the structure could likely support its own weight until repairs could be made (*ODOT 1981*). With today's computing power and the development of non-linear finite element programs, a more sophisticated analysis could be made to investigate various load paths under a failed flange scenario (*Morcos and Bjorhovde 1992*). These types of analysis are very complicated and hard to verify. Until further information is acquired on this subject, all of the fracture critical welds should be treated as fracture critical. Based on this position, failure of a fracture critical weld is an unacceptable event to the safety and serviceability of the structure.

5.2.1 Failure Assessment

The main concern of the standard gap ESW is the poor toughness when compared to modern requirements. Poor toughness can result in rapid and unstable crack growth as was found in the liberty ship failures in the 1940's. Steels of high toughness can tolerate missed fabrication flaws and other defects that may develop due to poor detailing or distortion-induced cracking under service conditions. Ideally, large cracks could exist in a member and it would not fail by brittle fracture, but by ductile tearing and yielding of the remaining section of the member.

Steels of low toughness are less tolerant to these common deficiencies in real structures and, under the right conditions, they can fail in a brittle manner at a load that is far below general yielding.

For this analysis a Failure Assessment Diagram (FAD) is appropriate. This approach looks at both ends of the failure mode spectrum and the interaction of both ductile and brittle failure modes. The FAD used in this analysis is based on the strip yield approximation. A failure envelope is defined in terms of the critical stress and fracture ratios S_r and K_r respectively. All points inside the envelope are expected to not fail in service.

5.2.1.1 Ductile failure mode:

The ductile failure mode for the flange plates on the box girders could be by yielding of the gross section if no defects were present. In this failure mode the critical stress for the flange plates, σ_c, can be considered to be the flow stress of the base metal. Once this stress level has been reached, the plate can no longer carry more load. For the A36 base metal this flow stress is 40.5 ksi. The flow stress of the weld metal is 72 ksi. Refer to Chapter 3 for material testing. For a ductile failure with gross section yielding, the base metal will have the limiting capacity. The maximum in-service stress that is put on any section of the flange plates is the sum of the dead, thermal, live and seismic loads, which are summarized in Table 5.1. If all of these loads were to occur at once, the magnitude of the stresses in the flange plates would vary from 0 to 20.4 ksi. Thus for a completely ductile failure of the flange plates the worst-case stress ratio S_r is 0.50, where S_r is the ratio of the maximum stress to the ductile failure stress:

$$S_r = \text{maximum service stress} / \text{ductile failure stress} = 0.50 \qquad \textbf{(5-1)}$$

Table 5.1: Summary of flange plate maximum service stresses

Load Source	Top Flange Stress (ksi)	Bottom Flange Stress (ksi)
Dead Load	9.3	6.8
Live Load	2.3	2.8
Thermal Load	4.8	4.8
Seismic Load	4.0	4.0
Total	20.4	18.4

5.2.1.2 Brittle failure mode:

The brittle failure mode for the flange plates would require a critical sized flaw to be present in one of the ESWs, since they have inferior crack tolerance when compared to the base metal. As discussed in Chapter 3, the response of the weld metal to a crack or other severe defect is best represented using the LEFM approach. This approach attributes crack growth, both stable and unstable, to the single parameter term – the stress intensity, K. K is a function of applied stress around the crack tip and the size and shape of the crack. In a constant stress field, as the crack gets bigger, the stress intensity raises until it reaches a critical level; then unstable crack growth occurs, which is generally considered ultimate failure in a brittle material.

The critical level of K at which this occurs is often a function of plate thickness, surrounding stress field, strain rate and temperature; it is not an intrinsic material property like the elastic modulus or Poisson's ratio. One-inch thick by three-inch diameter test specimens were tested from various metallurgical regions within the ESW to best predict the toughness of the full section flange plates at the lowest anticipated service temperature and strain rates. The lowest toughness was found to be in HAZ with a critical stress intensity of 97 ksi-in^{½}, as determined from brittle failure modes in J-Integral testing, K_{Jssy}.

In order to quantify the maximum stress intensity in service conditions, two parameters must be evaluated: 1) the flaw size, shape and location; and 2) the maximum stress the flaw is subjected to. As found in the ductile failure mode analysis above, the maximum far field stress from a global view of the structures is 20.4 ksi. As discussed in Chapter 2, the weld residual stresses are much higher than this but are neglected for the current failure scenario.

From Chapter 4 the present UT code rejectable defect indications are not considered to be crack-like, but crack-like flaws statistically may exist in the structure. The maximum flaw size to escape the NDT performed to date is less than ½ inch in length. As previously discussed, quality NDT can do much better than this, but this is a conservative estimate. Based on the ability to perform surface inspections on the welds (VT and MT) with excellent reliability and based on the fact that there are large magnitude compressive stresses on and near the surface of these ESWs, the most likely flaw to escape detection is in the core of the weld and or HAZ.

If one assumes a circular or penny shaped crack of radius a, in a plate of finite width b, the maximum stress intensity K, can be expressed as shown in Figure 5.1. With a ½ inch diameter crack and a far field stress of 20.4 ksi, K = 11.7 ksi-in^{½}. The brittle failure stress intensity, K_{Jssy}, is 97 ksi-in^{½}; thus the Stress Intensity ratio K_r is equal to 0.12:

K_r = (service stress intensity) / (critical stress intensity) **(5-2)**

K_r =.12 and S_r = 0.5 most probable maximum service condition

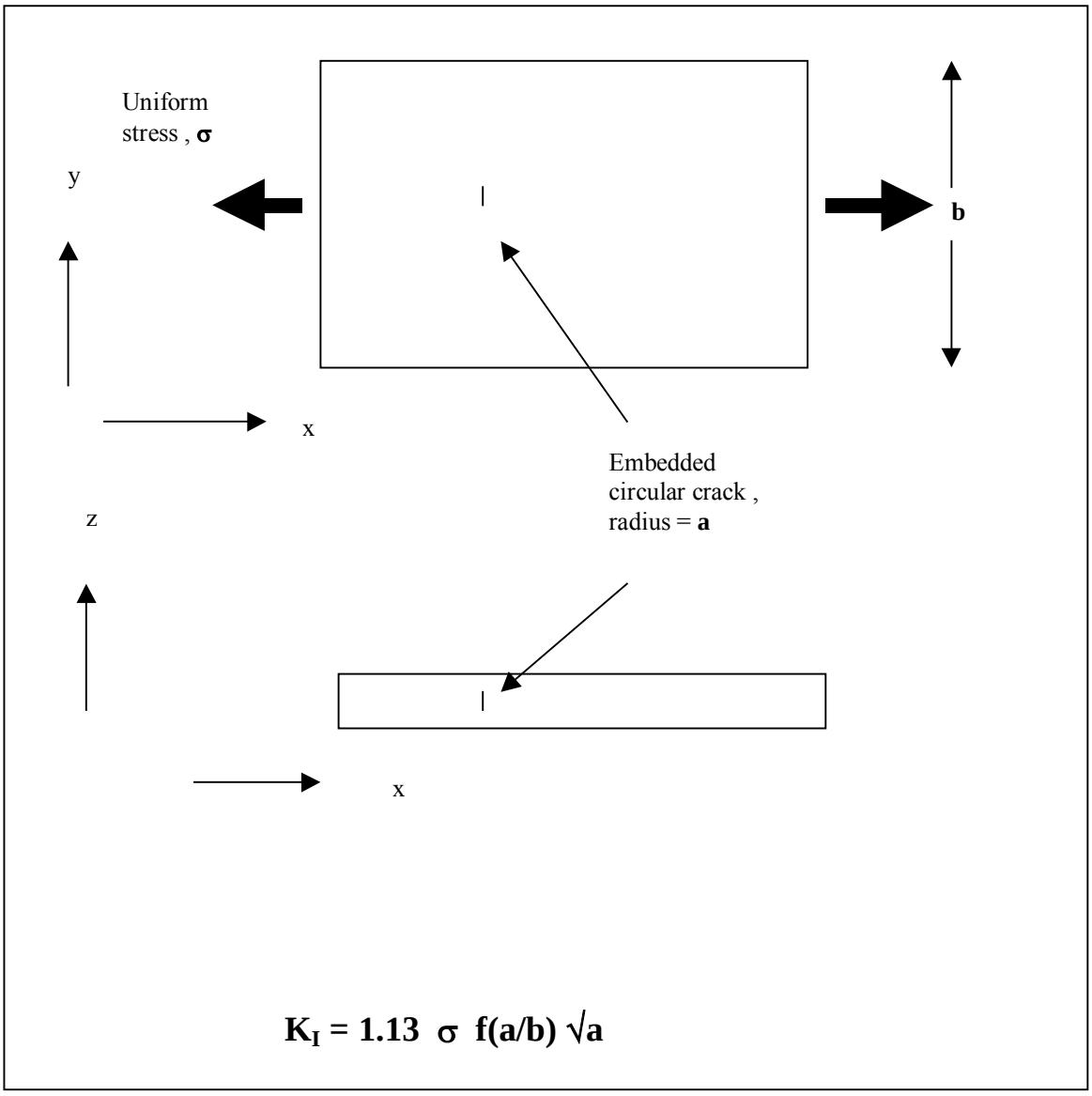

Figure 5.1: Stress Intensity equation for an embedded circular crack in a plate of finite width and uniform stress field

In the case that some welds exhibit even lower toughness than predicted by K_{Jssy}, and K_Q is a better representation of the actual toughness than the K ratio and would be $K_r = 0.24$:

$K_r = .24$ and $S_r = 0.5$ extreme service condition

Figure 5.2 show the failure assessment diagram (FAD) for the strip yield model of a through-thickness crack as developed by Dowling and Townley, and Harrison, et al. (*Dowling and Townley 1975; Harrison, et al. 1976*).

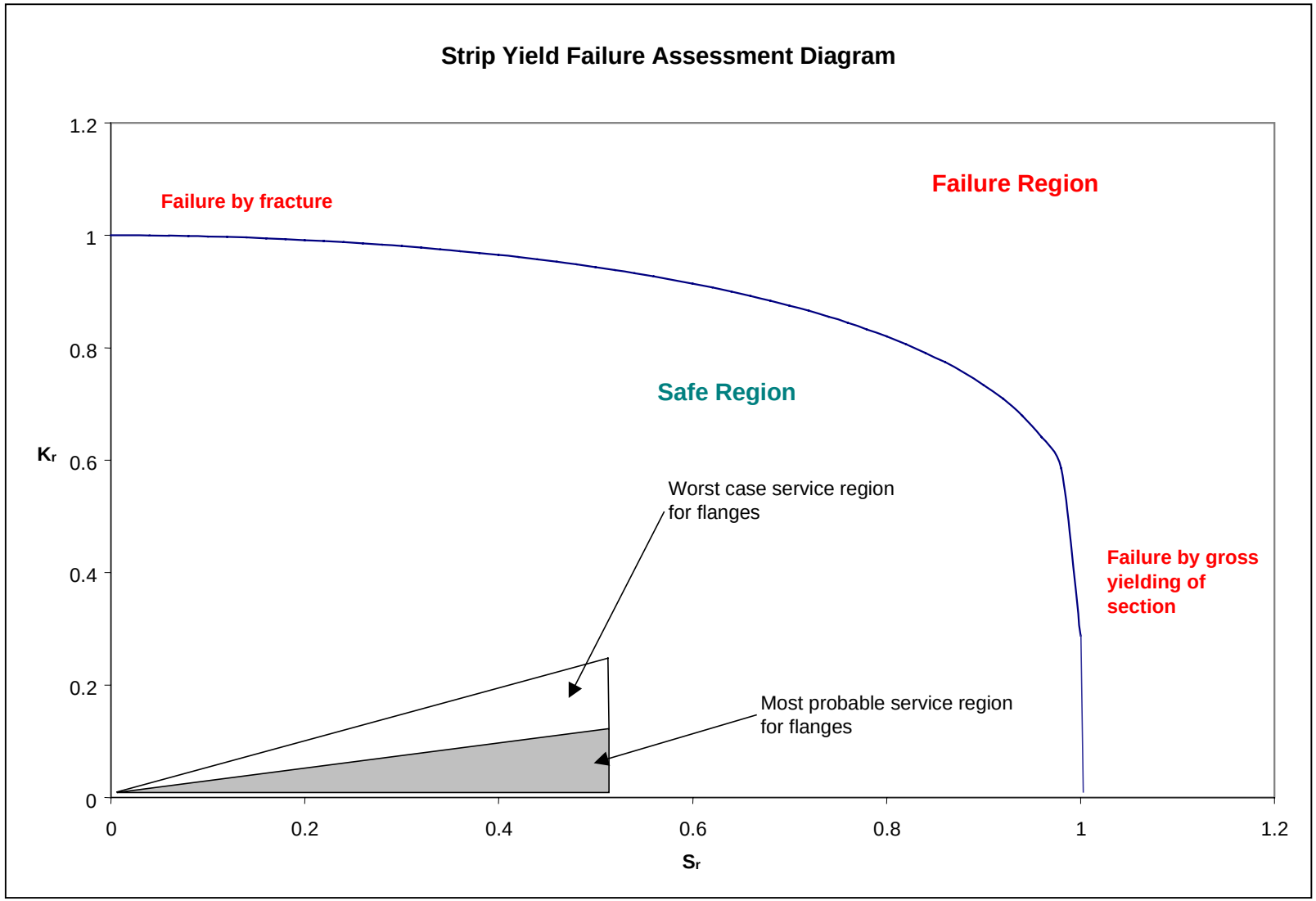

Figure 5.2: Failure assessment diagram for box girder ESW

The vertical axis defines brittle failure modes and the horizontal axis defines ductile failure modes. The plot shows the locus of predicted points of failure. All points inside the line are predicted not to fail, and those outside the line are to fail.

The flange plates operate in the region shown by the smaller triangle. This is the best estimate of maximum service conditions based on a ½-inch diameter crack escaping NDT, the sum of all design loads occurring simultaneously, using the lowest toughness measured in the welds. The second triangle area is for the same conditions with the exception of extremely brittle behavior in the welds with the toughness being on the order of 50 ksi-in^{½}. None of the test data indicate a toughness this low, but only nine toughness tests were used to quantify the toughness of all 112 fracture critical welds. It is improbable but not impossible for the toughness of a few welds to be this low.

5.3 DEFECTS AND HIGH RESIDUAL STRESSES

Another failure scenario that needs to be addressed is the flaw or defect subjected to the residual stresses in the ESW. The failure scenario above included the potential of a sub-critical defect being affected by extreme service loads and high residual stresses but neglected the residual stresses for the actual calculation of critical crack size. From the load analysis in Chapter 2 it was shown that the outer shell or fusion zone of the standard gap ESW is subjected to large compressive residual stresses; thus it was inferred that the core of the weld is subject to large magnitude, triaxial tensile stresses.

These weld regions with steep stress gradients are typically not addressed in structural designs and are assumed to develop at least the same strength as the base metal. Experience has shown this to be a generally good assumption. However, given the lower toughness of the weld metal, the course grain structure which could present crack initiation sites, and the high triaxiality of the stress which decrease ductility, it becomes necessary to address the probability of a subcritical flaw in the core of a weld growing into a large and potentially hazardous crack.

Standard gap ESWs have several different crystalline grain structures depending on the welding parameters and cooling rates (*Culp 1979*). All of these types can typically have long columnar grains in the middle of the weld metal. Let us assume that a few of these grains represent an embedded elliptical crack in the weld metal with a length of 1.5 inches and a width of 0.25 inches. The stress intensity for this case is calculated to be near 40 ksi-in^{½} if weld metal yield stresses are assumed. With a critical stress intensity of 97 to 178 ksi-in^{½}, even the high magnitude residual stresses are not expected to fail the assumed defect. See Figure 5.3 for assumed geometry.

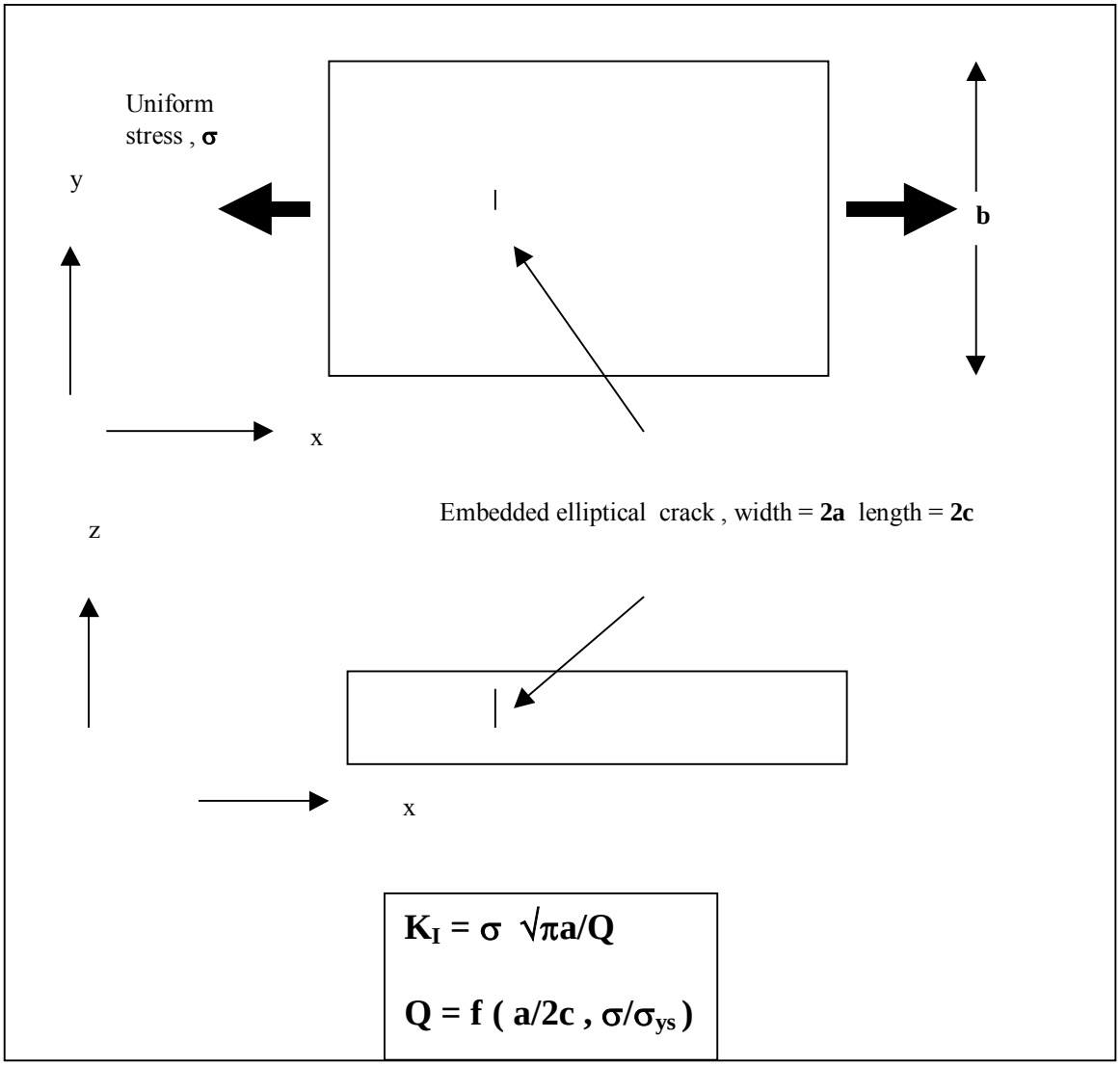

Figure 5.3: Stress intensity equation for an embedded elliptical crack in a finite width plate with uniform stress field

5.3.1 Fatigue Crack Growth

Fatigue crack growth can be separated into three regions of behavior: initiation, stable growth and unstable growth. Initiation is the process of developing a very small flaw into an actively growing fatigue crack. In welded structures this portion of the fatigue life is often neglected under the assumption that crack-like flaws may have escaped NDT. Once a crack is located in a structural component, it will grow in a stable manner, provided that the stress intensity range, ΔK, at the crack tip(s) is greater than a threshold value ΔK_{th}, and that the combination of all stresses adds to a tensile value. The dead and live load stresses on all fracture critical welds are tensile by definition and the residual stresses are assumed to be tensile at the core of the weld.

Thus if the live load range and flaw sizes are large enough, a small defect could grow into a fully active fatigue crack.

As discussed in Chapter 4, the NDT performed on this structure will very likely detect defects and flaws less than 0.5 inches in dimension. The maximum live load stress range was found to be less than 3 ksi at any weld location. The maximum stress intensity range from this combination of flaw size and stress range is 1.7 ksi-in^{½} or less. The lowest crack growth threshold calculated from core data was 10.9 ksi-in^{½}. Thus the largest flaw expected to escape NDT would not be expected to grow or propagate under the live load stress range.

From another perspective, based on the measured, ΔK_{th}, nearly an eight-inch long by two-inch wide elliptical crack would be the maximum sized flaw expected to remain dormant under current live loads. Thus developing and propagating an active fatigue within the ESW in the flange plates is a very unlikely event. Proper NDT can assure this with a very high probability of success.

5.3.2 S-N Approach

Looking at these ESWs from a design perspective, the fatigue life is typically characterized by the number of stress cycles at a particular stress amplitude. Prior research has shown that non-tapered standard gap ESWs can be characterized as having an AASHTO fatigue strength of Category B and Category C for tapered butt joints (*Schilling and Klippstein 1981*). Category C is also representative of the stud welds attached to the top flange plates for composite action with the concrete deck. The constant amplitude fatigue limit (CAFL) for two million stress cycles or more for Categories B and C are 16 and 9 ksi, respectively.

Using the estimation of fatigue life procedures suggested by Yen, et al., the measured effective stress range should be compared with the CAFL (*Yen, et al. 1990*). The largest effective stress ranges measured at the six strain gauge locations ranged from 425 to 1060 psi. The maximum stress cycle measured ranged from 1233 to 2175 psi. Both of these parameters are seen to be substantially below the CAFL, and thus infinite fatigue life is predicted under the loading measured.

It should be noted that there is a fatigue Category E′ detail fabricated into the box girders. At the access hole in each diaphragm, a ¾ inch thick plate has been welded to the bottom flange. Figure 5.4 shows a picture of one of these details. The CAFL for Category E′ is 1.3 ksi, which, using the above procedures, is predicted to have a finite fatigue life because the maximum stress range measured exceeds the CAFL. Using an effective stress range of 1000 psi and an ADTT per direction of traffic of 3500, the estimated remaining fatigue life of these details is 280 years. None of these details is attached to an ESW in this structure and thus does not effect the fatigue lives of the welds in question.

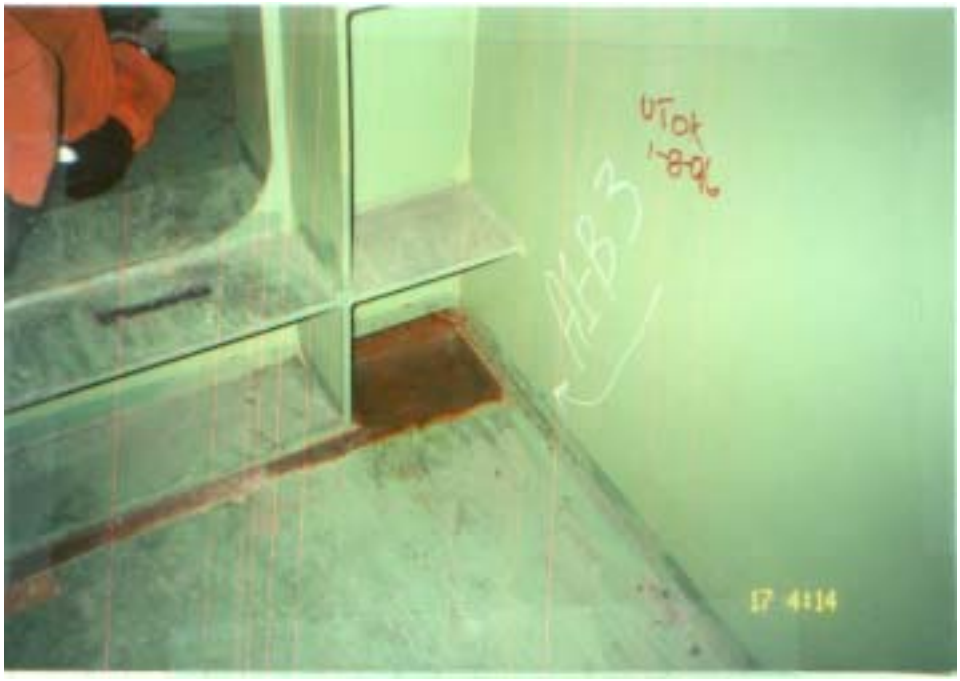

Figure 5.4: Fatigue Category E' detail found in box girders at diaphram connection to flange. The detail does not effect the butt welds.

6.0 SUMMARY AND CONCLUSIONS OF STUDY

6.1 SUMMARY

A fitness-for-purpose evaluation was performed on the flange butt welds on the I-205 West Linn bridge as per the request of FHWA notices N5040.23 and 5040.29, dated 2/16/77 and 2/23/77, respectively, as well as Memorandum HNG-30, dated 6/21/78. This evaluation requires gathering knowledge of the material properties, flaw or defect population from fabrication and service loads pertaining to the weldments. With these data the serviceability of the weldments can be assessed and repair or inspection requirements can be developed to assure public safety and reasonable operational costs.

Service Loads – From the original design calculations the maximum dead load stress was 9.3 ksi. The maximum live load stress was 2.8 ksi. Measured live load stresses were found to have an effective stress range of less than 600 psi. Other analyses indicated that the maximum thermal induced stress was 4.8 ksi and the maximum seismic stress was 4.0 ksi. The total maximum combination of these structural loads was 20.4 ksi.

Fabrication Stresses – Residual stresses from the welding process were shown to have a core of triaxial tension and a compressive outer shell surrounding the weld region. The magnitude of these stresses was on the order of the yield stress of the weld metal.

Material Properties – The tensile, toughness and crack growth threshold properties of the base, HAZ and weld metals were quantified. The lowest measured toughness as defined by the small scale yielding criteria applied to ASTM 813 test data was found to be 97 ksi-in^{½} in the HAZ at 0ºF. The minimum fatigue crack growth threshold measured, as defined by ASTM E647, was 10.9 ksi-in^{½}.

Non-destructive Testing – Based on the original fabrication inspection document, UT / RT testing in 1978, and UT / MT testing in 1996 and 2000, the most likely size of crack-like weld defects to escape inspection was less than ¼ inch in maximum dimension. The largest sized flaw to possibly escape detection was ½ inch in maximum dimension. Four of the 112 fracture critical ESWs contained UT rejectable defects based on the AWS D1.5-88 Bridge Welding code. These defects were only rejectable on one of four scan angles used and were located in low stress range regions of the girders. Based on repeated testing, these defect indications were not considered to be crack-like.

Failure Analysis – Based on the quantified data above, a failure assessment was made considering two modes of failure – brittle and ductile. Based on the strip yield theory of combined failure modes, the ESWs were found to be very unlikely to fail under even the most extreme combination of service loads and minimal material crack tolerance. Critical crack dimensions were on the order of four inches for an assumed through-thickness crack in a finite width plate. Given the maximum crack size to escape NDT, the fatigue crack growth threshold

and service loads, fatigue crack growth under live load was not anticipated for the service life of this structure. From a traditional S-N approach, infinite fatigue life was predicted based on comparison with fatigue testing of similar ESW beams.

6.2 CONCLUSIONS

1) The ESW metal is stronger yet less ductile then the base metal. The toughness is substantially lower than the base metal, yet adequate to sustain all anticipated service loads.

2) The fatigue crack growth threshold indicates that fatigue crack growth is very unlikely under service loads.

3) The fabrication and inspection quality of these welds is very good. It is highly unlikely that any crack-like flaw larger than ½ inch exists in any of the ESWs; they are more likely less than ¼ inch.

4) From a conventional S-N approach the ESWs are expected to have an infinite fatigue life.

5) Retrofitting of the ESWs is not necessary nor is it recommended.

6) A rigorous yet reasonable NDT program can insure public safety and maintain acceptable maintenance costs.

7.0 FRACTURE CONTROL PROGRAM FOR THE BOX GIRDERS

7.1 OVERVIEW

Between 1977 and 1999 ODOT carried out the fracture control program for the fracture critical ESWs in the box girders of the George Abernethy Bridge at West Linn, Oregon. This plan characterized the fracture potential of these welds by quantifying the structural loading, material toughness and weld defects present. The results of this study concluded that the ESWs were fit for continued service without any modifications or repairs. Under the National Bridge Inspection Standards (NBIS) act of 1967 the box girders are required to be visually inspected by a licensed lead bridge inspector every two years. Details of fracture critical inspections can be found in FHWA report FHWA-IP-86-26 (*FHWA 1986*). Oregon has been granted an exception to this standard, in that engineered fracture critical inspection periods can be developed for our fracture critical structures on a case by case basis. These inspection periods can be extended out to 10 years but rely on quality inspection. It should be noted that these modified inspection periods do not apply to the routine biennial NBIS inspection defined in FHWA report FHWA-PD-91-015 (*FHWA 1991*).

7.2 FRACTURE CONTROL PLAN FOR REMAINING LIFE OF STRUCTURE

In addition to the biennial NBIS inspections, the four box girders shall receive the following inspections at the specified periods:

1) **Modified Biennial Inspection** – In addition to the current biennial (NBIS) inspections, all four box girders shall have visual testing (VT) performed on the fracture critical welds as defined in Drawing #32000 and performed on the cored and plugged compression welds . This inspection shall be performed from inside of the box girders. All of these welds have had the paint removed from the inside surface. As part of this inspection, a protective coating such as WD-40 will be applied to these surfaces. The surface must be free of rust, dirt, etc. for proper inspection.

   All Fatigue Category E′ details shall also be given VT. These details will be permanently marked and coded inside the box girders for ease of identification and tracking. The paint system shall be removed in the vicinity of these details to assist inspection. They will also be coated with a protective coating such as WD-40. These additional inspections shall be performed with every biennial inspection.

2) **Fracture Critical Inspection** – In addition to the NBIS biennial inspection as modified above, a fracture critical inspection shall be performed on all four box girders every 10 years,

starting in 1996. This will be considered a major inspection and shall, at a minimum, include VT of 100 % of the exposed surface area of the box girders, inside and out.

All fracture critical ESWs shall receive 100% UT in accordance with AWS D1.5. This inspection will be performed from the inside of the box girders with the exception of the outer edges of the flange plates, which must be scanned from outside the box girders. The UT shall be overseen and approved by an ASNT level 3 UT inspector with at least 7 years experience with ESW inspection. All testing shall be performed by an ASNT level 2 inspector or higher. Techniques and data presentation shall be substantially similar to the testing performed in 1996 (*PSI 1996*). All code-rejectable UT indications shall be scanned from both surfaces of the flange plate. If the outside scan is inconclusive, then RT from two orthogonal directions will be performed. All UT described above shall be performed in 2006 and again in 2016. If no new code-rejectable UT indications are recorded after the 2016 inspection, only fracture critical ESWs with code-rejectable indications shall be required to be UT. All other inspections still apply.

All Fatigue Category E′ details shall receive MT. Any MT indications shall receive UT to establish depth of indication. All cored welds shall have the plug removed and be subject to MT on both inside and outside surfaces. Plugs shall be reinstalled after inspection.

3) The documentation for each inspection shall be preserved for the life of the structure.

8.0 REFERENCES

Anderson, T.L. and R.H. Dodds, Jr. 1991. Specimen Size Requirements for Fracture Toughness Testing in the Ductile-Brittle Transition Region. *Journal of Testing and Evaluation*, vol. 19, pp. 123-134.

Barsom, J.M. and S.T. Rolfe. 1987. *Fracture and Fatigue Control in Structures, Applications of Fracture Mechanics, 2nd edition*. Prentice-Hall, Inc. Englewood Cliffs, NJ.

Caltrans Transportation Laboratory. 1978. Report of Evaluation of Electroslag Weld Cores from West Linn Bridge in the State of Oregon. Test report for Oregon Department of Transportation. August 21.

Culp, J.D. 1979. Electroslag Weldments: Performance and Needed Research. *Welding Journal*, 58(7): pp. 27-41.

Dowling, A.R. and C.H.A. Townley. 1975. The Effects of Defects on Structural Failure: A Two-Criteria Approach. *International Journal of Pressure Vessels and Piping*, vol. 3, pp. 77-137.

Federal Highway Administration. 1986. *Inspection of Fracture Critical Bridge Members*. FHWA Report No. FHWA-IP-86-26.

Federal Highway Administration. 1991. *Bridge Inspector's Training Manual / 90.* FHWA Report No. FHWA-PD-91-015.

Ferrill, D.A., P.B. Juhl and D.R. Miller. 1966. Measurement of Residual Stresses in a Heavy Weldment. *Welding Research Supplement.* American Welding Society National Fall Meeting, St. Louis, MO. pp. 504s-514s.

Harrison, R.P., K. Loosemore, I. Milne and A.R. Dowling. 1976. Assessment of the Integrity of Structures Containing Defects. Central Electricity Generating Board, report CEGB R/H/R6, United Kingdom.

Koon-Hall-Adrian Metallurgical, Inc. 1997. Test report for Oregon Department of Transportation. December 30.

Longview Inspection, Inc. 1994. Final Report Ultrasonic Examination of Glenn Abernethy Bridge, report for Oregon Department of Transportation, August 15.

MEI-Charlton, Inc. 1999. Electroslag Butt Welds; West Linn I-205 Bridge; Residual Stress Measurements. Test report for Oregon Department of Transportation. Reference No. 6406040. March 16.

MEI-Charlton, Inc. 2001. Oregon City I-205 Bridge, No. 9403; Weld Compact Tension Specimen; Fatigue Crack Threshold and Metallurgical Testing. Reference No. 6607054. Test report for Oregon Department of Transportation, September 14.

Morcos, S.S. and R. Bjorhovde. 1992. Fracture in Continuous Composite Girders. Ninth International Bridge Conference. Engineers' Society of Western Pennsylvania. IBC-92-42. pp 262-276.

Oregon Department of Transportation. 1981. Bridge Engineering Section maintenance file for Bridge #9403. Calculations by Phil Rabb.

Oregon Department of Transportation. 1999. Willamette River (Abernethy) Bridge Main Spans and East Approach Seismic Retrofit. Calculation Books #4801-4805. ODOT Bridge Engineering Section, Salem, OR.

Oregon Graduate Institute of Science and Technology. 1999. Toughness and Fatigue Threshold Determination of Electroslag Welds Extracted from the West Linn Bridge. Test report for Oregon Department of Transportation. September 8.

Paton, B.E. 1962. *Electroslag Welding, 2nd ed*. American Welding Society. Miami, FL.

Pense, A.W., J.D. Wood and J.W. Fisher. 1981. Recent Experiences with Electroslag Welded Bridges. *Welding Journal*, December, pp. 33-42.

Physical Acoustics Corporation 1993. Acoustic Emission Monitoring of the I-205 Willamette River Bridge. Report R90-259 for Oregon Department of Transportation, April 30.

Professional Services Industries, Inc. 1996. Report of Inspection George Abernethy Bridge, Willamette I-205 Bridge 09403 January 08, 1996 – January 11, 1996. Report for Oregon Department of Transportation, January 15.

Ruud, C.O. and P. S. Dimascio. 1981. A Prediction of Residual Stress in Heavy Plate Butt Welds. American Society for Metals, Vol. 3, June, pp. 62-65.

Ruud, C.O., J.A. Josef and D.J. Snoha. 1993. Residual Stress Characterization of Thick-Plate Weldments Using X-Ray Diffraction. Supplement to *Welding Journal*, March, pp. 87s-91s.

Schilling, C.G. and K.H. Klippstein. 1981. Tests of Electroslag-Welded Bridge Girders. *Welding Journal,* December, pp. 23-30.

Watson, P. and B.J. Dabell. 1975. Cycle Counting and Fatigue Damage. *Proceedings from Symposium of the Society of Environmental Engineers*, vol. 2.

Wiss, Janney, Elstner Associates, Inc. 2001. West Linn (George Abernethy) Bridge, I-205 West Linn, Oregon for State of Oregon Department of Transportation. Report WJE No. 2000.3567 for Oregon Department of Transportation, June 22.

Yen, B.T., T.I. Huang, L.Y. Lai and J.W. Fisher. 1990. *Manual for Inspecting Bridges for Fatigue Damage Conditions*. Federal Highway Administration. Report No. FHWA-PA-89-022 +85-02.